

BL ✓

**FOR REFERENCE ONLY**

40 0786155 7



ProQuest Number: 10290215

All rights reserved

INFORMATION TO ALL USERS

The quality of this reproduction is dependent upon the quality of the copy submitted.

In the unlikely event that the author did not send a complete manuscript and there are missing pages, these will be noted. Also, if material had to be removed, a note will indicate the deletion.



ProQuest 10290215

Published by ProQuest LLC (2017). Copyright of the Dissertation is held by the Author.

All rights reserved.

This work is protected against unauthorized copying under Title 17, United States Code  
Microform Edition © ProQuest LLC.

ProQuest LLC.  
789 East Eisenhower Parkway  
P.O. Box 1346  
Ann Arbor, MI 48106 – 1346

# 'Nanoparticles for Use in Reactive Porous Polymer Latex Films'

Simon A. Mazengarb

Thesis submitted in partial fulfilment of the requirements of the Nottingham  
Trent University for the degree of Doctor of Philosophy

May 2006

The investigation which is the subject of this report was initiated by the director of CBD  
Sector, Defence Science and Technologies Laboratory (Dstl) Porton Down and was carried  
out under the terms of Contract No. RD013-930312

**“He who would search for pearls must dive below.”**

**John Dryden, 1631-1700**

## **Abstract**

Porous styrene divinylbenzene copolymers in the size range 50 - 100nm have been produced via a cross-linking emulsion copolymerisation technique. The effect of varying the initiator, surfactant and inert diluent type and concentration on particle size and specific surface area have been systematically evaluated. Toluene, xylene and heptane have been used as inert diluents to generate the internal porous network. Evaluation of the porosity has been carried out using nitrogen adsorption / desorption methods to calculate the BET specific surface area of the resulting latex and then comparing this with the theoretical surface area for a solid sphere of comparable size. The mean particle size was determined by photon correlation spectroscopy. Further evaluation of the nanoparticle porosity was achieved by interpreting the nitrogen desorption isotherm using the BJH equation to give a pore size distribution and using the Dubinin-Radushkevich equation to quantify the micropore volume.

A kinetic study on the formation of porous nanoparticles resulted in the dependency on the concentration of potassium persulphate and sodium dodecylsulphate being calculated together with a value of  $n$  for comparison with the Smith – Ewart theory.

The kinetics of the polymerisation of styrene using various redox couple ratios for initiation and different surfactants has been studied by dilatometry to optimise initiation efficiency and to produce hydrolysis resistant strong acid sulphonate functionality.

Amine functionalisation of both styrene and porous nanoparticles with chitosan has been achieved and the catalytic potential of redox initiated

porous nanoparticles in latex polymer film for the hydrolysis of ethyl formate has been examined and shown to be viable.

## **Acknowledgements**

I would sincerely like to thank Dr John Hearn for his supervision over the past three years; I would also like to express my gratitude to Dr Stuart Brewer and Dr Corinne Stone from DSTL for funding and advice throughout the course of my period of study. Thanks are also due to Mr Arthur Richards and Dr Fran Kapowicz for advice, patience and for keeping my feet on the ground. Finally I must thank my partner Lisa for her encouragement and tolerance.

Abstract.....	3
Acknowledgements.....	5
1.0. Introduction.....	10
1.1 Aims and Objectives.....	12
1.2 Emulsion Polymerisation.....	13
1.2.1 Basic Ingredients.....	13
1.2.2 The Emulsion Polymerisation Process.....	14
1.2.3 Characteristics of Emulsion Polymerisation in the Presence of Surfactant.....	15
1.2.4 Emulsifier Free Emulsion Polymerisation.....	18
1.2.5 Kinetics of Emulsion Polymerisation.....	20
1.2.6 The Smith-Ewart Equation.....	21
1.2.6.1 Derivation of The Smith-Ewart Equation.....	22
1.2.6.2 Case 1: $n \ll 1$ .....	23
1.2.6.3 Case 2: $n \approx 0.5$ .....	23
1.2.6.4 Case 3: $n > 1$ .....	24
1.2.7 Initiator Systems for Emulsion Polymerisation.....	24
1.2.7.1 Persulphate.....	24
1.2.7.2 Redox initiation.....	26
1.2.7.2.1 Redox initiation Reactions.....	27
1.2.7.2.1.1 Persulphate Activation.....	27
1.2.7.3 Effect on Initiator Decomposition from Emulsion Polymerisation Constituents.....	29
1.2.7.3.1 Effect of Surfactant.....	29
1.2.7.3.2 Effect of Monomers and Other Oxidisable Species.....	30
1.3 Cleaning Techniques for Polymer Colloids.....	30
1.3.1 Dialysis.....	31
1.3.1.1 Conventional Dialysis.....	31
1.3.2 Ion Exchange.....	32
1.3.3 Steam Stripping.....	33
1.3.4 Centrifugation / Decantation.....	34
1.3.5 Microfiltration / Serum Exchange.....	34
1.4 Styrene/Divinylbenzene Copolymers.....	35
1.4.1 Introduction.....	35
1.4.2 Pore Development in Styrene / Divinylbenzene Resins via Suspension Polymerisation.....	39
1.4.2.1 Pore Formation.....	39
1.4.3 Non-Solvating Porogen.....	44
1.4.4 Solvating Porogen.....	46
1.5 Chitin and Chitosan.....	47
1.5.1 Discovery of Chitin and Chitosan.....	49
1.5.2. Occurrence of Chitin and Chitosan in Nature.....	49
1.5.2.1 Chitin in Lower Plants.....	50
1.5.2.2 Chitin in Animals.....	50
1.5.3. Morphology of Chitin.....	51
1.5.4. Isolation of Chitin.....	52
1.5.5. Preparation of Chitosan.....	52
1.5.6. Degree of N-acetylation in Chitin and Chitosan.....	53
1.5.7. Methods for Determining the Degree of N-Acetylation of Chitin and Chitosan.....	54

1.5.7.1. Colorimetric Techniques.....	54
1.5.7.1.1. Dye Adsorption.....	54
1.5.7.1.2. Metachromatic Titration .....	54
1.5.7.1.3. Residual Salicylaldehyde .....	55
1.5.7.2 Titrimetric Techniques.....	55
1.5.7.3 Spectrophometric Techniques.....	55
1.5.7.3.1 UV Spectroscopy.....	55
1.5.7.3.2 IR Spectroscopy.....	56
1.5.7.4 Gas Chromatographic Techniques .....	56
1.5.7.5 NMR Spectroscopy.....	57
1.5.8 Adsorption of Metal Ions by Chitin and Chitosan .....	57
2 Instrumental Techniques and Background Theory .....	59
2.1 Surface Area and Pore Size Analysis Using Adsorption.....	59
2.1.1 Introduction.....	59
2.1.2 Adsorption Isotherms .....	60
2.1.3 Surface Area and The BET Equation .....	68
2.1.4. Pore Analysis by Adsorption .....	73
2.1.5. Adsorption by Non-Porous Solids.....	75
2.1.6. Adsorption by Microporous Solids .....	75
2.1.7. Adsorption by Mesoporous Solids .....	76
2.1.8 Quanasorb Surface Area Determination .....	76
2.2 Photon Correlation Spectroscopy.....	77
2.2.1 Diffusion and the Stokes-Einstein Equation.....	78
2.3 Pore Size Distribution.....	81
3.0 Experimental .....	87
3.1 Materials .....	87
3.1.1 Polymerisation Materials .....	87
3.1.2 Additives .....	87
3.1.3 Water.....	88
3.1.3 Gases.....	88
3.1.4 Chitosan .....	88
3.1.5 Jeffamine D2000 .....	88
3.2 Latex Preparation .....	88
3.2.1 Shaken Polymerisation .....	89
3.2.2 Stirred Polymerisation .....	91
3.2.3 Dilatometry .....	92
3.3 Cleaning.....	96
3.3.1 Continuous Liquid / Liquid Extraction.....	97
3.3.2 Steam Distillation.....	98
3.2.3 Dialysis .....	98
3.3 Drying.....	99
3.4 Latex Characterisation.....	99
3.4.1 Particle Size Determination .....	99
3.4.1.1 Photon Correlation Spectroscopy.....	99
3.4.1.2 Electron Microscopy.....	100
3.4.2 Surface Area Determination.....	100
3.4.3 Nitrogen Adsorption / Desorption Isotherms.....	102
3.4.4 Nonane Preadsorption.....	103
3.5 Chitosan Characterisation.....	104
3.5.1 Molecular Weight Determination.....	104

3.5.2 Determination of the degree of <i>N</i> -acetylation.....	106
3.5.2.1 Purification of CI Acid Orange 7.....	106
3.5.2.2 Determination of the degree of <i>N</i> -acetylation by Dye Adsorption.....	107
3.6 Vapour Adsorption.....	108
3.7 Functionalisation of particles with chitosan.....	110
3.7.1 Polymerisation in the Presence of Chitosan.....	111
3.7.2 Post Polymerisation Coating of Particles with Chitosan.....	111
3.8 Characterisation of Chitosan Containing Latices.....	112
3.8.1 Infrared Spectroscopy.....	112
3.8.2 Dye Adsorption.....	113
3.9 Conductometric titration.....	114
3.10 Films.....	114
3.11 Hydrolysis of Ethyl Formate.....	115
4.0 Results and Discussion.....	116
4.1 Porous Latex Nanoparticles.....	116
4.1.1 Introduction.....	116
4.1.2 Effect of initiator Concentration.....	117
4.1.2.1 Potassium Persulphate.....	117
4.1.2.2 Redox Initiator.....	119
4.1.2.3 Oil Soluble Initiators.....	121
4.1.3 Effect of surfactant concentration.....	122
4.1.3.1 Polymerisation in the presence of Sodium Dodecylsulphate.....	122
4.1.3.2 Emulsifier Free Polymerisation.....	124
4.1.4 Effect of Porogen Concentration and Type.....	125
4.1.4.1 Toluene.....	125
4.1.4.2 Xylene.....	127
4.1.4.3 Heptane.....	129
4.1.4.4 Comparison Between Solvating and Non Solvating Porogen.....	131
4.1.4.5 Linear Polymeric Porogen.....	132
4.1.5 Monomer Ratio.....	133
4.1.5.1 Persulphate Initiated Porous Nanoparticles.....	133
4.1.5.2 Redox Initiated Porous Nanoparticles.....	138
4.1.6 Effect of Temperature.....	139
4.1.7 Effect on Surface Area of Cleaning Technique.....	142
4.1.8 Pore Size Analysis.....	145
4.1.8.1 Introduction.....	145
4.1.8.2 Pore Size Distribution – Effect of Porogen.....	146
4.1.8.2.1 Toluene.....	147
4.1.8.2.2 Xylene.....	150
4.1.8.2.3 <i>n</i> -Heptane.....	153
4.1.8.3 Pore Size Distribution – Effect of Cross-Linker Concentration.....	155
4.1.8.3.1 Persulphate Only Porous Nanoparticles.....	156
4.1.8.3.2 Redox Initiated Porous Nanoparticles.....	158
4.1.8.3.3 Pore Size Distribution of Porous Nanoparticles Produced With a Redox couple – Effect of Monomer Ratio.....	162
4.1.8.3.4 XAD-4.....	164
4.1.8.4 Nonane Preadsorption.....	166
4.1.9 Vapour Adsorption by Porous Nanoparticles.....	168
4.1.9.1 Methanol Adsorption.....	169
4.1.9.2 Pentane Adsorption.....	173

4.1.9.3. Toluene Adsorption .....	176
4.2 Kinetics of Polymerisation.....	180
4.2.1 Kinetics of Styrene Polymerisation Using a Redox Couple Initiator.....	180
4.2.1.1 Sodium Dodecylsulphate .....	181
4.2.1.2 Aerosol OT.....	186
4.2.1.3 Igepal .....	188
4.2.2 Porous Nanoparticles.....	191
4.2.2.1 Kinetic Study By Dilatometry.....	191
4.2.2.2 Kinetic Study By Gravimetric Method.....	193
4.2.2.3 Rate Dependence on Divinylbenzene Concentration .....	197
4.3 Reactive particles .....	200
4.3.1 Introduction.....	200
4.3.2 Redox Initiated Porous Nanoparticles .....	200
4.3.3 Catalysis of Ethyl Formate by Redox Initiated Porous Nanoparticles.....	203
4.4 Chitosan Functionalisation .....	204
4.4.1 Chitosan Functionalised Solid Polystyrene .....	205
4.4.2 Chitosan Functionalised Spheres Produced Using Jeffamine D2000 .....	205
4.4.3 Chitosan Functionalised Solid Polystyrene Without Jeffamine D2000 .....	209
4.4.4 Chitosan Functionalised Porous Nanoparticles.....	211
5.0 Conclusions.....	214
6.0 Further Work.....	217
References.....	218

## **1.0. Introduction**

The use of polymers as supports for chemical reagents and for catalysts offers the prospect of cleaner and greener chemistry. Toxic, noxious and corrosive species are much safer to handle when immobilised on a polymeric support and expensively synthesised reagents and metal complexes are much easier to recover<sup>1</sup>.

Recently truly colloidal sized porous latex particles of poly(styrene) co-divinylbenzene have been prepared for the first time by emulsion polymerisation<sup>2</sup>

Much work has been carried out on coarse macroreticular resin beads that have found applications as ion exchange resins and as packing for chromatography columns<sup>3</sup>, however the activity of these resins is restricted, in part because of external mass transfer and intra-particle diffusion to the active sites<sup>4,5</sup>. The activity of non-porous polymer beads will increase as the particle diameter decreases due to the specific surface area (the surface area of 1 g) being inversely proportional to the particle diameter. Colloidal sized polymer particles such as latex particles are attractive due to their high specific surface area and their ability to concentrate organic reactants in the catalytic phase by adsorption from water<sup>6</sup>. Processes utilising aqueous colloidal dispersions instead of volatile organic solvents would also limit the need for solvent recovery and associated disposal problems.

Functionalised latex particles have proved to be viable catalysts for a variety of hydrolysis and oxidation reactions in which a high electrolyte concentration is not a requirement<sup>7</sup>. Several functional groups have been

employed, these include sulphonic acids<sup>8</sup>, primary amines<sup>9</sup> and imidazoles<sup>10</sup> for use in ester hydrolysis and cobalt complexes for autoxidation of organic compounds<sup>11,12,13,14</sup>.

Colloidal sized particles are much harder to recycle than large beads, needing to be both coagulated and redispersed or ultrafiltered<sup>7</sup>. Also under the usual conditions of phase transfer catalysis, charged particles are impractical due to rapid coagulation in the presence of electrolyte<sup>15</sup>. These disadvantages to the use of colloidal sized latex particles may be overcome if the functionalised latex is presented in the form of a film rather than an aqueous dispersion. Thin polymer films have for example been shown to offer better mechanical strength as well as improved chemical and temperature stability than soft gels such as alginate or polyacrylamide when used with trapped and immobilised viable microbial cells in biocatalytic applications<sup>16</sup>

## **1.1 Aims and Objectives**

The aims of the current work are:

To develop a novel cross-linking co-polymerisation reaction in order to produce a colloiddally stable dispersion of porous nanoparticles having specific surface areas approaching those of commercially available activated carbons for potential use in military protective clothing and respirators. Such dispersions could be simply blended with film forming latex binders and applied to textile binders and filter supports.

To produce the highest possible surface areas the effects of the reaction ingredients will be systematically investigated. Initiator concentration and type, surfactant concentration and type, porogen concentration and type, ratio of vinyl and divinyl monomers and temperature will all be investigated, as well as the most effective cleaning technique for removing post reaction contaminants such as porogen, residual unreacted monomer, low molecular weight polymer and surfactant .

To introduce functionality into the surface of polymer nanoparticles with a view to use as catalysts to decompose toxic chemicals rather than just adsorb them to improve handling and disposal problems. Redox initiator systems are to be used to introduce anionic functionality and protonated chitosan used for amine functionality.

To use the polymer nanoparticles supported in a binder film to evaluate, in a safe model system, the potentiality of catalysed surface reactivity in polymer latex films.

## **1.2 Emulsion Polymerisation**

Emulsion polymerisation has become a widely used process for the manufacture of synthetic latices since its first inception on an industrial scale in the mid 1930's<sup>17</sup>. Today polymer latices find applications in a wide range of industrial products such as synthetic rubber, paper coatings, high impact polymers, latex paints, adhesives and barrier coatings to name but a few. Polymer latices have also been used in a wide variety of more specialist areas such as diagnostic tests, immunoassays, drug delivery systems, size calibration standards and chromatography.

### **1.2.1 Basic Ingredients**

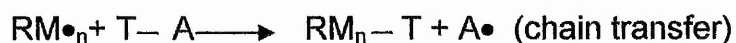
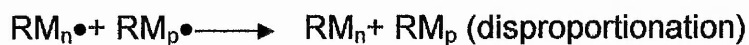
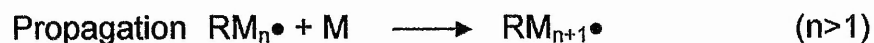
Emulsion polymerisation is a free radical initiated chain polymerisation in which a monomer or a mixture of monomers is polymerised in the presence an aqueous solution of surfactant to form the product known as a latex. Latex is defined as a colloidal sized dispersion of polymer particles in an aqueous medium.

The main ingredients included in an emulsion polymerisation are: water, monomer(s), initiator, surfactant and in certain circumstances chain-transfer agents.

### **1.2.2 The Emulsion Polymerisation Process**

The process of emulsion polymerisation can be divided into three stages, these are initiation, propagation and termination.

Initiation begins with the thermal decomposition of the initiator to form free radicals. The propagation step follows when the free radicals quickly react with a monomer unit to form a monomer radical. These monomer radicals continue to add further monomer units to form a growing polymeric radical. Termination can be brought about in one of three ways, these being 1) Combination: When two growing polymeric radicals combine to form one polymer molecule. 2) Disproportionation: A hydrogen atom is abstracted from one growing chain by another leading to the formation of two polymer molecules. 3) Chain transfer: When a polymeric radical abstracts a hydrogen atom from a molecular fragment, resulting in a dead polymer molecule and a new radical. This radical can then go on to react with a monomer molecule and initiate a new polymeric radical. These processes can be represented schematically:



Scheme 1.

### **1.2.3 Characteristics of Emulsion Polymerisation in the Presence of Surfactant**

Possibly the most important feature of emulsion polymerisation is its heterogeneity from the beginning of the process to the end. At the beginning when the monomer(s), water and surfactant(s) are mixed together, the surfactant molecules form micelles with the hydrophobic cores swollen with monomer. The diameter of these micelles is in the order of 5-15 nm<sup>18</sup>. The bulk of the monomer exists in the form of large emulsion droplets which have surfactant molecules adsorbed on the surface. The diameter of these

monomer droplets is in the order of 1-10  $\mu\text{m}$ . A schematic representation of the phases involved in the emulsion polymerisation process is shown in Fig. 1.

On addition of the initiator to the reaction mixture, initiator radicals are formed; these radicals then go on to form oligoradicals by reacting with the small amount of monomer that is dissolved in the aqueous phase. The oligoradicals become surface active when they are 3-5 repeat units long and become capable of dynamic exchange with the surfactant molecules in micelles. This is the point at which particle nucleation begins. Once the radical enters a micelle the radical continues to grow, forming polymer particles that swell with monomer via diffusion from the monomer droplets. The radical will continue to grow until a further radical enters the micelle causing termination. These monomer swollen polymer particles then become the main sites for further propagation to take place that results in particle growth. The growing particle is stabilised by the redistribution of the surfactant molecules from any micelles that have not been initiated and from the diminishing monomer droplets. The polymerisation is complete when all the monomer is converted to polymer. This results in a dispersion of sub-micron polymer spheres stabilised mainly by an adsorbed layer of surfactant molecule end groups.

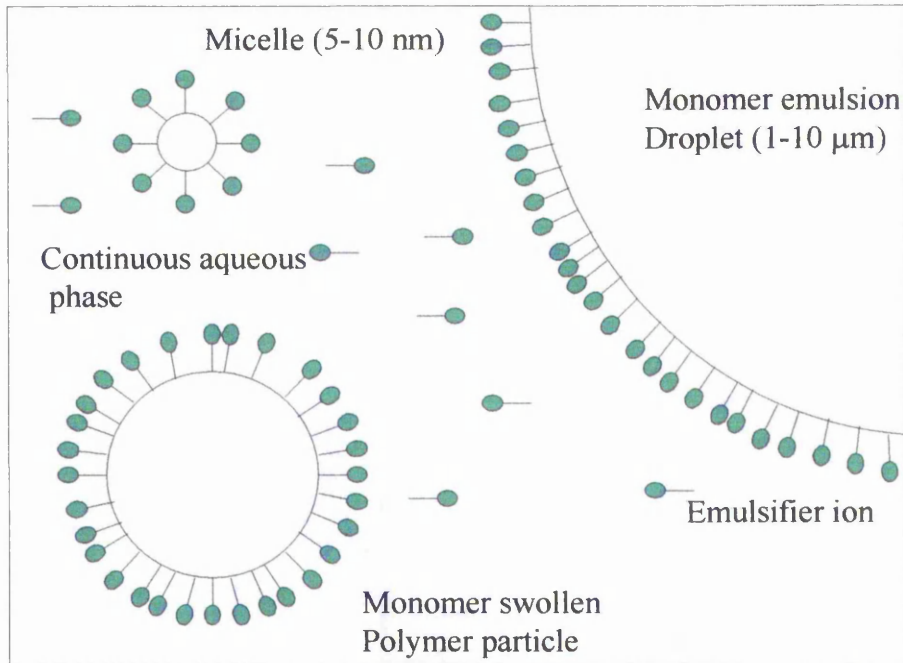


Fig. 1.1 Schematic diagram of the phases involved in an emulsion polymerisation

The final properties of the particle can be controlled at a given temperature by either varying the concentration of the initiator or the concentration of the surfactant. Varying these two parameters causes a change in the number of nucleated micelles in the early stages of polymerisation and therefore the number of growing polymer particles. Increasing the initiator concentration leads to an increase in the number of free radicals available for adsorption into micelles, and this leads to an increase in the number of nucleated micelles. This in turn leads to an increase in the number of growing polymer particles which compete for the available monomer, resulting in an increase in the reaction rate and a decrease in particle size. Increasing the surfactant concentration has a similar effect by increasing the number of micelles available for nucleation which leads to an increase in the number of growing particles, an increase in the rate of reaction and a decrease in particle size.

Smith and Ewart produced a quantitative treatment of emulsion polymerisation<sup>19</sup> and it was shown that the number of particles formed was proportional to the initiator concentration to the power of 0.4 and to the surfactant concentration to the power 0.6. This has been confirmed experimentally to be the case for monomers with limited water solubility such as styrene.

#### **1.2.4 Emulsifier Free Emulsion Polymerisation**

Matsumoto and Ochi<sup>20</sup> first described surfactant free emulsion polymerisation for producing monodisperse polystyrene latex in 1965. It derived from conventional emulsion polymerisation but the reaction was carried out in the absence of any added emulsifier. The lower particle number density resulting from the lack of stabilising surfactant is less attractive commercially than conventional emulsion polymerisation, but from an academic point of view being able to produce monodisperse model colloids with well characterised surface properties is of great interest.

Several mechanisms for the formation of stable latices in the absence of added surfactant have been proposed. These include, homogenous nucleation<sup>21, 22</sup>, oligomer "micellisation"<sup>23</sup> and coagulation<sup>24, 25</sup>.

Studies carried out on the surfactant free polymerisation of styrene initiated by potassium persulphate in an aqueous continuous phase<sup>23</sup> showed the presence of styrene oligomers in the nucleation stage of the reaction. Nuclei are formed by the aggregation of oligomers until the particles reach a sufficient charge density for stability in line with the DLVO theory of colloidal

stability<sup>26</sup>. The rate of aggregation follows second order kinetics, thus in the early stage there is a rapid decrease in the particle number density. The Fuchs' ratio  $W$  increases as the surface charge density increases and the rate of coagulation tends toward zero. At this point a constant number density is reached and the polymerisation continues as in a conventional emulsion polymerisation. The final particle size can be controlled by use of the equation<sup>27</sup>

$$\text{Log}D = 0.238 \left( \frac{\text{Log}[I][M]^{1.723}}{[P]} + \frac{4929}{T} \right) - .827$$

where:

$I$  = Ionic Strength

$[P]$  = Persulphate initiator concentration

$[M]$  = Monomer concentration

$T$  = Temperature (K)

This relationship means that higher temperatures and higher initiator concentrations result in a greater number of smaller particles, this in turn means higher charge densities are reached more rapidly, which leads to polymers with lower molecular weights. High ionic strengths therefore favour fewer larger particles and increased monomer concentrations allow particles to grow to a larger size.

Colloidal stability for polymer latices prepared by a surfactant free method is provided by electrostatic repulsion between the like charged end groups of the polymer chains at the particle surface<sup>28</sup>

### **1.2.5 Kinetics of Emulsion Polymerisation**

Studies on the kinetics of emulsion polymerisation are normally focused on the determination of the rate of polymerisation and its dependence on the parameters of polymerisation, such as initiator type and concentration, surfactant type and concentration, the type of monomer or monomers in copolymerisation and the temperature.

The usual experimental approach is to determine the percentage conversion against time curve by varying the individual parameters. A typical conversion versus time plot is illustrated in Fig. 2. It can be seen that there are three distinct regions marked I, II and III corresponding to the three stages of polymerisation.

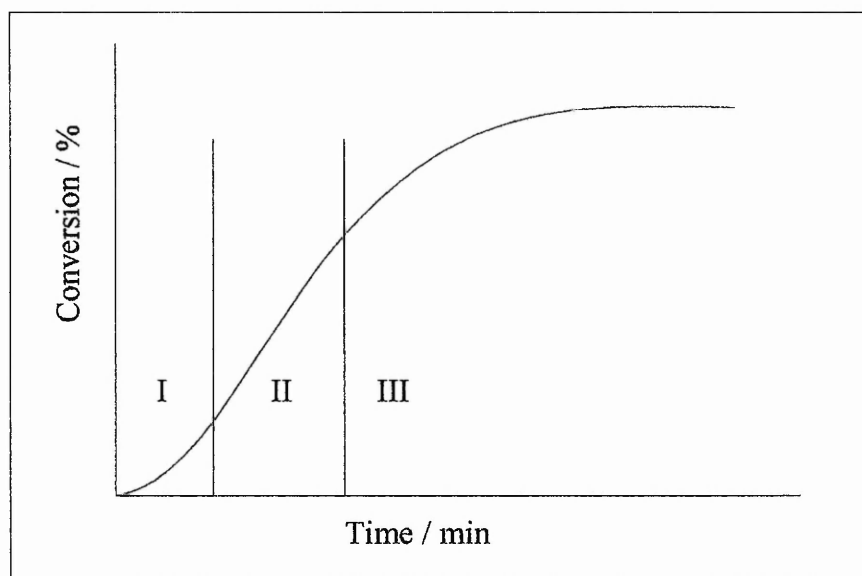


Fig. 1.2. Typical conversion versus time plot showing the three distinct regions

Region I corresponds to the initial stage of the nucleation of particles. The system is characterised by the presence of monomer-swollen micelles, monomer droplets and nucleated particles. This stage usually corresponds to a monomer conversion of 0-10 %. This region shows an increasing rate of conversion due to the generation of free radicals from the decomposition of the initiator, the number of nucleated particles increases leading to more sites for polymerisation and ultimately to an increase in the rate of conversion. Region II begins when particle nucleation is complete. This region is characterised by the absence of surfactant micelles, a constant number of polymer particles swollen with monomer, a constant concentration of monomer within the growing particles and an increase in particle size. The rate of conversion in this region is constant and usually corresponds to a monomer conversion of 10-40 %. Region III begins when all of the monomer droplets have been depleted and the remaining monomer is confined to the swollen polymer particles. This region is characterised by a constant number of polymer particles and decreasing monomer concentration within those particles. As the monomer concentration within the particles decreases the rate of conversion also decreases. This final region usually corresponds to a monomer conversion of 40-100 %.

### **1.2.6 The Smith-Ewart Equation**

The Smith-Ewart equation was devised in 1948<sup>29</sup> in a quantitative treatment on the work carried out by Harkins<sup>30</sup>. They managed to obtain an

equation for the particle number as a function of the surfactant concentration and initiation and polymerisation rates.

### **1.2.6.1 Derivation of The Smith-Ewart Equation**

If we consider a system of  $1 \text{ dm}^3$  of aqueous phase in which  $N$  particles of latex are dispersed, each particle has a volume of  $v$  and an interfacial area of  $a$ . As free-radicals are generated they are captured by the particles at a rate  $\rho_a$ . The increase in the number of radicals  $n$  in the particles with time is given by:

$$\frac{dn}{dt} = \rho_a \quad 1.1$$

The molecular concentration within a particle is given by:

$$n/v$$

And the molecular concentration of radicals with which any of the  $n$  radicals within the particle may react is given by:

$$(n-1)/v$$

The molecular termination rate coefficient  $k'_t$  is given by:

$$k'_t = N_A k_t \quad 1.2$$

Where  $k_t$  is the molar termination constant. Thus the rate at which the number of radicals decreases by mutual termination is given by:

$$-dn/dt = 2 k'_t n[(n-1)/v] \quad 1.3$$

Radicals may also leave the particles and go into the aqueous phase (subsequent to a transfer reaction). This depends on their concentration and the interfacial area of the particle. This process is characterised by the molecular rate coefficient  $k'_d$  and so:

$$-dn/dt = k'_d a(n/v) \quad 1.4$$

therefore the number of latex particles,  $N_0, N_1, N_2, \dots, N_n$  which contain 0, 1, 2, .....n radicals respectively will, under steady state, be given by:

$$N_{n-1} \rho_a + N_{n+1} k'_d a[(n-1)/v] + N_{n+2} k'_t [n+2](n+14)/v = N_n \rho_a + k'_d a(n/v) + k'_t n[(n-1)/v] \quad 1.5$$

Smith and Ewart discussed three limiting cases, these being 1)  $n \ll 1$ , 2)  $n \approx 0.5$  and 3)  $n > 1$ .

### **1.2.6.2 Case 1: $n \ll 1$**

Smith-Ewart case 1 kinetics apply when the rate at which a radical is transferred from the polymerisation loci via diffusion is much greater than the rate at which the radicals are captured from the aqueous phase

### **1.2.6.3 Case 2: $n \approx 0.5$**

Smith-Ewart case 2 kinetics apply if there is no readily available mechanism for the activity of a growing radical to be transferred from the polymerisation loci back into the aqueous phase, and that mutual termination

of the propagating centre occurs almost instantaneously when a second radical is adsorbed by the locus.

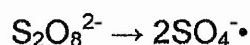
#### **1.2.6.4 Case 3: $n > 1$**

Smith-Ewart case 3 kinetics apply if radicals can enter the polymerisation loci more rapidly than they can be destroyed by mutual termination. Hence in this situation it is possible to have more than one propagating polymer chain in each polymerisation locus as the growing particles are large enough to accommodate more than one radical without termination occurring.

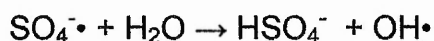
### **1.2.7 Initiator Systems for Emulsion Polymerisation**

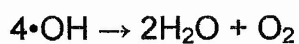
#### **1.2.7.1 Persulphate**

The use of persulphates for initiating emulsion polymerisation is widespread; Kolthoff and Miller<sup>31</sup> studied the decomposition of potassium persulphate in oxygen 18 enriched water at different pH levels. At acid pH it was found that all the oxygen produced came from the decomposition of the persulphate, whereas under alkaline conditions the oxygen came from the water. The reaction scheme as proposed by these workers is:

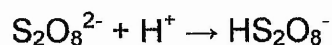


Uncatalysed





Acid Catalysed



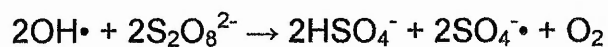
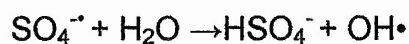
Dilute Acid



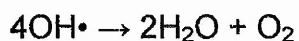
Strong Acid



Work carried out by Bartlett and Cotmann<sup>32</sup> studied the kinetics of the uncatalysed reaction and proposed the following alternative chain mechanism:



Whilst Fronaeus and Ostman<sup>33</sup> suggested:



In both of the studies performed by Kolthoff and Miller<sup>31</sup> and by Froneaus and Ostman<sup>33</sup> the rate of decomposition in alkaline conditions was independent of ionic strength, however under acid conditions there was a negative salt effect.

### **1.2.7.2 Redox initiation**

A redox couple consists of two components, these being an initiator (oxidant) and an activator (reductant). The discovery that such a system could be used to initiate emulsion polymerisation was made independently by Bacon<sup>34</sup> and by Evans *et al.*<sup>35</sup> in 1940.

There are several significant features involved in the initiation of emulsion polymerisation using a redox couple, these being:

- The induction period is very short
- The comparative rate at which high yields of high molecular weight polymer can be achieved is much faster
- Small activation energy

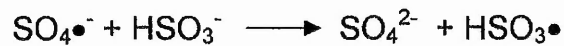
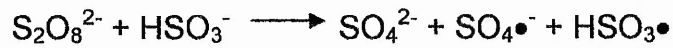
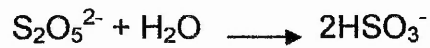
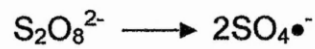
- Polymerisation can be initiated and maintained at a satisfactory rate at low temperatures.

### **1.2.7.2.1 Redox initiation Reactions**

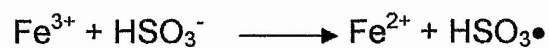
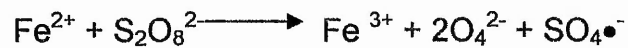
#### **1.2.7.2.1.1 Persulphate Activation**

The use of persulphates for the initiation of emulsion polymerisation both alone and with activators is extensive. Bacon was able to activate persulphates using a range of reducing agents which include metals, oxidisable metal salts, hydroxylamine, hydrazine, hydrogen sulphide, thiols, sulphates, dithionite, thiosulphates and polyhydric phenols. The kinetics of polymerisation initiated by  $\text{Fe}^{2+}$  ion activated persulphate was studied by Bury and Peterson<sup>36</sup> and Fordham and Williams<sup>37</sup>. Other activators for persulphates include ferricyanide<sup>38</sup>, however these systems are very complex as multivalent metal ions are capable of initiating polymerisation without the need for peroxide substances. Two of the most widely exploited redox couples are persulphate / thiol and persulphate / bisulphite. Some metal anions can act as promoters in these two component system, such as  $\text{Fe}^{2+}$ ,  $\text{Cu}^{2+}$ .

Although this system of initiating emulsion polymerisation was patented as early as 1940<sup>39</sup>, there are still aspects of the system which are not fully understood<sup>40</sup> particularly with regard to the relative proportions of oxidant and reductant required. The key reaction thought to be involved in the thermal initiation process for the potassium persulphate / sodium bisulphite system is<sup>41</sup>:



If trace metals are present in the feed water then further promotion of initiator decomposition can occur<sup>42</sup>, e.g.



Although both Morgan and Whitby *et. al.*<sup>43</sup> have suggested initiation by hydroxy radicals.

### **1.2.7.3 Effect on Initiator Decomposition from Emulsion Polymerisation**

#### **Constituents**

##### **1.2.7.3.1 Effect of Surfactant**

Kolthoff and Miller<sup>31</sup> showed that the decomposition of persulphate was significantly effected by the presence of fatty acid soaps. They observed that the rate of decomposition was greater in the presence of soap, a four fold increase in the rate was observed with potassium laurate at 323 K. The persulphate oxidised the soap causing decarboxylation. In a further series of studies by Ivanchoff and Yurzhenko<sup>44</sup> the rate of initiator decomposition and the rate of polymerisation of styrene was examined in the presence of a series of fatty acid soaps from formate to palminate, they reported that the rates of decomposition and of polymerisation were directly proportional. Morris and Parts<sup>45</sup> found that for polymerisations carried out in the presence of sodium dodecylsulphate and sodium hexadecylsulphate the rate at which the persulphate ions disappeared increased, whereas if polymerisation was carried out in the presence of a fully fluorinated anionic surfactant there was no apparent change in the rate of decomposition. They did not feel that the enhanced rate of decomposition contributed to initiation. Friend and Alexander<sup>46</sup> examined the polymerisation of water soluble monomer in the presence of sodium dodecylsulphate at concentrations above and below its CMC. They found that the rate of polymerisation was not effected by the concentration in the reaction mixture. Allen<sup>47</sup> also studied the effect of sodium dodecylsulphate concentration below the CMC with methyl methacrylate and

ammonium persulphate and observed constant persulphate efficiency across the range studied.

#### **1.2.7.3.2 Effect of Monomers and Other Oxidisable Species**

Limited studies have been carried out on the effect of monomers and other oxidisable compounds present in emulsion polymerisation reaction mixtures. Sturzenhofecker<sup>48</sup> reported that the rate of persulphate decomposition was accelerated in the presence of hydrocarbons such as styrene, toluene and ethylbenzene, and a similar increase was observed by Vanderhoff for *n*-octane and benzene.

### **1.3 Cleaning Techniques for Polymer Colloids**

In the study of polymer colloids it is important to have well characterised products. An important part of producing model colloids for study is to ensure adequate cleaning of the latex<sup>49</sup>. The cleaning process must be capable of removing any impurities from the bulk polymer and also from the suspending media (in most cases water). This must be achieved without affecting the nature of the latex i.e. particle size, functionality (surface group nature and concentration) and particle morphology.

The most commonly studied model colloids are polystyrene latices and the major impurities encountered are unreacted monomer, low molecular weight oligomers, thermally polymerised material, by-products from the monomer (benzaldehyde, formaldehyde and benzoic acid from styrene), by-products

from the initiator ( $K^+$  and  $H_2SO_4$  from potassium persulphate), emulsifier, pH buffers, inhibitors, dissolved atmospheric gases (e.g.  $CO_2$ ), bacteria and fungal spores and material leached from reaction vessels and containers.

Several methods for cleaning polymer colloids have been employed, dialysis and ion exchange have been used for many years, but these techniques have been shown to have problems associated with them. This has led to the development of other techniques that include, hollow fibre dialysis<sup>50</sup>, steam-stripping<sup>51, 52</sup>, serum exchange<sup>53</sup>, centrifugation / decantation<sup>54</sup>, ultrafiltration<sup>55</sup>, diafiltration<sup>56</sup> and microfiltration<sup>57</sup>.

The ease with which impurities are removed from colloidal suspension varies greatly, for example electrolytes can be readily removed by conventional dialysis or ion-exchange but unreacted styrene monomer is only removed very slowly by these techniques.

### **1.3.1 Dialysis**

#### **1.3.1.1 Conventional Dialysis**

Conventional dialysis is the most widely used technique for the cleaning of model colloids<sup>58</sup>. This is a slow process that relies on the concentration gradient across the membrane as its driving force and can take several weeks to complete. As the concentration of the impurities decrease so the concentration gradient decreases and so with low levels of impurities removal by dialysis is very slow. Dialysis also uses a large amount of water, typically around twenty changes at a latex to water ratio of about 1:20. For efficient

removal the impurities must be readily soluble thus poorly soluble non-ionic materials will be removed very slowly.

Other problems encountered with the dialysis technique arise from the tubing material itself, there is a possibility of material, weak acid sulphur compounds, leaching from the dialysis tubing and over the protracted times associated with the technique post reaction changes and contamination (such as bacterial) can occur. The removal of unreacted monomer, oligomeric material and reaction by-products is also not fully achieved with conventional dialysis. Dialysis in conjunction with another cleaning process is still the most widely used technique.

#### **1.3.1.2 Hollow Fibre Dialysis**

Hollow fibre dialysis is a much more rapid technique, the time taken to reach equilibrium is usually hours instead of weeks, but the amount of water required is significantly greater. In hollow fibre dialysis water is circulated through the system at approximately  $40 \text{ cm}^3 \text{ min}^{-1}$  this means that in excess of 30 litres of water is required to clean 100ml of latex. There is also the chance of significant metal cation exchange even when ultra pure Analar water is used.

#### **1.3.2 Ion Exchange**

A technique for the use of ion exchange for the cleaning of polymer latices was first proposed by Vanderhoff and co-workers<sup>59</sup>. It was necessary for a procedure to be developed for highly efficient purification of the resin as

Schenkel and Kitchener<sup>60</sup> had previously reported that the use of ion exchange should be discouraged due to possible leaching of polyelectrolyte contaminants from the resin onto the polymer surface, this could lead to an alteration of the surface charge on the latex, possibly even charge reversal.

Although Vanderhoff and co-workers have carried out a large amount of work using ion exchange resins to clean polymer latices<sup>61, 62, 63</sup> other workers have encountered severe difficulties when working with these materials.

Ion exchange resins are very effective at removing ionic materials and surface-active species but are significantly less effective in removing polyelectrolytes and unreacted monomer. A further complication in the use of ion exchange resins is the intimate contact made between the resin beads and the latex particles, making the possibility of contaminant exchange very high, also a proportion of the latex particles will be left adhering to the resin beads which may lead to a shift in the particle size distribution if the latex is not monodisperse.

### **1.3.3 Steam Stripping**

The use of steam stripping to remove unreacted monomer and low molecular weight oligomer is a widely used commercial process and can be easily achieved in the laboratory. Although steam stripping is the most efficient method for the removal of these impurities it is not effective in the removal of surface-active species or polyelectrolytes and should therefore be used in conjunction with another cleaning technique such as dialysis or microfiltration.

### **1.3.4 Centrifugation / Decantation**

This is a very simple technique that has been applied by several groups<sup>64</sup>,<sup>65</sup>,<sup>66</sup> and involves centrifuging the polymer latex at high spin speeds (approx. 25 000 rpm for 45 min.). The supernatant can then be decanted and fresh water added and the process repeated until the conductance and surface tension correspond to that of pure water. The latex can also be acid washed in situ to ensure complete protonation of the surface groups.

The primary disadvantage of this technique is the problem of redispersion of the latex. After cleaning latices that have only a small amount of stabilising surface groups are likely to be irreversibly coagulated, and even those that have a high concentration of stabilising groups may need to be subjected to long periods of vigorous redispersion by ultrasound to redisperse satisfactorily.

### **1.3.5 Microfiltration / Serum Exchange**

In this technique as in dialysis a semi-permeable membrane is used to retain the latex. However whereas in dialysis transfer across the membrane is dependant on the concentration gradient, in microfiltration techniques hydrostatic pressure is employed to force the aqueous phase (serum) through the membrane whilst pure water is fed in to replenish the lost serum.

Microfiltration shows several distinct advantages over other cleaning methods. It avoids the long preparation times associated with ion exchange techniques and is much more efficient at the rapid removal of surface active materials than dialysis, also the quantities of water used are much reduced

compared to dialysis. Unreacted monomer can also be effectively removed. Acid washing of the latex to ensure full protonation can also be carried out using this technique.

The main disadvantage associated with this technique is filter clogging, it is therefore essential to maintain an adequate degree of mixing to prevent forced sedimentation of the latex particles leading to blocking of the filter pores.

## **1.4 Styrene/Divinylbenzene Copolymers**

### **1.4.1 Introduction**

The first results to be published on the copolymerisation reaction of styrene with divinylbenzene were those of Staudinger in 1935<sup>67</sup>. He reported that in the copolymerisation, even with only small quantities of the difunctional monomer, a polymer was produced that was insoluble in solvents. He concluded that this was due to a three-dimensional polymer network being formed in which the divinylbenzene molecules cross-linked with polystyrene chains. This led to applications that exploited this insolubility of these new copolymers. It was through the work of D'Alelio<sup>68</sup> however who used sulphonation to produce the first cationic exchanger that the styrene/divinylbenzene copolymer became of technical importance<sup>69</sup>. Further research into the copolymerisation of styrene with divinylbenzene finally revealed that varying the ratio of the monomers was not sufficient to be able to produce enough variation in the ion-exchange properties to satisfy needs.

This led to the development of macroporous structures. The basis of pore production is the copolymerisation of styrene with divinylbenzene in the presence of an inert component, which can subsequently be removed from the final product, thus leaving a porous structure. The inert compound, which must not polymerise or be permanently incorporated into the polymer network, must be soluble or miscible with the monomer. It is also important that it is insoluble or sparingly soluble in water so that it does not partition into the aqueous phase.

These copolymers are now used extensively in a number of chemical applications<sup>70, 71, 72, 73</sup> and are found in various forms such as hydrophobic or hydrophilic, gel-type or macroporous. Copolymers produced with low levels of difunctional cross-linker (<4% difunctional monomer) are generally associated with the production of gel-type resins, these resins are also generally produced without including the inert diluent (porogen). Macroreticular resins are produced using much higher levels of difunctional monomer (>20%) and a porogen is also included in the reaction ingredients. The type of resin is dependant on the particular application e.g. in Affinity Chromatography a macroporous hydrophobic resin is used. Although other monomers can be used to produce similar structures the vinyl-divinyl system is still the most prevalent due to the chemical inertness of the final product.

The general method for producing these polymer supports is via suspension polymerisation. This method for polymerisation requires the monomers and a free radical initiator to be dispersed in an immiscible liquid. The monomer phase is maintained as small droplets by mechanical agitation and the use of a stabiliser within the continuous phase<sup>74</sup>. Initiation is generally

started thermally using an oil soluble free-radical initiator and the final product is a suspension of polymer beads whose size is comparable to the initial size of the monomer droplets, thus allowing control of the final size by controlling the level of agitation. In contrast to emulsion polymerisation suspension polymerisation leads to much larger particles.

Kun and Kunin<sup>75, 76</sup> have carried out studies on the various types of resin and they defined the difference between ion exchange and macroreticular resins. They defined ion exchange resins as cross-linked gel-type whose pore structure is defined as the distance between the polymeric chains. Porosity is only present in these structures when the polymer is hydrated and the polymer network fully expanded, if the resin is dehydrated then the polymer network collapses and the porosity is lost. The definition of macroreticular resins was either a continuous non-gel structure or a continuous gel structure that is permeated with holes and channels that are not part of the gel structure, similar to those found in alumina, therefore the size and shape of these holes and channels is not greatly effected by the state of the polymer either hydrated or dehydrated and hence porosity is permanent and not lost as the polymer dries. Gel-type resins will swell and contract with addition or removal of a good solvent and will not adsorb bad solvent into the structure, macroporous resins however show little variation in their overall volume and will adsorb both good and bad solvents.

Kunin extended the definitions and related his ideas in relation to porous and non-porous solid adsorbents, porous adsorbents being solids containing permeating pores that are larger in diameter than the molecular distribution, and non-porous adsorbents consisted of very finely divided solids that had a

high surface area due to the small particle size. The surface area of these finely divided solids is however much less than that of porous adsorbents.

Gels that have dry porosity and therefore permanent porosity have over time been described as "macroporous"<sup>77</sup>, "macroreticular"<sup>78</sup> and "visibly porous"<sup>79</sup>, the latter term has not been widely adopted but relates to the visible appearance of the beads which can be translucent or opaque which is dependant on the extent of light scattering and the pore size distribution rather than the pores being visible. The terms "macroreticular " and "macroporous" have found favour however the term "macro" in this instance refers to the porosity of the resin as defined by Miller<sup>79</sup>. Miller defined resins as macroporous if the quantity of cyclohexane adsorbed was greater than 0.1 ml g<sup>-1</sup>. It is therefore important to distinguish the term "macroporous" when dealing with these gel type polymers and macroporous as defined by the IUPAC which refers to the pore size distribution within the resin where microporous, mesoporous and macroporous have specific definitions in terms of pore diameter (section 2.1.4).

Through minor modification of the production technique it has been possible to prepare resins with varying morphologies from gel-type through to macroporous, and by incorporating compounds such as pigments, magnetic particles and small carbon blacks into the aqueous phase<sup>80</sup> resins with specific properties that are easily identifiable can be produced for example different resins incorporated into a pigmented mixed bed ion exchange system. In a similar way other species such as enzymes<sup>81</sup> can be incorporated into the resin system.

## **1.4.2 Pore Development in Styrene / Divinylbenzene Resins via**

### **Suspension Polymerisation**

#### **1.4.2.1 Pore Formation**

The methods employed by Sederel<sup>82,84</sup> in the production of porous resins are based around three types of porogenic systems. These are:

- Porogens which are solvents for the copolymer
- Porogens which are non-solvents for the copolymer
- Macromolecular materials

The type of porogen used in the polymerisation process has a distinct effect on the type of porosity formed. Inclusion of a porogen that is a good solvent for the copolymer, such as toluene xylene and dichloroethane<sup>83</sup>, resulted in a polymer that was characterised by a high specific surface area ( $50 - 500 \text{ m}^2 \text{ g}^{-1}$ ) with relatively low pore volumes (up to  $0.8 \text{ ml g}^{-1}$ ) and a small average pore diameter<sup>79</sup>.

Resins produced in the presence of a non-solvating porogen such as *n*-heptane or octane, resulted in resins that had a low specific surface area (between  $10 - 100 \text{ m}^2 \text{ g}^{-1}$ ), a large pore volume ( $0.6 - 2.0 \text{ ml g}^{-1}$ ) and large average pore diameter.

The preparation of porous resins using macromolecular material such as low molecular weight linear polystyrene, resulted in resins with low pore

volumes (up to  $0.5 \text{ ml g}^{-1}$ ) low specific surface areas (between  $0 - 10 \text{ m}^2 \text{ g}^{-1}$ ) and very large average pore diameters.

By combining together two types of porogen it is possible to produce resins with a combination of the properties associated with the porogenic species.

The other major factor governing the development of the porous structure is the monomer ratio of the vinyl to divinyl component<sup>84</sup>. Resins produced with low levels of divinyl monomer will have an expanded gel type structure where the pores are formed between the polymer chains. Porosity is lost due to collapse of the porous network upon removal of the porogen. Resins like these with no permanent dry porosity are used solvated in GPC, or when functionalised for example by sulphonation with oleum in ion-exchange. As the cross-link density is increased by increasing the divinyl monomer in the reaction mixture, a more rigid polymer is formed that is able to maintain a porous network even after all of the porogen has been removed.

During suspension polymerisation it is thought, as first suggested by Kun and Kunin<sup>75</sup>, that there are three separate substructures involved in the development of the porous network, these are:

- Nuclei – The nuclei are the primary particles and are formed from the agglomeration of cross-linked polymer chains. The size of the nuclei are in the region of  $5 - 20 \text{ nm}$
- Microspheres – Microspheres are secondary particles formed by the agglomeration of nuclei during phase separation. The size of the microspheres in the region of  $60 - 100 \text{ nm}$

- Beads – The beads are the final structure formed, they are in the size region of  $10^5 - 10^6$  nm are made up of agglomerates of microspheres.

The experimental procedure employed by Kun and Kunin<sup>75</sup> was to remove a series of aliquots from the suspension polymerisation reaction mixture over time and examine the physical and chemical characteristics of the fractions. Cross-link density was indirectly measured by comparing the swelling ratios (as cross-link density increases the ability of the fraction to swell in good solvent will decrease) and as was expected it was found that the degree of cross-linking of the fractions increased as the polymerisation reaction proceeded, however they did observe a maxima in the rate at which cross-links were formed early in the reaction. Examination of the pendant vinyl bond concentration of each fraction was performed by infrared spectroscopy and the relative concentration of the unreacted pendant vinyl bond decreased as the polymerisation reaction proceeded. From this series of experiments they were able to determine that at divinylbenzene levels below 10% the rate of fractional loss of the vinyl pendant group was unaffected by the divinylbenene concentration and that where the concentration is sufficiently high the polymer is sufficiently rigid to freeze in some unreacted pendant vinyl groups. The change in surface area of the polymer with polymerisation time was also followed and as the polymerisation proceeded the total surface area also increased. It was also noted from total pore volume studies that the non-gel porosity first decreases and then increases during the time that there is an increase in the total surface area. These changes in the total porosity of the

polymer reflect the structural changes that take place whilst the resin is forming.

From their data Kun and Kunin proposed a mode of pore formation.

#### Stage 1

- i. The initial droplets containing monomer, initiator and diluent are suspended in the aqueous phase with the suspension stabiliser adsorbed at the interface
- ii. Straight chain polymers are formed within the droplets, pendant vinyl groups are present.
- iii. Intramolecular cross-links are formed resulting in a co-polymer. High molecular weight straight chain polymer is still present
- iv. After sufficient time has elapsed (depending on reaction temperature, monomer ratio diluent concentration etc.) phase separation will occur. This results in a droplet that comprises monomer, co-polymer and low molecular weight polymer phase and a monomer / diluent phase.
- v. Interfacial tension within the polymer rich phase leads to the formation of microspheres
- vi. Macrogelation occurs.

#### Stage 2

- i. The microspheres bind together as the polymerisation continues

- ii. The styrene / divinylbenzene ratio varies depending on the relative reactivity also the monomer in diluent concentration decreases.

### Stage 3

- i. The concentration of the monomer in the diluent becomes low and the rate of polymerisation begins to fall

The fine pore characteristics of the polymer are dependant upon stage 1 and the non-gel structure is dependant upon stage 2. Mikes<sup>85</sup> further elaborated and confirmed the Kun and Kunin theory of pore formation

Work carried out by Tager and Tailipotkina<sup>86</sup> on the porosity of styrene / divinylbenzene porous resins focused mostly on monomer ratios whilst using the non-solvating diluent heptane as the porogenic species. Analysis of the final polymer was based on sorption methods, density determination and swellability in benzene. The specific surface area, pore volume and size distribution were determined. Results obtained showed an increase in the specific surface area as the divinylbenzene concentration was increased whilst the total pore volume passed through a maximum, density and swellability decreased as the cross-link concentration was increased. They recorded specific surface areas in the region of 10 – 100 m<sup>2</sup> g<sup>-1</sup> with the higher surface area achieved with the highest concentration of both cross-linker and diluent. Pore size distributions were found to be wide.

The mechanism by which the nature of the porous structure within the resins can be controlled by the diluent type, whether solvating or non-

solvating, may be explained in terms of the stages of formation of the resin beads.

### **1.4.3 Non-Solvating Porogen**

For porous polymer produced in the presence of a non-solvating diluent and with a sufficiently high cross-linker content, then during stage 1 the growing polymer chains become entangled by the continuing polymerisation. Further entanglement and increase in molecular weight leads to stage 2 in which the growing chains compact to form microspheres, further entanglements cause the microspheres to compact, during this stage the pore volume increases dramatically. During the polymerisation process the solvating power of the dispersed liquid will decrease as the monomer is consumed until at a certain point the growing polymer nuclei will precipitate. The point at which phase separation occurs will be determined by the concentration of the cross-linker and porogen as well as the reaction temperature. Once phase separation has occurred the remaining monomer will polymerise between the coalescing agglomerates formed by the nuclei leading to a decrease in the surface area due to infilling<sup>87</sup>. Phase separation is induced prior to the gel point as the solvating power of the non-solvating porogen decreases due to polymer nuclei growth and depletion of monomer, until a point is reached at which the polymer is no longer soluble in the diluent and hence phase separation occurs.

Hauptke and Hoffman<sup>88</sup> also studied the effect of varying the organic components on pore formation, they produced polymers with varying

divinylbenzene content from 5% to 50% and with a mixture of alkanes with boiling points between 150°C and 200°C as diluent, they also varied the diluent concentration with respect to the organic phase from 10% to 70%. From the results they were able to determine four distinct porous domains.

1. Gel type polymer. These polymers were produced with low divinylbenzene content and a low diluent concentration; they had no measurable surface area and had a translucent appearance.
2. Semi-porous polymers. These polymers were semi-opaque in physical appearance but still with no measurable surface area. This type of pore domain was produced for polymerisations that were carried out with low divinylbenzene content and a medium diluent concentration, and with polymerisations produced with a higher divinylbenzene content but with a low diluent concentration.
3. Flocculent polymers. These polymers were produced with very high diluent concentrations and were opaque powders in appearance and a low surface area.
4. Macroreticular polymers. These polymers were again opaque in appearance and had a reasonable surface area. This type of porous domain was achieved for polymers produced with a high divinylbenzene content and medium diluent concentration

#### **1.4.4 Solvating Porogen**

Guyot *et. al.*<sup>89</sup> studied the formation of porous styrene / divinylbenzene copolymers in the presence of a solvating porogen. In comparison to the studies carried out with non-solvating porogens only two levels of substructure were observed.

1. Large nuclei in the size range of approx. 20 – 50 nm
2. Agglomerates of the nuclei.

i.e. no small, 5 – 20 nm, primary nuclei were observed.

During the polymerisation phase separation occurs at a later stage than with a non-solvating diluent and the chains are no longer extended. The result of this is the growing chains become entangled inside the growing nuclei resulting in larger final nuclei when phase separation occurs. When the concentration of divinylbenzene in the reaction mixture is low then the structure formed is an expanded gel because the chains remain fully solvated throughout the polymerisation process.

In the case of solvating diluents phase separation occurs after the gel point has been reached. At high divinylbenzene concentrations there is an increase in the cross-link density and therefore the diluent is no longer able to fill all the available volume, leading to phase separation. At low divinylbenzene concentrations the cross-link density is low and therefore the diluent is able to fill all the available volume and in this case there is no phase separation.

## 1.5 Chitin and Chitosan

Chitin and its deacetylated derivative chitosan are naturally occurring polysaccharides obtained primarily from the exoskeletons of crustacea, molluscs and insects. Chitin is the second most abundant biopolymer, after cellulose; the material used for this study came from the thousands of tons of waste material produced by the seafood industry.

Chitin is poly[ $\beta$ -(1-4)-2-acetamido-2-deoxy-D-glucopyranose] and its idealised structure is given in Fig.1.1. Chitosan is poly[ $\beta$ -(1-4)-2-amino-2-deoxy-D-glucopyranose] and its idealised structure is given in Fig. 1.2. However in reality these are two extremes of a continuous series of copolymers of the two monomer residue units, anhydro *N*-acetyl-D-glucosamine and anhydro D-glucosamine, chitosan being defined as the range of these copolymers soluble in dilute organic acid.

In recent years interest has grown in naturally occurring polymers, and the rise of environmental issues regarding the recycling of waste products generated by industrial processors has led to an increase in investigations into the potential use of chitin and chitosan in various applications.

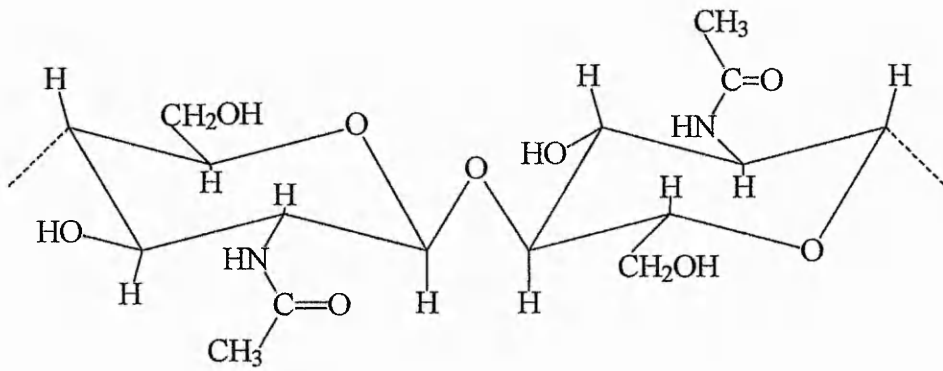


Fig 1.3 Idealised structure of Chitin

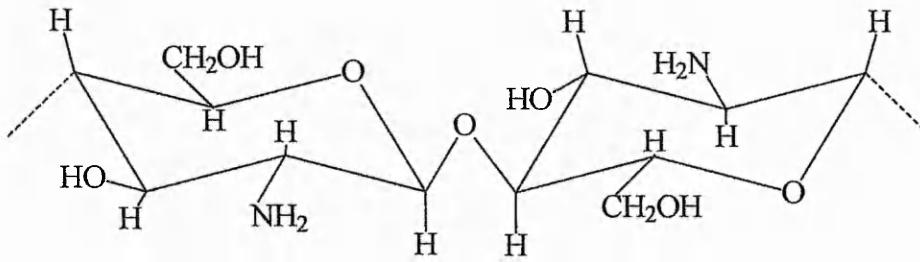


Fig 1.4 Idealised Structure of Chitosan

### **1.5.1 Discovery of Chitin and Chitosan**

Chitin was first described in 1811 by Braconnot<sup>90</sup>, when he isolated a product from fungi, which he named fungine. In 1823, Odier<sup>91</sup> established the relationship between plant tissue and insect cuticle and it was he who named the isolated product chitin. The term chitin was derived from the Greek for tunic or envelope. The presence of nitrogen in chitin was first demonstrated by Lassaigne<sup>92</sup> in 1843 in his work with silkworms. Ledderhose<sup>93</sup> proposed that chitin was composed of glucosamine and acetic acid and the presence of glucosamine was confirmed in 1894 by Gilson.<sup>94</sup>

Chitosan, which is now known to be the primary derivative of chitin, was first prepared in 1859 by Rouget<sup>95</sup>, when he treated chitin with concentrated potassium hydroxide. This "modified Chitin" was named chitosan in 1894 by Hoppe-Seyler<sup>96</sup>.

Research continued into the twentieth century concerning the occurrence of chitin in living organisms and into its chemical constitution. In 1946 after much controversy surrounding the chemical form of the nitrogen, Purchase and Braun<sup>97</sup> described chitin as a polymer of *N*-acetyl-*D*-glucosamine.

### **1.5.2. Occurrence of Chitin and Chitosan in Nature**

Chitin abounds in nature. It is the major structural polysaccharide used by most invertebrates, arthropods being the most significant group. However chitin is also found in less evolved groups as well as in lower plants such as

fungi. Both fungal and animal chitin has been shown to have the same identity<sup>98,99,100,101,102,103,104,105</sup>.

### **1.5.2.1 Chitin in Lower Plants**

Chitin is present as a major structural component in the cell wall of plants such as fungi and moulds. These plants metabolise considerable amounts of nitrogen. Wisselingh<sup>106</sup> showed that the cell wall of fungi consists of either cellulose or chitin and that they are responsible for the shape and rigidity of the cells.

### **1.5.2.2 Chitin in Animals**

Chitin is the major structural polysaccharide in most invertebrates, but whereas in plants the chitin is associated with other polysaccharides, in animals it is associated with proteins, particularly collagen<sup>107</sup> as well as mineral salts. Chitin is found in all major classes of arthropods both in their exoskeletons as well as in internal organs. The dry organic matter found in their cuticle can contain up to 80% chitin. This abundance has led to the arthropods being a major source of chitin for industrial use. Chitin is also found in the shells of various mollusc species, however the shells of molluscs only contain between 1-5% chitin, the rest being calcium carbonate. Although mollusc shells are available in large quantities the low level of chitin in them means that they are not a suitable source for chitin on an industrial scale.

### **1.5.3. Morphology of Chitin**

Studies using X-ray diffraction<sup>108, 109</sup> have shown that chitin exists in three polymorphic forms,  $\alpha$ ,  $\beta$ , and  $\gamma$  chitin. The three forms differ in the arrangement of polymer chains within the unit cell. In  $\alpha$  chitin the chains have an anti-parallel arrangement, which makes this the most stable and compact form of chitin. In  $\beta$  chitin, which exists as a crystalline hydrate<sup>110, 111</sup>, the chains are arranged in parallel, the lower stability of this form being attributed to the relative ease with which water can penetrate the lattice. Chitin in the  $\gamma$  form is the least stable, in this form the chains are in a two chains “up” to every one chain “down” arrangement.

The reason for the existence of these three polymorphic forms has been attributed to function<sup>112</sup>;  $\alpha$  chitin is associated where extreme hardness is required, such as the exoskeletons of crustacea.  $\beta$  and  $\gamma$  chitin are associated with collagen type proteins and are found where toughness and flexibility are required. The three forms have been found within the same organism; in the squid *Loligo* the beak is formed from  $\alpha$  chitin, the pen is formed from  $\beta$  chitin, and the lining of the stomach from  $\gamma$  chitin. This appears to confirm the link between morphology and function as opposed to taxonomic grouping.

In recent years doubt has been cast as to the existence of  $\gamma$  chitin since its first description by Rudall<sup>113</sup>. It is now suggested that what Rudall thought to be  $\gamma$  chitin is a distorted form of either  $\alpha$  or  $\beta$  and not a true polymorphic form.

#### **1.5.4. Isolation of Chitin**

Chitin is usually found in conjunction with other substances. In crustacea, which is the most abundant source for chitin, it is closely associated with calcium carbonate and proteins. The isolation of chitin generally involves harsh chemical treatment, typically decalcification with acid followed by deproteination with hot alkali, but not necessarily in that order. These harsh treatments generally lead to a certain amount of degradation of the polymer, decrease of molecular weight due to acid hydrolysis and deacetylation in the alkali. Several methods of isolating chitin have been proposed and these have been reviewed by Roberts<sup>113</sup>.

#### **1.5.5. Preparation of Chitosan**

Chitosan has been found in the cell wall of certain fungi<sup>114, 115</sup>, but this has not so far been used as a source for chitosan. Chitosan used for commercial purposes is generally produced by the deacetylation of chitin from crustacea.

The cleavage of acetamido groups adjacent to *trans*-related hydroxyl groups, as is the case with chitin, requires much harsher conditions than the cleavage of *cis*-related analogues. Therefore the deacetylation of chitin is carried out in concentrated alkali.

A comprehensive review of the techniques used in the deacetylation of chitin has been carried out by Roberts<sup>24</sup>.

### **1.5.6. Degree of N-acetylation in Chitin and Chitosan**

As has already been discussed chitin and chitosan exist as a series of copolymers, chitosan being described as the members of this series which are soluble in dilute organic acid. This implies that the distribution and amount of the minor structural components, anhydro-D-glucosamine in chitin and anhydro *N*-acetyl-D-glucosamine in chitosan, have a considerable effect on the properties of the polymer. Studies have shown that the solubility of chitin in organic solvents however is inversely dependent on the degree of deacetylation<sup>116</sup>. Further studies were carried out on the relationship between solubility and degree of *N*-acetylation by Sannan et al<sup>117</sup>, who found that samples deacetylated to about 50% residual *N*-acetyl content under homogenous conditions were water soluble. Samples of greater or lesser degrees of residual *N*-acetyl content were either gel forming or insoluble. It can be seen therefore that it is of vital importance that in any study carried out on chitin and chitosan, that the degree of *N*-acetylation of the materials under study should be determined.

## **1.5.7. Methods for Determining the Degree of N-Acetylation of Chitin and Chitosan**

### **1.5.7.1. Colorimetric Techniques**

#### **1.5.7.1.1. Dye Adsorption**

This is a relatively simple technique developed by Roberts<sup>118</sup>, and is based on the fact that at equilibrium there is a 1:1 stoichiometry<sup>119</sup> for the interaction of the sulphonic acid groups within anionic dyes with protonated amine groups along the polymer chain. A fuller description of this technique can be found in the experimental section of this work (section 3.5.2).

#### **1.5.7.1.2. Metachromatic Titration**

Metachromatic titration involves polyelectrolyte-induced metachromacy in suitable dyes. The absorbance at  $\lambda_{\max}$  of a dye showing polyelectrolyte-induced metachromacy, decreases with increasing added polyelectrolyte concentration, until a minimum is reached. After this point further addition of polyelectrolyte has no further effect. Using a plot of absorbance versus volume of added polyelectrolyte solution, the intersection represents the point at which the system contains an equivalent number of dye ions and charged groups on the polyelectrolyte.

Gummow and Roberts<sup>120</sup> observed chitosan induced metachromasy in C.I. Acid Red 88 and C.I. Acid Orange 7.

### **1.5.7.1.3. Residual Salicylaldehyde**

Domszy and Roberts<sup>121</sup> determined the amine group content of chitosan by utilising the reaction between the free amine groups within the chitosan chain and salicylaldehyde. The reaction forms the yellow Schiff's base, *N*-salicylidenechitosan. The basis for this technique involves reacting chitosan in excess salicylaldehyde and subsequent spectroscopic analysis of the remaining salicylaldehyde at the end of the reaction period.

### **1.5.7.2 Titrimetric Techniques**

The measurement of the primary amine groups of a sample shows significant advantages over the measurement of residual *N*-acetyl content<sup>122</sup>. It is a direct measure of the functional group of the polymer, it is readily measured by titration and is more sensitive than nitrogen analysis<sup>28, 31, 123, 124</sup>.

### **1.5.7.3 Spectrophometric Techniques**

#### **1.5.7.3.1 UV Spectroscopy**

The first attempt to use UV spectroscopy to determine the degree of *N*-acetylation of chitin or chitosan was carried out by Castle et. al.<sup>125</sup>, but the technique was found to be unsuitable for quantitative analysis.

Muzzarelli and Rochetti<sup>126</sup> reported a method for determining the degree of *N*-acetylation of chitosan using first derivative UV spectroscopy and *N*-acetyl-D-glucosamine solutions as calibrants.

#### **1.5.7.3.2 IR Spectroscopy**

The IR spectrum of  $\alpha$  chitin shows two adsorption bands at approximately 1655 and 1625  $\text{cm}^{-1}$ . These two bands are characteristic of hydrogen bonded amide groups. Darnen and Rudall<sup>127</sup> noted the disappearance of these bands during de-acetylation. It was however several years before their use in determining the degree of *N*-acetylation was proposed<sup>128</sup>. Several other workers have described infrared techniques utilising either the amide I or the amide II band<sup>129, 130, 131</sup>.

#### **1.5.7.4 Gas Chromatographic Techniques**

Radhakrishnamurthy<sup>132</sup> determined the quantity of *N*-acetyl groups in mucopolysaccharides by chromatographic techniques and Holan<sup>133</sup> proposed a similar method for determining chitin in yeast cell walls. Both methods involve hydrolysis of the polymer followed by chromatographic determination of the amount of released acetic acid.

Muzzarelli<sup>130</sup> used a gas chromatographic method with chitin and chitosan. In this method the degree of *N*-acetylation was determined by the retention time of methanol eluted through a column of polymer, the retention time increasing with increasing degree of *N*-acetylation.

#### **1.5.7.5 NMR Spectroscopy**

The determination of the degree of *N*-acetylation of chitin by NMR was first carried out by Hirano and Yamaguchi<sup>134</sup> in their work on *N*-acetylchitosan gels. This method is most accurate for samples with high levels of *N*-acetylation. It has also been reported that the extent of deacetylation of chitin may be determined by using solid state <sup>13</sup>C CP/MAS NMR spectroscopy<sup>135</sup>.

#### **1.5.8 Adsorption of Metal Ions by Chitin and Chitosan**

The chelation of metal ions with chitin and chitosan was first described by Muzzarelli<sup>136</sup>. Hauer<sup>137</sup> also studied the ability of chitosan to form chelated metal ion complexes, attributing the adsorption of metal ions to the NH<sub>2</sub> groups. Other work carried out by Yaku and Koshijima<sup>138</sup> involved the preparation of a *D*-glucosamine/Cu (II) complex from a water-soluble glucosamine oligomer as a model for the chitosan/Cu (II) complex. This work concluded that one mole of cupric ions was co-ordinated with four moles of *D*-glucosamine. This result is however in conflict with those obtained by Blair and Ho<sup>139</sup> who claimed that in chitosan film two moles of *D*-glucosamine were complexed with one mole of cupric ions, and those of Muzzarelli et al<sup>140</sup> who stated that at a pH of 4.0-5.0 one or two nitrogen atoms per cupric ion were involved, and that at higher pH the co-ordination number increased with OH groups becoming involved also. There are however considerable differences between complex formation of Cu (II) ions with water soluble oligomers on the one hand and with chitosan polymer chains in the solid state on the other. It is

therefore not surprising that differences in the number of amine groups complexed with a Cu (II) ion was found.

The exact mechanism for the adsorption of metal ions by chitin and chitosan has yet to be fully determined. Muzzarelli<sup>141</sup> has speculated that chelation, sorption and ion exchange may all be involved, and Yoshinara and Subramanian<sup>142</sup> suggest that all three processes have varying degrees of importance depending on the metal ion.

Although chitosan has a high affinity for the first row transition metals it remains relatively inert to alkali metal and alkali earth ions<sup>138</sup>.

Studies carried out by Mazengarb<sup>143</sup> focused on the adsorption of various textile dyes by chitin and chitosan both in solid state and in film form. Using CI direct Blue 15 and CI Direct Blue 218, both of which have the same structure apart from CI Direct Blue 218 being chelated to a copper ion with three available co-ordination sites free, the study clearly showed that a different mode of adsorption was taking place. In the case of CI Direct Blue 15 a Freundlich adsorption isotherm was produced signifying non-site specific adsorption whereas in the case of the coppered CI Direct Blue 218 a Langmuir adsorption isotherm was obtained indicating a site specific adsorption mechanism.

## **2 Instrumental Techniques and Background Theory**

### **2.1 Surface Area and Pore Size Analysis Using Adsorption**

#### **2.1.1 Introduction**

The ability for a porous solid to adsorb large amounts of condensable gas has been known for a long period of time, as early as 1777 Fontana<sup>144</sup> noted the ability of freshly calcined charcoal to adsorb several times its own volume of various gases when cooled under mercury. In the same year Shceele<sup>145</sup> noted that when charcoal was heated the gas driven off was re-adsorbed on cooling, he noted that the process of desorption and adsorption was reversible, and that the volume of gas desorbed on heating took up eight times the volume of the charcoal sample.

Further investigations soon led to the realisation that the quantity of gas expelled differed from one charcoal to another and in 1814 de Saussure<sup>146</sup> suggested that the efficiency of the charcoal to adsorb gas was dependent on the area of exposed surface. It was Mitscherlich<sup>147</sup> who in 1843 first emphasised the role of pores in the adsorption process and he was able to estimate the size of the pores to be  $1/2400$  in, it was also noted that when carbon dioxide was adsorbed a layer 0.005mm thick which closely resembled liquid carbon dioxide was formed on the surface of the charcoal. It is these two factors of surface area and pore volume that are now recognised as playing complementary roles in the adsorption of gases or vapours, not only on charcoal but on a wide variety of other solids. Therefore the measurement

of adsorption of gases or vapours can yield information as to the surface area and pore structure of the solid under study.

The term adsorption was introduced by Kayser<sup>148</sup> to denote the condensation of gases or vapours onto a free surface as opposed to absorption where the molecules of the gas or vapour penetrate into the bulk mass of the solid.

### **2.1.2 Adsorption Isotherms**

If a solid is exposed to a gas in an enclosed space the quantity of gas adsorbed by the solid will be dependent on certain parameters, these being the pressure, the temperature and the interaction potential between the adsorbate (gas or vapour) and the adsorbent (surface under study), therefore at equilibrium the amount (weight) of gas adsorbed can be expressed as:

$$W = F(PTE) \qquad 2.1$$

Where:

W = Weight of gas adsorbed

F = Constant

P= Pressure

T = Absolute temperature

E = Interaction potential

As it is usual to perform adsorption experiments at constant temperature equation 1.1 can be reduced to

$$W = F(PE) \quad 2.2$$

And if the temperature is below that of the critical temperature of the gas then,

$$W = F(P/P_0) \quad 2.3$$

is more useful ( $P_0$  = saturation vapour pressure of the adsorbate).

A plot of  $W$  against  $P/P_0$  at a constant temperature will yield a adsorption isotherm of the particular gas / solid system, indeed were it not for differences in  $E$  the interaction potential then all adsorption isotherms would be identical.

The classification of adsorption isotherms was put forward by Brunauer, Deming, Deming and Teller<sup>149</sup> who, after extensively reviewing the literature, observed that all adsorption isotherms fitted into one of five types, and found that this was enough to satisfy most situations. More recently a report from the International Union of Pure and Applied Chemistry (IUPAC)<sup>150</sup> built on the original work and reclassified the adsorption isotherms into six types (Fig.1.5). The IUPAC report also assigned the boundaries of the mesopore range, these being 2 to 50 nm in width, anything below 2 nm being classed as micropores and anything above 50 nm being classed as macropores.

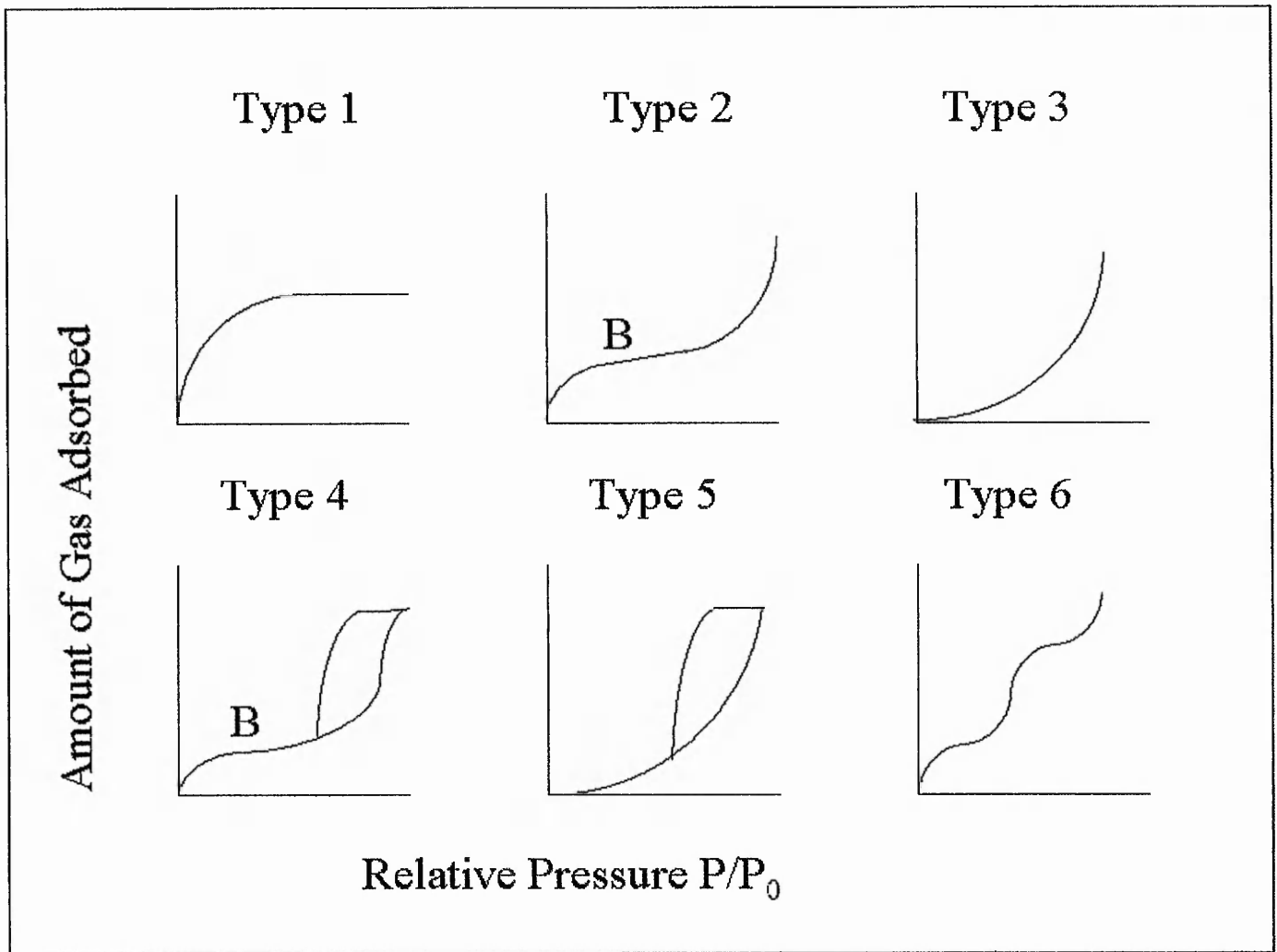


Fig.1.5 The six types of adsorption isotherms.

The six basic isotherm shapes into which the majority of adsorbate / adsorbent combinations will fit reflect specific conditions and are classified as follows.

Type I More commonly referred to as a Langmuir adsorption isotherm, occurs when the adsorption is limited to only a single molecular monolayer, This is the type of isotherm observed for chemisorption where adsorption is limited to specific sites where once all sites are occupied no further

adsorption takes place. In terms of physical adsorption type I isotherms are encountered with microporous solids in which the pore diameter does not exceed a few adsorbate molecules in size. When a molecule of the adsorbate is inside the pore it encounters the overlapping potentials of the pore walls, this enhances the amount of gas adsorbed at low  $P/P_0$ , at higher values of  $P/P_0$  the pores are full of condensed gas and this leads to the plateau. Thus when a type I isotherm results for physical adsorption it indicates that the solid under study is microporous and that the vast majority of the available surface for adsorption is contained within the pores, which once full leave very little external surface for further adsorption to occur.

Type II      The type II isotherm is generally associated with nonporous solids or porous solids whose pore diameters are greater than those in the micropore region, with an adsorbate having strong interactions with the surface. The inflection or knee of the isotherm seen at b in Fig. 1. is of significance as this is the point at which a single monolayer of adsorbate has been reached.. As  $P/P_0$  increases further layers are adsorbed until at saturation the number of adsorbed layer becomes infinite. This type of isotherm can be described by the BET equation.

- Type III      The type III isotherm differs from the type I and II in that there is no inflection or knee present and the curve does not rise above the x-axis until a finite value of  $P/P_0$  has been reached. After this point the curve continues to rise. This type of isotherm is associated with systems where the heat of adsorption is less than the adsorbate's heat of liquefaction, thus as the adsorption proceeds further adsorption occurs because the interaction of the adsorbate with the previously adsorbed layer is greater than that of the adsorbent surface. It applies to non-porous adsorbents with an adsorbate with weak interactions with the surface.
- Type IV      The type IV isotherm is related to the type II but with a high pressure hysteresis loop. This type of isotherm is generally associated with mesoporous adsorbents and an adsorbate with high interactions with the surface.
- Type V      The type V isotherm is related to the type III with the addition of a high pressure hysteresis loop. This type of isotherm is associated with a mesoporous adsorbent and an adsorbate with weak interactions with the surface.

Type VI      The type VI isotherm is quite unusual and is associated with stepwise multilayer adsorption. This will occur on a very energetically uniform surface.

Beside the six classical types of adsorption isotherms, as with all systems of classification there are numerous borderline cases which are difficult to assign to one group or another, indeed there are a number of isotherms that are difficult to fit into the classification at all.

The IUPAC report also focused on four types of hysteresis, illustrated in Fig 1.6. Hysteresis occurs due to a difference in the process of pore filling and pore emptying. In the simple case of cylindrical pores capillary condensation occurs on the pore walls and results in a cylindrical meniscus, however during the desorption process, capillary evaporation occurs from a concave hemispherical meniscus. This difference in mechanism means that the relative pressure at which a pore will empty due to capillary evaporation is lower than the relative pressure required for capillary condensation within the same pore.

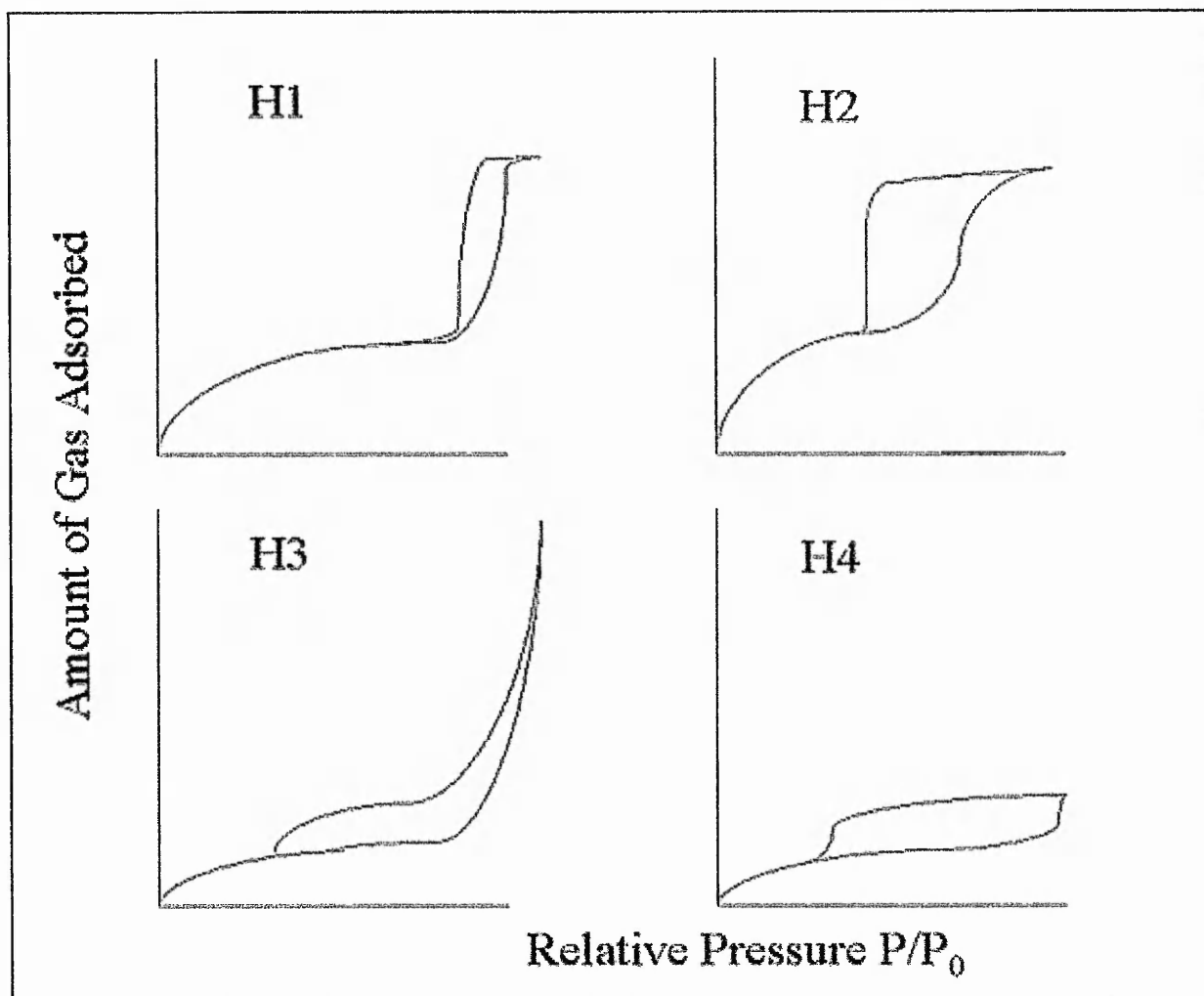


Fig. 1.6 Types of hysteresis observed on adsorption / desorption isotherms.

- Type H1      Type H1 hysteresis is generally associated with porous materials made up from agglomerates or compacts of uniform spheres packed in fairly uniform arrays.
- Type H2      The type H2 hysteresis loop has been especially difficult to interpret". The original idea of so called "ink bottle pores" pores with a narrow neck that open out towards the bottom of the pore has been recognised as being over simplified but the report stated that "the role of network effects must be taken into account.
- Type H3      Type H3 hysteresis is associated with agglomerates of flat plate like particles leading to the formation of slit shaped pores.
- Type H4      Type H4 hysteresis has also been associated with slit type pores but the overall type I character of the isotherm has been taken to suggest that this type of hysteresis is indicative of microporosity.

It has also been noted that a feature common to many hysteresis loops is that the region of the desorption branch will intersect with the adsorption branch at a point dependant on the adsorptive at a given temperature but at a relative pressure independent of the nature of the porous adsorbent, for example for nitrogen at its boiling point of 77 K closure of the hysteresis loop

is usually seen at  $P/P_0 = 0.42$  and for benzene at  $25^\circ\text{C}$  closure of the hysteresis loop occurs at  $P/P_0 = 0.28$ .

There have been several suggestions put forward as to the possible causes of low-pressure hysteresis where the desorption branch of the isotherm does not rejoin the adsorption branch. Some of these are:

- Irreversible chemical interaction between the adsorbate and the adsorbent.
- Uptake of adsorbate molecules into pores or through pore entrances that are of similar size as the adsorbate molecule
- Swelling of non-rigid porous structures.

### **2.1.3 Surface Area and The BET Equation**

The determination of the surface area of a solid by gas adsorption relies on the ability of the model to predict the number of adsorbate molecules required to form a complete monolayer, the monolayer capacity. The monolayer capacity is defined as the number of adsorbate molecules that can be accommodated in a single molecular layer that completely covers the surface of the solid of a unit mass of 1 g. and can be related to the specific surface area  $A$ , the surface area of 1 g of the solid by:

$$A = n_m a_m N_A \quad 2.4$$

Where  $a_m$  is the average area covered by a single molecule of the adsorbate,  $N_A$  is the Avogadro constant and  $n_m$  is the number of moles of adsorbate per gram of adsorbent.:

$$A = \frac{x_m}{M} a_m N_A \times 10^{-20} \quad 2.5$$

With the monolayer capacity  $x_m$  stated in grams of adsorbate per gram of adsorbent and the cross-sectional area  $a_m$  stated in  $\text{\AA}^2$  and the molecular weight of the adsorbate  $M$  in g, the specific surface area,  $A$ , is in  $\text{m}^2 \text{g}^{-1}$ .

In order to derive the monolayer capacity it is necessary to interpret the adsorption isotherm. There have been several theories put forward to achieve this, the best known and most widely used of these theories is the one derived by Brunauer, Emmett and Teller<sup>151</sup>.

The BET theory is built upon an idea first put forward by Langmuir<sup>152</sup> in 1916. Langmuir postulated that the surface of a solid could be regarded as an array of adsorption sites and at dynamic equilibrium the number of adsorbate molecules arriving at the surface and condensing onto free sites was equal to the rate at which adsorbate molecules were leaving the surface by evaporating from occupied sites.

If the fraction of occupied sites is  $\theta_1$  and the fraction of unoccupied sites is  $\theta_0$  (hence  $\theta_1 + \theta_0 = 1$ ), the rate of condensation on a unit area of surface is

$$pa_1k\theta_0,$$

$k$  is a constant given by the kinetic theory of gases  $k = \frac{1}{2} N_A / (MRT^{1/2})$ ,

$a_1$  is the condensation coefficient which is the fraction of incident molecules that actually condense on the surface, The process of

evaporation of an adsorbed molecule from the surface is one in which the isotheric heat of adsorption  $q_1$  is equated to the energy of activation, thus the rate of evaporation from the surface is,

$$a = z_m \theta_1 v_1 e^{-q_1/RT} \quad 2.6$$

in which  $z_m$  is the number of sites per unit area ( $z_m \theta_1$  is the corresponding number of adsorbed molecules) and  $v_1$  is the frequency of oscillation of the molecule in the direction normal to the surface. Hence at equilibrium,

$$a_1 k p \theta_0 = z_m \theta_1 v_1 e^{-q_1/RT} \quad 2.7$$

and since  $\theta_1 + \theta_0 = 1$  then,

$$\theta_1 = \frac{a_1 k p}{a_1 k p + z_m v_1 e^{-q_1/RT}} \quad 2.8$$

If  $n$  is the amount in moles adsorbed on 1 g of adsorbent then  $\theta_1 = n/n_m$  in which  $n_m$  is the monolayer capacity, which leads to the Langmuir equation when adsorption is limited to a single molecular layer,

$$\frac{n}{n_m} = \frac{Bp}{1 + Bp} \quad 2.9$$

Where

$$B = \frac{a_1 k}{z_m v_1} e^{q_1/RT} \quad 2.10$$

In reality B is an empirical constant and cannot be reached using the above relationship.

Langmuir<sup>153</sup> referred to the possibility of the evaporation-condensation mechanism extending to a second and higher molecular layers, but the equation he derived is very complex and thus little used. In 1938 Brunauer, Emmett and Teller<sup>24</sup> introduced their well-known equation for multilayer adsorption by introducing a number of simplifying assumptions into the equation derived by Langmuir.

When the Langmuir mechanism is extended to the second layer it requires that the rate of condensation from the gas phase onto molecules already adsorbed in the first layer be equal to the rate of evaporation from the second layer, i.e.

$$a_2 k_p \theta_1 = z_m \theta_2 v_2 e^{-q_2/RT} \quad 2.11$$

and for the  $n^{\text{th}}$  layer,

$$a_n k_p \theta_{i-1} = z_m \theta_i v_n e^{-q_n/RT} \quad 2.12$$

This implies that at any pressure below the saturation vapour pressure the fraction of the surface 1, 2, ...,  $i$  molecules will be  $\theta_1, \theta_2, \dots, \theta_i$  respectively, so that the thickness of the adsorbed layer will not be constant throughout. Thus on a specific surface area  $A$ , the number of molecules adsorbed  $Z$  will be

$$Z = Az_m(\theta_1 + 2\theta_2 + \dots + i\theta_i) \quad 2.13$$

And the amount adsorbed in moles  $n$  is,

$$n = \frac{Az_m}{N_A} \sum_1^i (i\theta_i) \quad 2.14$$

In theory each individual adsorbed layer will have its own value of  $a$ ,  $q$  and  $v$  hence the summation of the equation can not be carried out unless some simplifying assumptions are made. Brunauer, Emmet and Teller made three such assumptions.

- i) In all layers except the first the heat of adsorption is equal to the molar heat of condensation  $q_L$ .
- ii) In all layers except the first the evaporation-condensation conditions are identical, i.e.

$$v_2 = v_3 = \dots = v_i \quad \text{and} \quad a_2 = a_3 = \dots = a_i$$

- iii) When  $p = p_0$  the adsorptive condenses to a bulk liquid on the surface of the solid.

This leads to the BET equation

$$\frac{n}{n_m} = \frac{c(p/p_0)}{(1-p/p_0)(1+(c-1)p/p_0)} \quad 2.15$$

Which for convenience of plotting is usually written as,

$$\frac{p}{n(p_0 - p)} = \frac{1}{n_m c} + \frac{c-1}{n_m c} \frac{p}{p_0} \quad 2.16$$

$c$  is given by

$$c = \frac{a_1 v_2}{a_2 v_1} e^{(q_1 - q_L)/RT} \quad 2.17$$

But in practice it is nearly always taken as,

$$c = e^{(q_1 - q_L)/RT} \quad 2.18$$

The monolayer capacity  $n_m$  is equal to the reciprocal of the slope plus the intercept.

#### **2.1.4. Pore Analysis by Adsorption**

The analysis of surface area and pore size has to be limited to a certain extent to solids that are either finely divided or contain a significant pore system. If we consider the case of finely divided solids it is known that for a given mass of the solid the surface area is inversely proportional to the particle size. As primary particles aggregate due to surface forces to form secondary particles, the voids that form between the neighbouring primary particles will form a pore system. The size and shape of the pores will depend on the size and shape of the primary particle. Although almost any shape of primary particle is possible in practice the two most often encountered are the sphere and the plate. Voids formed between spherical particles will depend on the closeness of the packing, in an ideal situation where the spheres are monodisperse then a co-ordination number  $N$  (the average number of nearest neighbours) will be 12 (hexagonal close packing), 4 for tetrahedral packing but can be as low as 2 for a very loose open structure. For plate-like particles the pores tend to be wedge shape, however in the most favourable circumstances the walls of the pores can be parallel or nearly parallel and in this case slit shape pores are formed.

When discussing the surface properties of solids with a high specific surface area it is desirable to distinguish between the internal and external surfaces. For the two given idealised examples above it is easy to distinguish between the internal and external surfaces, however for real solids the distinction is not as straightforward. The surfaces of the primary particles may also contain imperfections such as cracks or fissures that may extend deep

into the interior of the particle, therefore it is necessary to make a distinction between what constitutes internal and external surface. This distinction is by necessity quite arbitrary but it is usual to define the internal surface to include all surface imperfections that are deeper than they are wide and that the external surface will be made up to include any surface imperfections that are wider than they are deep. Although arbitrary this system of classification works well in practice as a wide variety of porous solids have an internal surface area several orders of magnitude greater than that of the external surface. Porous solids that fall into this category are not only restricted to those formed by primary particle aggregation as described but also those in which the pore system is formed by removal of parts of the internal solid or by removal of an additive which can be incorporated into the solid during particle formation but that can subsequently be removed to leave a porous network.

Thus within a porous solid the pores may be of many different kinds and can vary a great deal in both size and shape. Dubinin<sup>154</sup> proposed a classification for pore sizes depending on their average width in the case of cylindrical pores. This classification has since been adopted by IUPAC, see section 2.1.2

The fundamental basis for this classification stems from the characteristic adsorption effects that can be distinguished from the adsorption isotherm. For micropores the close proximity of the pore walls means that there is a significantly higher interaction potential than in pores with wider dimensions and this leads to enhanced amount of adsorption at a given low relative pressure. For mesopores the effect of capillary condensation yields a pronounced hysteresis loop in the high-pressure region of the isotherm. With

macropores the pores are so wide that a detailed derivation of the pore size distribution from the isotherm is almost impossible due to the closeness of the relative pressures to unity.

### **2.1.5. Adsorption by Non-Porous Solids**

In the vast majority of cases when gases or vapours are adsorbed onto non-porous solids a type II isotherm is obtained.

### **2.1.6. Adsorption by Microporous Solids**

In a microporous solid the pore walls are in close proximity to each other and thus the potential fields from the neighbouring walls will overlap. This overlap of the potential fields within the pore means that the interaction energy between the solid adsorbent and the gaseous adsorbate will be significantly enhanced. This effect will cause a distortion in the low-pressure region of the isotherm in favour of increased adsorption; in many cases the interaction may be so strong as to bring about the complete filling of the pores at low values of  $P/P_0$ . In the simplest case of adsorption by microporous solids a type I isotherm is derived.

### **2.1.7. Adsorption by Mesoporous Solids**

The adsorption of gases by mesoporous solids will give rise to a type IV isotherm. A characteristic feature of the type IV isotherm is the hysteresis loop. The exact shape of the loop may vary from one adsorbent / adsorbate system to another but the desorption branch of the isotherm will always be above the adsorption branch until a point of intersection occurs.

### **2.1.8 Quantasorb Surface Area Determination**

Specific surface area measurements may be performed using a Quantasorb apparatus (Quantachrome Corporation). This apparatus utilises a continuous flow method that is very sensitive and eliminates the dead space correction uncertainty of static methods, allowing very low specific surface areas to be measured<sup>155</sup>, The instrument operates by passing nitrogen across the sample in a carrier stream, in this case helium. The partial pressure of the nitrogen is varied by adjusting the flow rate of both the nitrogen and the helium carrier.

$$\frac{P}{P_0} = \frac{f_N}{f_H + f_N} \quad 2.19$$

Where:

$f_N$  = nitrogen flow rate

$f_H$  = helium flow rate

Once the instrument has reached equilibrium and the base line set, the sample holder is immersed in liquid nitrogen at 77 K. This promotes adsorption of nitrogen from the gas stream onto the sample surface. When the system reaches equilibrium the liquid nitrogen is removed and the sample holder warmed to desorb the nitrogen back into the gas stream, which is passed over a thermal conductivity detector and the area under the peak above the base line is integrated. A calibration is performed by inserting a known volume of nitrogen gas into the carrier stream at each partial pressure and the quantity of nitrogen adsorbed per gram of sample at each partial pressure can be calculated.

## **2.2 Photon Correlation Spectroscopy**

Photon Correlation Spectroscopy (PCS) is a light scattering technique that exploits the fact that small particles in dilute liquid suspension undergo random thermal motion (Brownian Motion). When small particles such as colloidal sized latex particles are suspended in a fluid they collide randomly with the fluid molecules and this movement is known as diffusion. The diffusion coefficient is a measure of the rate at which diffusion occurs and this is a function of the particle size.

When a particle is irradiated by a laser beam the light is scattered by the particle over a wide range of angles. When many particles are irradiated at the same time the scattered light by individual particles interacts to form an interference pattern. This will include regions of constructive and destructive interference and results in regions of high and low intensity. Since the particles are in motion the regions of varying intensity will also be in motion

and therefore a detector capable of detecting the changes in intensity, such as a photon counter, maintained at a fixed position can be used to measure the fluctuations in intensity. The rate of change of intensity is a function of the rate of diffusion of the particles which is as already stated a function of particle size.

### **2.2.1 Diffusion and the Stokes-Einstein Equation**

The diffusion coefficient of a particle is a measure of the rate at which it moves through the suspending fluid and it is also a function of particle size, fluid viscosity and temperature. Figure 3 shows Brownian motion schematically.

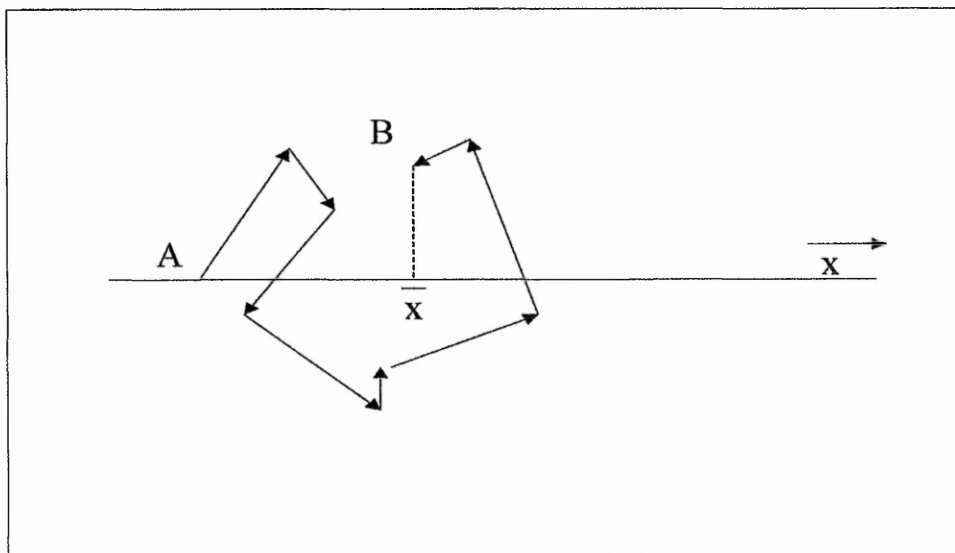


Figure 3. Random Movement Due to Brownian Motion

At time  $t$  the particle is at position A, at some time later  $dt$  it is at position B. Due to the erratic nature of the particle motion the mean distance  $\bar{x}$  will not increase linearly with time but with its square root,

$$\bar{x}^2 = Dt \quad 2.20$$

where  $D$  = Diffusion coefficient

The movement of a particle through a fluid is affected by its size and the viscous drag of the fluid as related by Stokes law, where  $F_d$  is the viscous drag

$$F_d = 6\pi\eta r\bar{V} \quad 2.21$$

and as  $\frac{\bar{x}}{t}$  is the mean velocity  $\bar{V}$  of the particle then,

$$F_d = \frac{6\pi\eta r\bar{x}}{t} \quad 2.22$$

where:  $\eta$  = fluid viscosity

$r$  = hydrodynamic particle radius

The viscous drag of the particle is also dependant on the kinetic energy  $E$  of the system by the relationship,

$$E = Fd\bar{x} \quad 2.23$$

and

$$E = kT \quad 2.24$$

where  $k$  = Boltzmann's constant ( $1.38 \times 10^{-23} \text{ J K}^{-1} \text{ mol}^{-1}$ )

$T$  = Absolute temperature in degrees Kelvin

thus 
$$E = \frac{6\pi\eta r \sqrt{\bar{x}^2}}{t} = kT = Fd\bar{x} \quad 2.25$$

Since the diffusion coefficient  $D = \frac{\bar{x}^2}{t}$  and  $r = \frac{d}{2}$

then

$$kT = \frac{6\pi\eta d D}{2} \quad 2.26$$

which when arranged for  $d$  yields

$$d = \frac{kT}{3\pi\eta D} \quad 2.27$$

which is the Stokes-Einstein equation

The Stokes Einstein equation implies conditions of ideality, such as an infinitely dilute dispersion and monodisperse spherical particles. Results obtained from this relationship are statistical in nature and therefore apply to the population of particles as a whole and not a single particle.

As the particles within the sample chamber undergo Brownian motion and the intensity of the scattered light fluctuates, the time scale of these fluctuations can be found by correlating sections of the output signal with themselves at different periods of time. This is termed "auto-correlation" and the auto-correlation function is defined as:

$$G(\tau) = \langle I(t) \cdot I(t+\tau) \rangle \quad 2.28$$

Where:  $I(t)$  = Intensity detected at time  $t$

$I(t+\tau)$  = Intensity detected at time  $t+\tau$

$\tau$  = delay time ( $\mu\text{s}$ )

$\langle \rangle$  = Average time

$G$  = auto-correlation function

If the value of  $G(\tau)$  is large then the correlation between the intensity at any instant is strong and means that the particles have not diffused very far during the measurement interval. If  $G(\tau)$  remains large for a long delay time, this indicates that the particles are slowly moving large particles.

Calculating the value of  $G(\tau)$  for a large range of delay times will give a quantitative measurement of the rapidity of the light fluctuations and this measurement, termed the decay time, is directly related to the particle size.

If the particles under observation are monodisperse, i.e. the same size, then the auto-correlation function of the scattered light intensity is a single decaying exponential.

For a fluid of a given viscosity at constant temperature, the rate of diffusion of a particle is inversely proportional to its diameter, in other words the smaller the particle the faster it will move, therefore only the temperature and the viscosity of the suspending fluid need to be known for the particle size to be calculated from the diffusion coefficient.

### **2.3 Pore Size Distribution**

For the calculation of pore size distributions it is generally accepted that the desorption branch of the isotherm be used on thermodynamic grounds. The exception to this rule are “bottle neck” pores which exhibit type IV

hysteresis, where the equilibrium isotherm corresponds to the adsorption branch due to the instability associated due to the inability of the adsorbate to evaporate in the wider portion of the pores until the narrow neck is emptied. Whichever branch of the isotherm is chosen the mathematical treatment of the data remains the same.

If nitrogen is used as the adsorbate then at its normal boiling point of 77 K the Kelvin equation can be written as

$$r_k = \frac{4.15}{\log(P/P_0)} \quad 2.29$$

where  $r_k$  is the Kelvin radius in Å into which condensation will occur at the selected relative pressure. The Kelvin radius is not the actual radius of the pore since some adsorption will already have occurred on the pore walls prior to condensation, therefore leaving a central core of radius equal to that of the Kelvin radius. During desorption this adsorbed film on the pore walls remains when evaporation of the central core takes place.

To calculate the actual pore radius it is necessary to know the thickness of the adsorbed film  $t$  since

$$r_p = r_k + t \quad 2.30$$

where  $r_p$  = pore radius and  $t$  = film thickness. It can be assumed that the depth of the adsorbed film will be the same on the pore walls as it is on a plane surface at the same value of the relative pressure  $P/P_0$ , therefore the film thickness  $t$  can be stated as

$$t = \left(\frac{W_a}{W_m}\right)\tau \quad 2.31$$

where  $W_a$  and  $W_m$  are the weight adsorbed at a specific relative pressure and the weight that corresponds to the BET monolayer respectively and  $\tau$  is the thickness of the monolayer.

The value of  $\tau$  may be calculated using the area  $S$  and volume  $\bar{V}$  that is occupied by one mole of liquid nitrogen if it were spread across a plane surface to the depth of one molecular layer.

$$S = (16.2)(6.02 * 10^{23}) = 97.5 * 10^{23} \text{ \AA}^2 \quad 2.32$$

$$\bar{V} = (34.6 * 10^{24}) \text{ \AA}^3 \quad 2.33$$

$$\tau = \frac{\bar{V}}{S} = 3.54 \text{ \AA} \quad 2.34$$

It should be noted that the value of 3.54 Å is significantly smaller than the diameter of a nitrogen molecule based on the cross sectional area of 16.2 Å<sup>2</sup>, 4.54 Å, but it is considered that the liquid structure is hexagonal close packed. It is now possible to rewrite the equation for  $t$  in the form

$$t = \left(\frac{W_a}{W_m}\right)3.54 \text{ \AA} \quad 2.35$$

For a non porous solid it has been shown that if  $W_a / W_m$  is plotted against  $P/P_0$  a common type II isotherm is described above a relative pressure of 0.3. This common curve is closely described by the Halsey equation which can be written for nitrogen as

$$t = 3.54 \left( \frac{5}{2.303 \log P_0 / P} \right)^{\frac{1}{3}} \quad 2.36$$

In order to calculate the pore size distribution it is useful to enter the desorption data into a worksheet similar to that shown in table 2.1. Columns 1 and 2 contain the data taken directly from the experiment, the relative pressures being selected to give small decrements at high values where  $r_k$  is very sensitive. Column 3 is the Kelvin radius  $r_k$ , and column 4 is the film thickness  $t$  calculated using the Hasley equation. Column 5 gives the pore radius from the equation  $r_p = r_k + t$ . Columns 6 and 7 are the average Kelvin radius  $\bar{r}_k$  and the average pore  $\bar{r}_p$  radius calculated from the mean difference of successive values. Column 8 is the change in film thickness  $t$  calculated from the difference of successive values of  $t$ . Column 9  $\Delta V_{gas}$  is the change in adsorbed volume between successive values of  $P/P_0$  and is calculated by subtracting successive values from column 2. Column 10  $\Delta V_{liq}$  is the liquid volume that corresponds to  $\Delta V_{gas}$ , this can be done by calculating the moles of gas and then multiplying by the liquid molar volume. For nitrogen at STP this is given by

$$\Delta V_{liq} = \frac{\Delta V_{gas}}{22.4 * 10^3} * 34.6 = \Delta V_{gas} (1.54 * 10^{-3}) cm^3 \quad 2.37$$

Column 11 is the change in volume of the adsorbed film that remains on the walls of the pores after evaporation from the centre core. This volume is the product of the film area  $\sum S$  (column 14) and the change in film thickness  $\Delta t$ , assuming that there are no pores present greater than 950 Å which

corresponds to a value of  $P/P_0$  0.99; the first value in column 10 is 0 since there is no film area from previously emptied pores.

	1	2	3	4	5	6	7	8	9	10	11	12	13	14		
nmHg	PF0	Mass (mg)	NE (g-g-1)	V	rk	t	ip	Avip	Avik	$\Delta$	$\Delta V$	$\Delta F$	$\Delta K$	$\Delta p$	$\Delta Sp$	$\Sigma \Delta Sp$
739399	0.999999	64.65	0.482798	385.5628	7244849	546.1113	7245395	3622804	3622523	529.7042	1.100132	0	1.100132	1.10032	6.07E-07	6.07E-07
724	0.992632	64.59	0.481422	394.8627	196.441	16.40705	2128481	147.1421	133.1277	4.786362	34.66415	1.86E-07	34.66415	42.33427	0.57542	0.575421
663	0.872368	62.7	0.483073	350.2085	69.81443	11.6217	81.43613	73.55927	62.39261	0.890073	24.38625	0.032779	24.35347	33.86005	0.920494	1.495915
639	0.840789	61.37	0.407589	325.8223	54.97078	10.73163	65.70241	57.25411	47.09373	1.142302	42.35507	0.109881	42.24639	62.44035	2.181187	3.677102
596	0.784211	59.05	0.354587	283.4672	39.21668	9.599129	48.80381	41.31022	32.35155	1.283944	90.94421	0.30145	90.64276	147.703	7.150916	10.82802
523	0.668158	54.1	0.240826	192.523	25.57345	8.305186	33.81463	30.11657	22.21524	0.789508	51.33948	0.547124	50.79235	93.44553	6.205163	17.03318
459	0.603947	51.3	0.176305	141.1835	18.90403	7.516577	26.42271	23.8118	16.62365	0.65105	14.66942	0.720357	13.94778	28.61783	2.403667	19.43365
391	0.514474	50.5	0.153257	126.5151	14.34328	6.857617	21.209	19.32263	12.74198	0.55398	9.901185	0.689035	9.212119	21.1845	2.192713	21.62965
323	0.425	49.95	0.145872	116.614	11.14038	6.313637	17.44437	16.20349	10.11049	0.415371	7.884277	0.574894	7.309283	18.78155	2.317685	23.94722
266	0.35	49.53	0.136009	108.7297	9.08302	5.888316	14.96862	13.88031	8.204885	0.405772	7.700921	0.621895	7.079026	20.28863	2.921263	26.86948
207	0.272368	49.11	0.126376	101.0288	7.329467	5.482544	12.81201	12.04605	6.723725	0.320429	6.234079	0.551004	5.683075	18.24119	3.028575	29.89705
160	0.210526	48.77	0.118578	94.73467	6.117983	5.162115	11.2801	10.67694	5.662885	0.276125	6.61079	0.528342	6.072448	21.66292	4.057889	33.95465
121	0.159211	48.41	0.110321	88.19389	5.187785	4.88899	10.07378	9.595287	4.827937	0.237278	5.684013	0.515533	5.16838	20.4149	4.255194	38.21014
90	0.118421	48.1	0.103211	82.50987	4.468087	4.648711	9.116798	8.471228	3.998383	0.351733	9.167164	0.880146	8.307617	37.23039	8.804081	47.01422
51	0.067105	47.6	0.091743	73.34211	3.52868	4.236978	7.826688	7.365313	3.208201	0.277733	8.230367	0.836573	7.415315	39.09389	10.61418	57.6284
28	0.036842	47.15	0.081422	65.09112	2.887723	4.019245	6.909688	6.489444	2.615425	0.270452	8.984408	0.937485	7.988924	49.32278	15.17754	72.80394
13	0.017105	46.65	0.070183	55.10571	2.345125	3.748794	6.09192	5.850761	2.189405	0.172875	7.150365	0.805526	6.345329	45.35494	15.50391	88.30995
7	0.009211	46.27	0.051239	48.96686	2.036683	3.575918	5.603601									

Table 2.1 Example of pore size calculation

## **3.0 Experimental**

### **3.1 Materials**

#### **3.1.1 Polymerisation Materials**

- Styrene 99%– Supplied by Sigma Aldrich Ltd, Gillingham, UK. Styrene was distilled under reduced pressure to remove the inhibitor prior to use
- Divinylbenzene 80% mixture of isomers– Supplied by Sigma Aldrich Ltd, Gillingham, UK. Washed three times with equal volume of 10% w/v of sodium hydroxide, then three times with equal volumes of double distilled water. Then distilled under reduced pressure
- Potassium Persulphate > 98% - Supplied by Fischer Scientific UK, Loughborough, UK. Recrystallised twice from double distilled water.
- Sodium metabisulphite >97% - Supplied by Fischer Scientific UK, Loughborough, UK. Used as supplied
- Sodium dodecylsulphate >97% - Supplied by Sigma Aldrich Ltd, Gillingham, UK. Used as supplied

#### **3.1.2 Additives**

- Toluene – 68%, Sigma-Aldrich Co. Ltd. Gillingham Dorset.
- Heptane – BDH Ltd. Poole, England
- Xylene - BDH Ltd. Poole, England

### **3.1.3 Water**

All water used throughout the project was prepared in the laboratory using an all pyrex double still.

### **3.1.3 Gases**

- Nitrogen – Supplied by BOC
- Helium – Supplied by BOC

### **3.1.4 Chitosan**

The chitosan used was kindly donated by Prof G. A. F. Roberts, Nottingham Trent University, Design of Materials Group, and was characterised for molecular weight and % deacetylation.

### **3.1.5 Jeffamine D2000**

Jeffamine D200 was kindly supplied by Robnor Resins Ltd., Swindon

## **3.2 Latex Preparation**

To ensure that good reproducibility is achieved between each polymerisation run the procedure and the conditions must be controlled meticulously. All glassware must be clean and free from contaminants. Initial trials were carried out to ensure repeatability and only after this had been achieved were latices prepared for use in the study.

The preparation of porous nanoparticles was based on the mechanism devised for the production of macroreticular resins, only rather than using suspension polymerisation particles were produced using a direct emulsion polymerisation. The organic phase of the reaction mixture consisted of the monomers and porogen and the aqueous phase contained the surfactant and initiator. Two techniques were used to produce porous nanoparticles, these being shaken polymerisation where polymerisation was carried out on a small scale in glass jars which were agitated by rapid side to side shaking and stirred reactions carried out in more conventional apparatus consisting of a Pyrex round bottom flask and agitation achieved by stirring with a PTFE paddle.

### **3.2.1 Shaken Polymerisation**

Prior to the preparation of the reaction mixtures all components were thoroughly out-gassed with nitrogen to purge them of oxygen. Oxygen is a scavenger for free radicals and if present in a free radical polymerisation will retard the progress of the reaction. All subsequent preparation was carried out under a nitrogen atmosphere. The reaction mixtures were prepared in several steps before addition to the reaction vessel. First the organic phase was prepared by mixing the monomers and porogen together in the reaction vessel, next the surfactant was dissolved in 75% of the aqueous phase, 25% being retained to dissolve the initiator and for washing the initiator in to the reaction vessel. Next the surfactant solution was added to the reaction vessel and was then mechanically homogenised using a Silverson mixer to produce an emulsion, further purging with nitrogen was carried out at this stage to

ensure that any oxygen that may have got into the mixture during homogenisation was removed. The flushed vessels were then sealed and the reaction mixture brought up to temperature and allowed to achieve thermal equilibrium. Further reaction mixtures were prepared to this point to ensure that all the vessels in each run had consistent preparation conditions. Once the reaction vessels reached thermal equilibrium the initiator which had been dissolved in the water retained from the preparation of the emulsion, was quickly added to the corresponding reaction vessel and the vessel was resealed. Polymerisation was carried out at 80°C for 8 hours in a Grant shaker water bath.

After the polymerisation was complete the jars were removed from the water bath, the lids were removed and the resulting latex filtered through glass wool to remove any large lumps of coagulum. Samples for percent solids determination and PCS analysis were taken at this point.

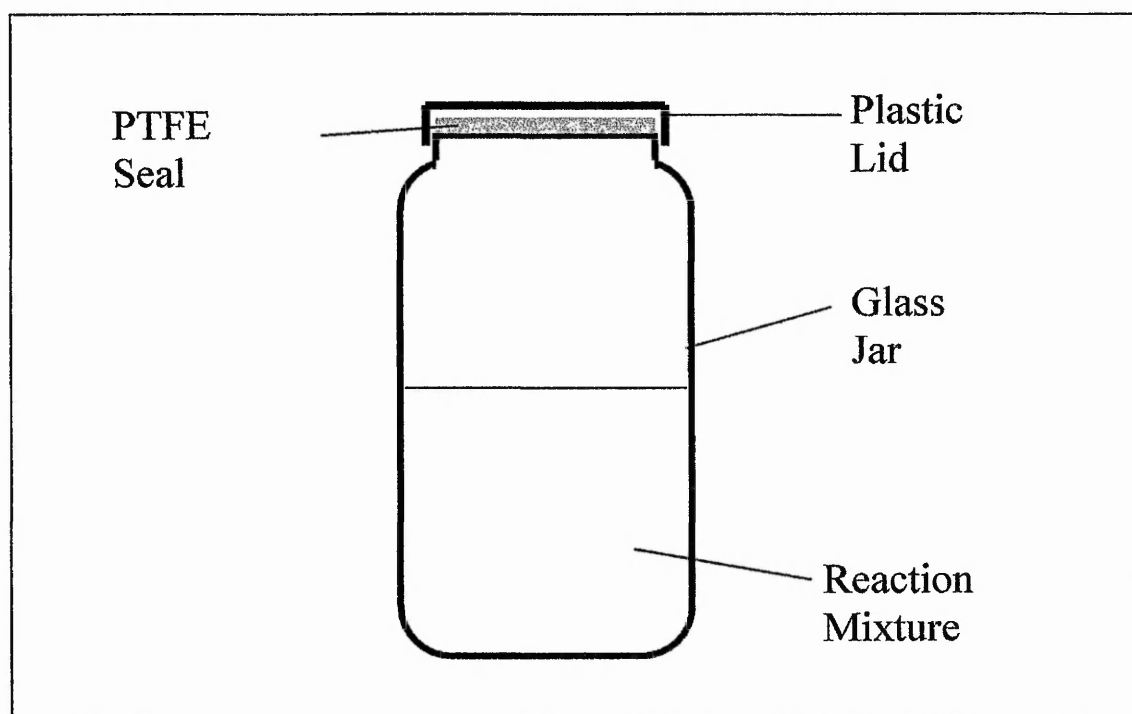


Fig.3.1 Shaken reaction vessel

### **3.2.2 Stirred Polymerisation**

All of the components were thoroughly out-gassed with nitrogen prior to the preparation of the reaction mixture to ensure complete removal of any oxygen. All subsequent steps in the preparation of the reaction mixture were carried out under a nitrogen atmosphere. First the organic phase was produced by adding the monomers and porogen to a conical flask, the surfactant was then dissolved in 75% of the water the remaining 25% being retained for dissolution of the initiator and for washing the initiator solution into the reaction vessel. The surfactant solution was then added to the organic phase and mechanically homogenised using a Silverson mixer to produce an emulsion. The emulsion was then transferred to the reaction vessel in this case a Pyrex three necked round bottom flask connected to a nitrogen inlet, a water cooled condenser and a PTFE stirrer. An air trap was fitted to the open end of the condenser to prevent any oxygen being sucked into the reaction vessel. The reaction mixture was allowed to reach thermal equilibrium at 80°C whilst having nitrogen flowing through the stirred system. Once thermal equilibrium was attained the nitrogen inlet was exchanged from a long feed which dipped under the surface of the reaction mixture to a short feed which sat above the surface, this prevented any build up of polymer on the end of the nitrogen feed causing a blockage. The initiator was added to the system by removing the air trap from the condenser and washing the initiator solution down the condenser and the air trap replaced. The reaction was then allowed to proceed for 8 hours.

Once the polymerisation was complete the resulting latex was filtered through glass wool to remove any large lumps of coagulum and samples for percent solids and PCS analysis were also taken at this point. The latex then moved on to the cleaning steps.

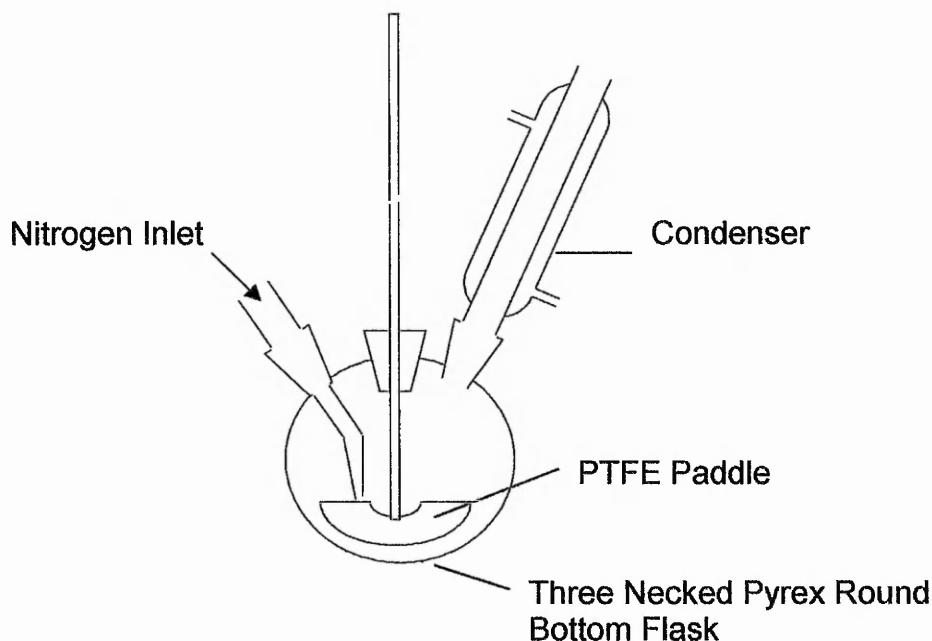


Fig. 3.2, Stirred polymerisation apparatus.

### **3.2.3 Dilatometry**

Dilatometry is a technique that allows a kinetic study of a reaction to be followed by observing the change in density, the change in density over time being directly proportional to the rate of reaction. However due to the small scale of the apparatus certain modifications in the preparation of the emulsion had to be made. All ingredients were flushed thoroughly with nitrogen prior to use to ensure complete removal of oxygen from the system, all subsequent preparation of the reaction mixture was carried out under a nitrogen atmosphere. The organic phase was prepared by mixing the monomers and

the porogen together in a conical flask. The aqueous phase was prepared by dissolving the surfactant in about 75% of the water and the initiator in the remaining 25%. The surfactant solution was then added to the organic phase and mechanically homogenised using a Silverson mixer, further purging with nitrogen was carried out at this point to ensure that no oxygen had been pulled into the system by the homogenisation process. The flask was sealed and placed in a water bath set to the reaction temperature and allowed to reach thermal equilibrium. Once the reaction mixture had reached thermal equilibrium the initiator was added and the mixture then quickly transferred to the dilatometer. Care must be taken at this stage to ensure that no air is introduced. The dilatometer stem was then fixed into place and the whole of the dilatometer apparatus transferred to a constant temperature water bath. The progress of the reaction could then be followed by observing the change in the height of the meniscus of the reaction mixture in the capillary over time. Using a cathetometer it is possible to record changes in the height of the reaction mixture in the dilatometer capillary to an accuracy of 0.01 mm. Agitation of the reaction mixture is achieved by placing a magnetic stirrer bar in the dilatometer prior to adding the reaction mixture, a magnetic stirrer placed under the water bath can then be used to agitate the system.

At the end of the polymerisation process the resulting latex was filtered through glass wool to remove any large lumps of coagulum and sample for percent solids and PCS analysis were taken at this point.

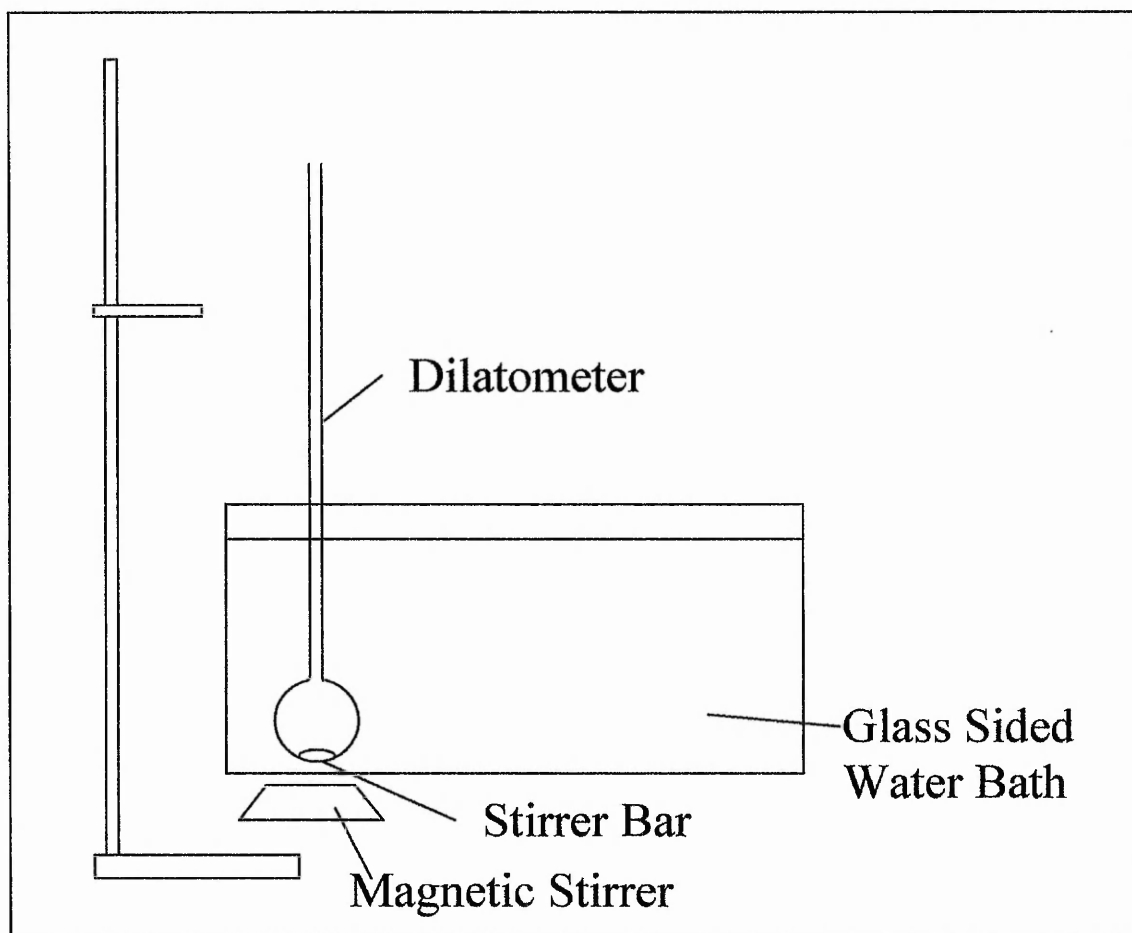


Fig 3.3 Kinetic apparatus

This technique was satisfactory for producing latices from styrene however when divinylbenzene was introduced into the system significant difficulties arose due to cavitations within the dilatometer bulb which caused gas to be trapped in the capillary leading to unreliable measurements. Recent studies on preparing surfactant free emulsions and cavitation at hydrophobic surfaces<sup>156,157,158</sup> have highlighted the importance of removing dissolved gases from the aqueous phase, which improves the stability of emulsions. The removal of dissolved gas requires several repetitions of a freeze thaw process carried out under vacuum. This was achieved by placing the prepared

emulsion in ice then evacuating the vessel using a water pump over a two hour period, the prepared emulsion was then removed from the ice and whilst still being pumped out allowed to return to room temperature. Once at room temperature pumping was continued for 30 minutes and then the freeze thaw routine repeated. Whilst more care was needed in preparing the reaction mixtures for styrene / divinylbenzene copolymerisation this technique improved the results dramatically, allowing the reaction to be followed with confidence.

The information gathered from the dilatometry experiments was used to calculate the value of  $\bar{n}$  in order to assign Smith –Ewart case 1, 2 or 3 to the system. In order to do this a worksheet was designed. A typical worksheet is shown in table 4.12. Column 1 is the ratio of sodium metabisulphite to potassium persulphate in the redox couple. Column 2 is the rate of polymerisation,  $R_p$ , calculated from:

$$R_p = \frac{\pi r^2 D}{0.154 * 60 * 104.5 * v} * 1000 \quad 3.1$$

where D is the rate of contraction in  $\text{cm min}^{-1}$ , r is the radius of the capillary stem of the dilatometer and v is the total volume of the dilatometer bulb and stem. Column 3 is the mean particle size obtained from PCS analysis of the final latex. Column 4 is the number density of particles calculated from:

$$N_d = \frac{\text{mass of styrene}}{\text{mass of 1 particle}} \quad 3.2$$

$$\text{with the mass of 1 particle} = \frac{4}{3}\pi\left(\frac{d}{2} * 10^{-7}\right)\rho^3 \quad 3.3$$

Where  $d$  is the particle size from column 3 and  $\rho$  is the density of styrene.

Column 5 is  $\bar{n}$  and is calculated from

$$\bar{n} = \frac{R_p N_A}{k_p [M] N_d * 1000} \quad 3.4$$

$$\text{where (Propagation rate constant) } k_p = 10^{7.04} \text{Exp}\left(\frac{-29500}{(8.314(T + 273))}\right) \quad 3.5$$

$$\text{( Monomer concentration) } [M] = \left(\text{Exp}\left(\frac{1}{T + 273}\right)\right) * .205381 \quad 3.6$$

$N_A$  = Avogadro's number

### **3.3 Cleaning**

For the study of model colloids it is necessary first to remove all of the residual components of the reaction mixture such as unreacted monomer, low molecular weight polymer, residual initiator fragments and surfactant before further study is undertaken. In the case of porous nanoparticles it is also necessary to fully remove the porogen component to develop the full porosity. This requires quite a complex cleaning process involving several stages.

### 3.3.1 Continuous Liquid / Liquid Extraction

In order to remove any low molecular weight polymer the latices were first extracted with 2,2,4 trimethylpentane (iso-octane). This was achieved by continuous liquid / liquid extraction over 9 hours using the apparatus illustrated in Fig.3.4.

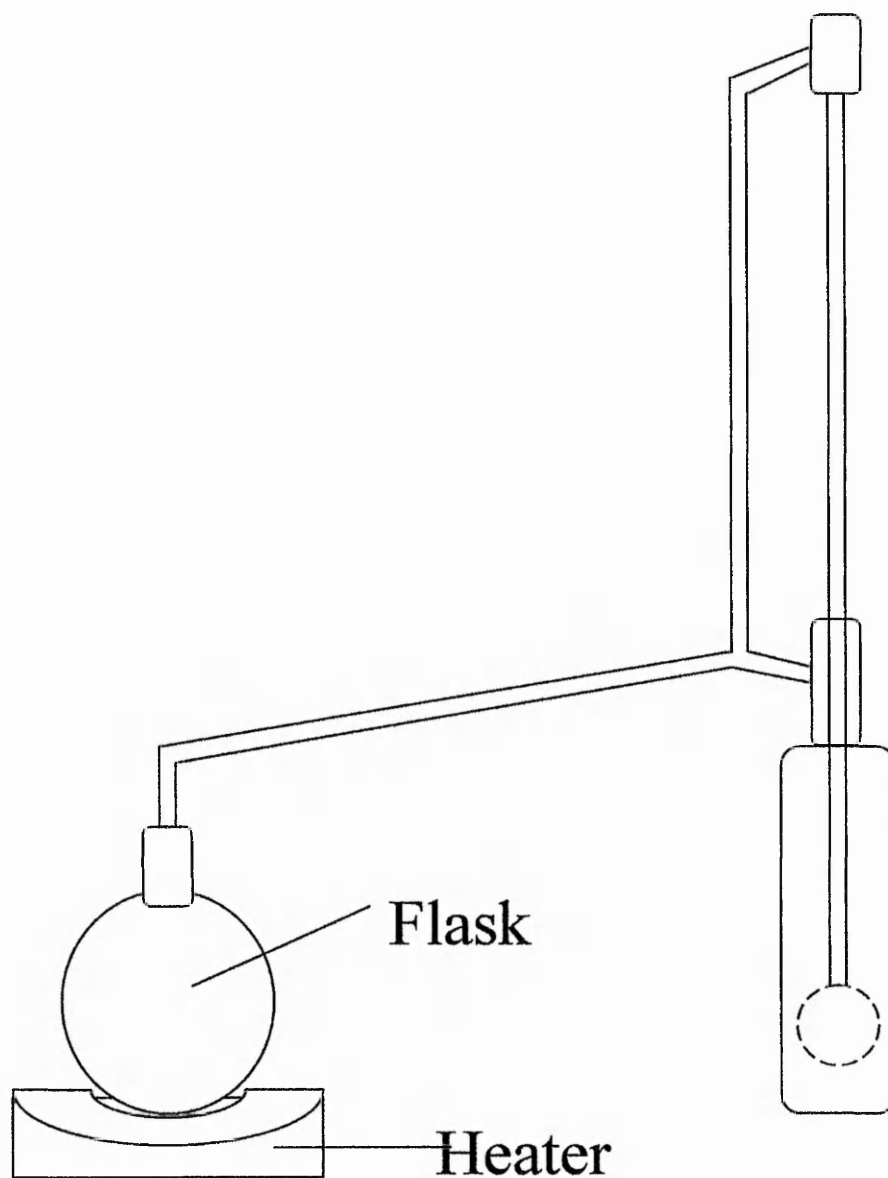


Fig. 3.4 Liquid / liquid extraction apparatus

### **3.3.2 Steam Distillation**

The next step in the cleaning of the porous nanoparticles was to remove any unreacted monomer, the porogen component and also to remove any residual 2,2,4 trimethylpentane from the aqueous dispersion. This was achieved using a rotary evaporation apparatus under reduced pressure. Care must be taken not to boil the aqueous dispersion too vigorously as this can lead to rapid evaporation leaving the solid latex in too small a volume of water to maintain colloidal stability. As the evaporation proceeds fresh water must be added to maintain a similar percent solids as the starting latex. The latex was deemed to be clean after the total volume of the aqueous phase had been changed four times and no organic extract could be detected.

### **3.2.3 Dialysis**

The final stage of cleaning of the porous polymer latices was by dialysis. The latex was placed in a length of semi-permeable membrane (Visking dialysis tubing) that had been previously activated by boiling twice in double distilled water. The ends of the dialysis tube were closed and then immersed in double distilled water. The tubing was agitated occasionally by stirring and the water changed at least once a day, more frequently during the early stages of dialysis, until the wash water maintained the same conductivity of pure double distilled water for 24 hours. After cleaning a further sample of the latex was taken for PCS analysis.

### **3.3 Drying**

For further study, such as surface area and nitrogen adsorption analysis, it was necessary to obtain a dry sample of the latex. This was achieved by freeze drying a sample of the latex on an Edwards freeze dryer. A portion of the wet latex was transferred to a round bottom flask. The latex was immobilised by freezing it to the inside of the flask by gently rotating it in a slush bath containing methylated spirits cooled to  $-80^{\circ}\text{C}$  with liquid nitrogen. The immobilised sample was then attached to the freeze dryer apparatus and allowed to dry at reduced pressure until a fine free flowing white powder was achieved.

### **3.4 Latex Characterisation**

#### **3.4.1 Particle Size Determination**

##### **3.4.1.1 Photon Correlation Spectroscopy**

As has been stated earlier two samples were taken for PCS analysis, one at the end of the polymerisation and one after the cleaning process had been completed. PCS analysis was carried out on a Coulter N4 Plus sub micron particle size analyser supplied by Beckman – Coulter Ltd.

Samples needed to be carefully prepared to avoid any contamination from dust or any other airborne particles, the water used for diluting the samples had previously been filtered through a  $1\mu\text{m}$  Millipore filter and kept in a clean stoppered flask. The sample cuvettes were also kept sealed to

prevent contamination. Samples were prepared from the latex by diluting with double distilled water until the conditions within the sample cuvette reached those required by the instrument with an intensity between  $5e^{+4}$  and  $1e^{+6}$ . The cuvette was then closed and placed in the sample holder. The sample was allowed to reach thermal equilibrium before any measurements were taken. Measurements were made at a  $90^\circ$  angle with sample times of 5 minutes.

#### **3.4.1.2 Electron Microscopy**

Samples of the latex were dried onto a sample grid, and the dried grids were analysed on a Joel 2010 Transmission electron microscope. Digital images were obtained via a CCD camera.

#### **3.4.2 Surface Area Determination**

Surface area measurements were made on a Quatasorb apparatus (Quatachrome Ltd). A sample of the dried polymer was accurately weighed into the sample holder, the sample and holder were then transferred to the Quatasorb apparatus and a dynamic flow of helium was passed over the sample whilst it was heated at  $100^\circ\text{C}$  until the thermal conductivity detectors response settled back to zero. This outgassing at elevated temperature was performed in order to ensure that all moisture and any adsorbed species on the surface of the polymer had been removed from the sample prior to the determination of the surface area.

The outgassed sample was then ready for surface area measurements to be made. Nitrogen was passed over the sample in a helium carrier; the

partial pressure of the nitrogen could be altered by adjusting the flow rates of the two gases. At the required partial pressure ( $P/P_0$ ) the sample holder was immersed in liquid nitrogen. This enabled nitrogen from the carrier stream to be adsorbed onto the surface of the sample, once equilibrium has been reached the liquid nitrogen was removed and the sample warmed to room temperature. This drives the adsorbed nitrogen off the sample and the thermal conductivity bridge will register a response. The response from the conductivity bridge can be converted to the quantity of nitrogen by injecting a calibration shot of nitrogen of known volume into the carrier stream and recording the subsequent response from the thermal conductivity bridge. This procedure was repeated five times for partial pressures in the region of 0.1 to 0.3. Linear regression was carried out on the resulting straight line portion of the desorption isotherm and a further check on the accuracy of the results was done by examining the  $R^2$  value, if the  $R^2$  value was below 0.98 then the experiment was repeated. The results obtained were then incorporated into the BET equation and the total surface area calculated for the sample under test.

The results obtained gave the total surface area of the sample. To gain an idea of the additional surface created by introducing pores into the latex it was necessary to take the particle size determined by PCS and calculate the surface area associated with a non-porous sphere of the same particle radius using the equation.

$$S = \frac{6}{d_{vs} \rho} \quad 3.7$$

Where:

$S$  = Surface area

$d_{vp}$  = Mean volume to surface diameter

$\rho$  = Density of the particle

Assuming monodispersity  $d_{vs}$  becomes the mean particle diameter obtained from the PCS measurements

### **3.4.3 Nitrogen Adsorption / Desorption Isotherms**

Full adsorption and desorption isotherms for nitrogen at 77K were determined using a vacuum frame. The basic components of the vacuum frame are illustrated in Fig. 3.5. The main feature of the frame is an enclosed microbalance that can be completely evacuated of air.

The sample is placed in a bucket at the end of a drop tube that facilitates immersion in liquid nitrogen to cool the sample and its surrounding area to  $-77\text{K}$ . Prior to determining the isotherm the sample was first out-gassed at room temperature and under a vacuum of  $5 \cdot 10^{-3}$  mm Hg for several hours until constant weight was achieved, this was done to ensure that any moisture was completely removed from the system and that the surface of the sample was clean. Once this point had been reached the sample and the counterbalance tubes were immersed in liquid nitrogen and allowed to reach thermal equilibrium. It is important that the level of liquid nitrogen is sufficiently high up both the sample and the counterbalance tubes to negate buoyancy effects. When the system has reached thermal equilibrium nitrogen is introduced in small increments and the weight of nitrogen adsorbed measured

at each pressure point. It is important to allow sufficient time for the system to reach equilibrium because in solids with very small pores nitrogen adsorption into the pores is dependant on diffusion, thus each step was only recorded when the mass of adsorbed nitrogen had remained steady for five minutes.

The desorption branch of the isotherm was generated by reducing the pressure in the system and allowing the nitrogen to desorb. Readings were taken when both the pressure and the weight reached a constant value that was stable for five minutes.

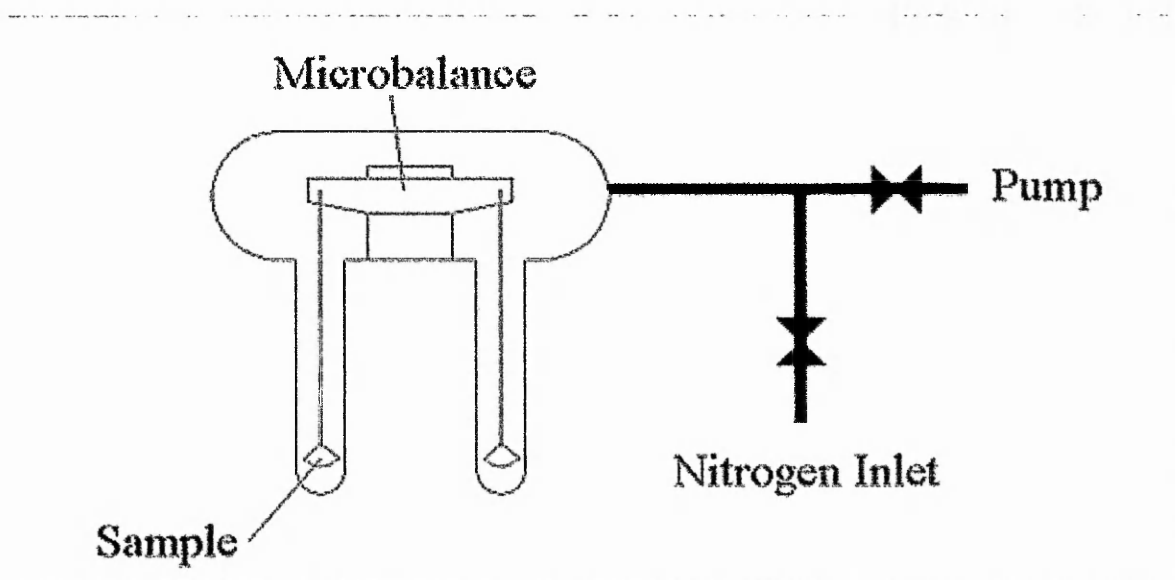


Fig. 3.5 Vacuum frame apparatus for deriving nitrogen adsorption / desorption isotherms.

#### **3.4.4 Nonane Preadsorption**

A simple way to evaluate the microporosity of a sample is to fill the micropores up with an adsorbate leaving the free surface and any pores larger than micropores free. Gregg and Langford<sup>159</sup> found that *n*-nonane could be used as its rate of removal from micropores is very slow.

Nonane preadsorption was achieved by exposing the sample under test to *n*-nonane vapour by suspending the sample above a reservoir of *n*-nonane inside a sealed vessel. The vessel was then evacuated of air. This allowed the atmosphere inside the vessel to become saturated with *n*-nonane vapour. The samples were left for 48 hours to ensure full adsorption of the vapour had been achieved.

### **3.5 Chitosan Characterisation**

Three samples of chitosan were available for study, one of very low molecular weight and two others with relatively low molecular weights but substantially higher than that of the first. It is important that these samples were characterised for both molecular weight and degree of *N*-acetylation.

#### **3.5.1 Molecular Weight Determination**

The molecular weight of the chitosan samples was determined by viscometry. The flow times of several solutions of chitosan of varying concentration were measured using a suspended level viscometer of modified Ubbelohde type. The solvent system for the dissolution of the chitosan samples consisted of 0.1 M acetic acid and 0.2 M sodium chloride. The viscometer was thoroughly rinsed with the sample and then placed in a constant temperature water bath set to 25°C and allowed to achieve thermal equilibrium. Once thermal equilibrium had been achieved the flow time for the sample was measured; measurements of the sample flow time were repeated

until three consecutive readings were made within 0.2 s of each other. From these readings it was then possible to calculate the viscosity number for each of the samples using the equation.

$$\text{Viscosity number} = [(t_{\text{sample}}/t_{\text{solvent}}) - 1] / \text{concentration} \quad 3.8$$

where the concentration is in  $\text{g l}^{-1}$ . A plot of viscosity number against time should yield a straight line. Extrapolating back to a concentration of 0 yields the limiting viscosity number and this can be related to the average molecular weight, AMW, by the equation.

$$\text{Log AMW} = (\text{Log LVN} - \text{Log}(1.81 \cdot 10^{-3}))/0.93 \quad 3.9$$

This gave average molecular weights of:

Sample	Molecular Weight
Chitosan (Low Molecular Weight)	$1.3 \cdot 10^2$
Chitosan 2	$4.01 \cdot 10^2$
Chitosan 3	$6.2 \cdot 10^2$

Table 3.1

### **3.5.2 Determination of the degree of *N*-acetylation**

The degree of *N*-acetylation of the chitosan samples was determined by dye adsorption. When chitosan is treated with dilute acetic acid protonation of the amine groups along the polymer chain occurs. These groups can then act as dye sites for anionic dyes. Although chitosan is normally soluble in dilute organic acids it is not soluble if the acid solution contains an excess of anionic dye<sup>160</sup>. This effect allows for the determination of the concentration of the amine groups and thus the degree of *N*-acetylation.

#### **3.5.2.1 Purification of CI Acid Orange 7**

As the amine groups within the chitosan chain form a 1:1 stoichiometry with ionic dyes it is important that with any technique utilising this phenomena that there are no competing species present, thus it is vital that the dye used to determine the degree of *N*-acetylation is of very high purity. It was therefore necessary to purify the dye to a high degree before use. A sample of commercially supplied CI acid orange 7 was extracted using boiling methanol in a Soxhlet apparatus. Refluxing of the methanol was continued until the concentration in the receiver flask reached saturation, i.e. crystals of dye began to appear in the receiver flask. At this point the refluxing was terminated and the receiver flask removed from the apparatus, sealed and placed on a cork ring. Once the flask had cooled sufficiently it was placed in a refrigerator for 24 hours. The recrystallised dye was then filtered off washed with methanol and dried under vacuum.

### **3.5.2.2 Determination of the degree of N-acetylation by Dye Adsorption**

Chitosan (0.2 g) was accurately weighed into a conical flask with a ground glass stopper. A stock dye solution prepared from purified CI acid orange 7 ( $1.75 \text{ g l}^{-1}$ ) in 0.1 M acetic acid to give a  $5 \times 10^{-5} \text{ M}$  solution, 200 ml aliquots of the solution were then added to the conical flask containing the chitosan and a blank containing just the dye solution was also prepared for reference purposes. The flasks were stoppered and placed in a water bath set to  $60^\circ\text{C}$  and allowed to achieve thermal equilibrium. Once thermal equilibrium had been achieved the pressure in the flask was released by briefly lifting the stoppers and the flasks sealed using laboratory film. The flasks were left at temperature for 16 hours to allow the adsorption process to reach equilibrium. The flasks were then removed from the bath one at a time and the content filtered through glass wool, this must be done quickly to avoid any diffuse adsorption of the dye as the flask and contents cool. The filtered solutions were also sealed to avoid evaporation. Once the filtered solution had cooled to ambient temperature the adsorbance of each solution and the blank was measured at 484 nm using a Helios Delta UV / visible spectrophotometer, using 0.1 M acetic acid to set the zero and the blank dye solution was used as the reference (a dilution factor of 100 is normally necessary). The degree of N-acetylation was then calculated using the formula:

$$EW = (w \cdot 22500) / (\Delta A \cdot f \cdot V) \quad 3.10$$

where:

EW = Equivalent weight of amine groups

w = Oven dry weight of chitosan

22500 = Extinction coefficient of Acid Orange 7

$\Delta A$  = Difference between the absorbance of the reference and the sample

f = dilution factor

V = Volume of solution in litres

The degree of *N*-acetylation can then be calculated:

$$\% = [(EW-161)*100]/(EW+42) \quad 3.11$$

Where 161 and 42 are the weights of the acetyl and amine groups respectively

### **3.6 Vapour Adsorption**

Vapour adsorption experiments were carried out on a similar apparatus as used for nitrogen adsorption except that the nitrogen source was exchanged for a vessel containing the volatile under study. Adsorption measurements were made at 298 K instead of 77 K as for nitrogen by surrounding both the sample tube and the counterweight tube with water kept at constant temperature using a thermostated circulating system. Saturation vapour pressure  $P_0$  was calculated for each of the volatiles under study using the Antoine equation:

$$\log_{10}(P) = A - (B / (T + C))$$

3.12

Where:

P = Vapour pressure

T = Temperature (K)

and the parameters A, B and C were obtained from the literature for each of the volatiles.

Volatile	A	B	C
Pentane <sup>161</sup>	3.9892	1070.617	-40.454
Methanol <sup>162</sup>	5.15853	1569.613	-34.846
Toluene <sup>163</sup>	4.23679	1426.448	-45.957

Table 3.2 Antoine Equation Parameters

The samples were pumped under a vacuum of  $5 \times 10^{-3}$  mm Hg for 8 hours at room temperature to ensure that all moisture was removed from them and that their surfaces were clean. The circulator was left running to ensure that thermal stability was achieved before any measurements were taken. Vapour was slowly added to the system and the increase in the sample mass recorded as well as the pressure. Measurements were only recorded once both the mass and the pressure readings remained steady for five minutes. Desorption isotherms were also made by slowly evacuating the system and recording the reduction in the sample mass and the final pressure

of the system, again measurements were not recorded until both the mass and pressure remained stable for five minutes.

In vapour adsorption experiments it is very important to ensure that all vapour is expelled from the system before a new sample is introduced. Due to the nature of the volatiles under study the system was cleaned after each run by removing the sample and replacing it with a sample of activated carbon, the system was then evacuated to  $5 \cdot 10^{-3}$  mm Hg and the sample immersed in liquid nitrogen for 2 hours. The liquid nitrogen was then removed and the system was then brought up to atmospheric pressure by introducing nitrogen. This was repeated three times to ensure any residual vapour was removed prior to a new sample being introduced. It was also found necessary to replace some of the seals within the vacuum system when changing volatiles due to degradation of the seals.

Plots of  $P / P_0$  against amount of volatile adsorbed were produced to give isotherms in the same way as those produced for nitrogen.

### **3.7 Functionalisation of particles with chitosan**

Two methods for functionalising the particles with chitosan were investigated. Direct polymerisation in which the chitosan was included at the beginning of the polymerisation and post polymerisation were the final latex was subjected to a coating process.

### **3.7.1 Polymerisation in the Presence of Chitosan**

When chitosan was included in the polymerisation process, the polymerisations were carried out in both the stirred reactors and shaken reactors the only difference between these polymerisations and those carried out in the absence of chitosan was that in place of the water used to produce the aqueous phase of the emulsion a solution of chitosan dissolved in 0.1 M acetic acid was used instead.

### **3.7.2 Post Polymerisation Coating of Particles with Chitosan**

For the production of particles functionalised by chitosan after polymerisation was complete the following steps were taken.

After polymerisation the latices were cleaned in the usual manner (see section 3.3 for details). These latices as aqueous colloidal dispersions were then stirred in a solution of chitosan dissolved in 0.1 M acetic acid. After the required time of stirring the latices were transferred to a centrifuge tube and spun down, the supernatant was then decanted off, replaced with double distilled water and the spinning down process repeated. The alternate steps of spinning down and washing with fresh double distilled water were continued until the conductivity of the supernatant decanted off was the same as that of the fresh double distilled water. These spinning / decantation steps were necessary to ensure that only chitosan that had been adsorbed on to the particles remained as any chitosan remaining in the supernatant would simply be deposited when the samples were freeze dried.

### **3.8 Characterisation of Chitosan Containing Latices**

To evaluate the effectiveness of the two methods of functionalising the latices with chitosan it was necessary to positively confirm the presence of chitosan and also to try and assess the quantity of chitosan present in each sample.

#### **3.8.1 Infrared Spectroscopy**

The energies associated with infrared (IR) radiation cause vibrations, either of the whole molecule or of individual bonds within a molecule when it is irradiated. If we consider a simple chemical bond X-Y, this can be approximated to two spheres connected via a spring and will therefore obey Hooke's law, When the bond is subjected to IR radiation stretching of the bond will occur, the frequency of the vibration (stretching) will be directly proportional to the strength of the bond and the masses of both X and Y. As a consequence of this different bonds within a molecule will vibrate at different frequencies depending on the nature of the bond, thus many different organic species can be easily identified from their IR adsorption properties.

The species of most interest in chitosan is the amine group as this group is a highly reactive species, Amine bonds show up in the infrared spectrum at a frequency around  $3500-3000\text{ cm}^{-1}$ . As there are no species in the polymer that produce a peak in this region of the IR spectrum it is a convenient method for detecting the presence of chitosan in the sample. Care

must be taken however to ensure that moisture is kept out of the instrument as O-H bonds also show a peak in this area.

In order to obtain IR spectra of the samples it was first necessary to support (a small amount of) the sample under study in a KBr disc. The disc was produced by mixing a small amount of the sample with finely ground dry KBr and subjecting this to a pressure in the region of  $10\,000\text{ Kg m}^{-2}$ . It was not possible to suspend a sample of pure chitosan in a KBr disc as the particle size of the chitosan sample was too large and further grinding of the sample proved to be difficult. To obtain spectra from pure chitosan it was necessary to cast a thin film from a solution of chitosan in 0.1 M acetic acid onto a clean and flat glass plate, the film was then dried in an oven. When dry the film was neutralised by immersing the plate in 0.1 M ammonia followed by several rinsings with fresh double distilled water, before being returned to the oven and redried. This film could then be analysed directly in the instrument.

### **3.8.2 Dye Adsorption**

A similar technique to that used for determining the degree of *N*-acetylation for chitosan was employed to evaluate the quantity of available amine groups available on the polymer surface. The technique is fully described in section 3.5.2.2 except that instead of 0.2 g of chitosan 0.2 g of chitosan containing dried polymer was used. The same equation was employed to give the amount of available amine groups expressed as a percentage of the total polymer.

### **3.9 Conductometric titration**

The concentration of accessible sulphonate groups within the porous nanoparticles was determined by conductometric titration. The porous nanoparticles were first protonated by washing with 0.05 M HCl within a microfiltration cell. The serum was changed several times with fresh HCl to ensure full protonation of the latex and then exchanged with double distilled water until the conductance of the serum leaving the microfiltration cell matched that of the double distilled water entering the cell.

Before titrating it was necessary to obtain the % solids content of the latex dispersion, this was done gravimetrically. 50 cm<sup>3</sup> of the latex dispersion was then titrated with 0.05 M NaOH. The surface charge was calculated in the same manner as used by Chainey *et al*<sup>164</sup>.

### **3.10 Films**

Hodges<sup>165</sup> has previously shown that a porous film can be produced by incorporating a soluble diluent within the film prior to casting. A similar technique was initially tried to incorporate porous nanoparticles into a film, however it was found that the films produced in this manner were very brittle and were not suitable for further use. Therefore an alternative approach was employed. A polybutylmethacrylate film was first cast onto a clean glass slide and dried, next a dispersion of porous nanoparticles was cast over the PBMA film and the slide placed in an oven set at a temperature slightly above that of the critical film forming temperature of PBMA, this allowed the surface of the

PBMA film to become tacky and for the porous nanoparticles to adhere to the surface of the film. Any excess porous nanoparticles were rinsed off when the film was dry, and the film finally dried at a low temperature and re-weighed to give the weight of porous nanoparticles present in the film.

### **3.11 Hydrolysis of Ethyl Formate**

The catalytic properties of the redox initiated porous latex particles were evaluated by their ability to catalyse the acid hydrolysis of ethyl formate by the sulphonate groups introduced into the particles. This reaction results in the production of formic acid which can be followed by conductometric titration.

Films prepared as described in section 3.10 were introduced into 100 ml of double distilled water in a conical flask which was then mechanically stirred. Once thermal equilibrium was achieved 1 ml of ethyl formate was introduced and the change in conductance with time recorded.

## **4.0 Results and Discussion**

### **4.1 Porous Latex Nanoparticles**

#### **4.1.1 Introduction**

The preparation of porous latex nanoparticles has been based on the methods used in the production of coarse macroreticular resins. Macroreticular resin beads have a diameter in the region of 10  $\mu\text{m}$  and are produced by suspension polymerisation whereas the porous latex nanoparticles reported here are much smaller, typically of the order of 50 nm and are produced directly by cross-linking emulsion co-polymerisation.

In the case of macroreticular resin production the effect on the porosity and final character of the beads can be controlled by varying the reactants used. In order to evaluate the production of porous latex nanoparticles a systematic investigation into the effect of each of the reaction components was carried out.

The basic components of the polymerisation reaction are initiator, surfactant, monomers and porogen. For each component a series of polymerisations were carried out in which the component under study was varied whilst maintaining the concentration of all the others at constant levels. The reproducibility of the polymerisation reactions was examined by repeating the runs several times.

Polymerisation was carried out in a shaken reaction vessel. Comparison of the results obtained for shaken polymerisations with a more

conventional stirred method showed that the final product obtained from the shaken system was the same as those produced using a stirred reactor.

## 4.1.2 Effect of initiator Concentration

### 4.1.2.1 Potassium Persulphate

In this series of experiments the effect on particle size and surface area of the final latex was examined in relation to the concentration of the initiator, potassium persulphate, by maintaining a constant concentration of all the reaction components apart from the potassium persulphate.

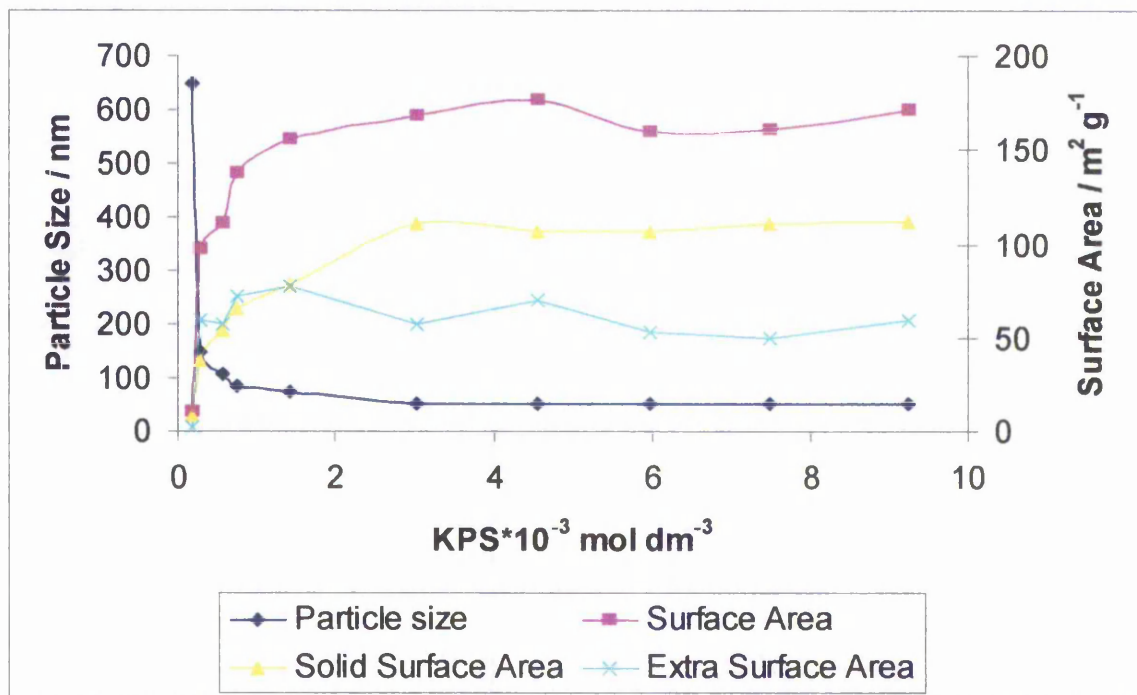


Fig. 4.1. Effect of initiator potassium persulphate concentration on surface area and particle size. Styrene / divinylbenzene ratio = 1:1, monomer to porogen (toluene) ratio = 1:0.5, surfactant (sodium dodecylsulphate) = 0.014 mol dm<sup>-3</sup>. Surface area = BET surface area, solid surface area = surface area of a smooth sphere of equal size, extra surface area = additional internal surface area.

Fig 4.1 shows the specific surface area found experimentally, the surface area calculated from the particle size for a non-porous sphere of equal size and by difference the additional surface area arising from the internal pore network. It can be seen from Fig. 4.1. that the initiator concentration only has an effect at very low concentrations and once a concentration of approximately  $1.5 \times 10^{-3} \text{ mol dm}^{-3}$  is reached additional potassium persulphate has little effect on either the surface area or the particle size of the final latex. This would suggest that at concentrations below  $1.5 \times 10^{-3} \text{ mol dm}^{-3}$  not all of the monomer containing micelles are initiated which results in a lower number of growing particles. This will lead to an increase in particle size, as there is still a large supply of available monomer and a reduced number growing particles. This will result in particles of lower specific surface area, however as can be seen there is still a significant amount of additional surface area developed as the initiator concentration tends towards  $1.5 \times 10^{-3} \text{ mol dm}^{-3}$ . As the potassium persulphate concentration increases the additional internal surface area developed also increases, and since the rate of reaction will be slower at low concentrations, then the development of additional internal surface may be linked with rate of reaction.

At potassium persulphate concentrations above  $1.5 \times 10^{-3} \text{ mol dm}^{-3}$  there is no further effect on either particle size or surface area which would suggest that all of the available loci for reaction are initiated leading to a constant number of growing particles and no further development of additional internal surface area occurs.

From this evidence it would suggest that whilst the rate of polymerisation is important in the formation of the porous structure the

potassium persulphate concentration does not affect the formation of a porous structure provided that a limiting value is exceeded.

All of the latices produced went to completion with conversion to polymer above 95% and with very low levels of coagulum, with reproducibility being good, typically particle size +/- 5 nm and surface area +/- 20%. The polydispersity index from photon correlation spectroscopy was typically 0.1 – 0.2.

#### **4.1.2.2 Redox Initiator**

The initiation of emulsion polymerisation reactions with a redox couple consisting of potassium persulphate and sodium metabisulphite was also examined for the production of porous latex nanoparticles. Although this method of initiating polymerisation reactions has been known for many years first patented as early as 1940<sup>166</sup>, there are still aspects of the system, such as the optimum ratio of the redox components, which are not fully understood. When a redox couple is used to initiate an emulsion polymerisation reaction the rate of reaction depends on the ratio of the two components. A fuller investigation into the redox couple will be dealt with in the kinetics section, here the results obtained for particle size and surface area are presented.

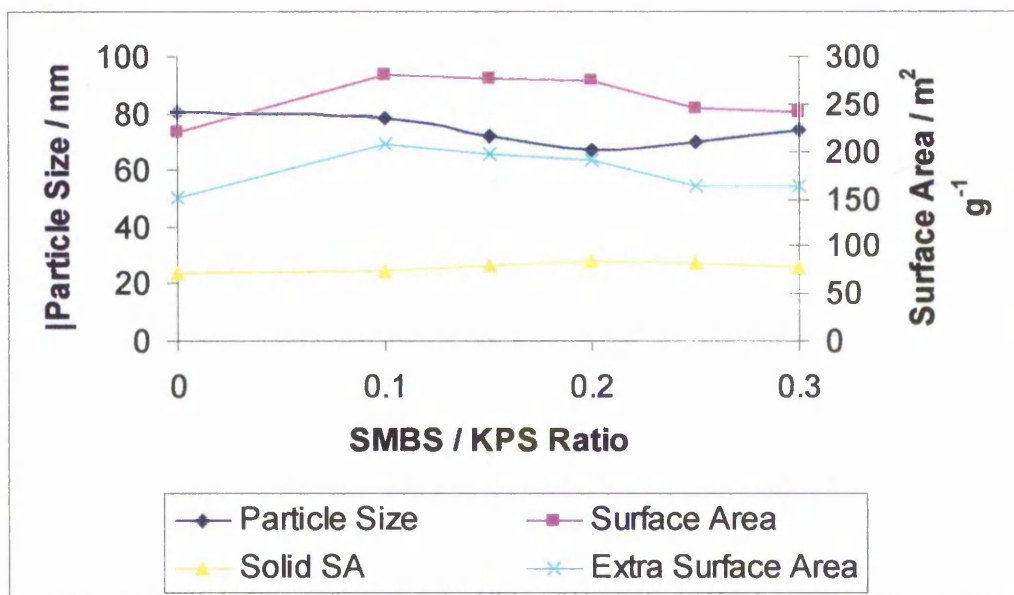


Fig. 4.2. Effect of redox couple ratio on surface area and particle size, potassium persulphate =  $7.0 \times 10^{-3} \text{ mol dm}^{-3}$ , styrene / divinylbenzene ratio = 1:1, monomer porogen (toluene) ratio 1:0.5, sodium dodecylsulphate  $0.014 \text{ mol dm}^{-3}$ , temperature =  $80^\circ\text{C}$ .

From Fig. 4.2. it can be seen that although the redox couple ratio has only a small effect on the particle size of the resulting latex there is a more noticeable effect on both the final surface area and thus the additional surface area (the surface area above that expected for a solid sphere of equal diameter). As the potassium persulphate concentration is well above the limiting value discussed above it is assumed that all of the loci available for initiation have been initiated but as will be discussed in the kinetics section the use of the redox couple gives rise to an increase in the overall rate of reaction. This can be seen in the increase of both total surface area and additional surface area upon introduction of the sodium metabisulphite component of the redox couple. Also of interest is the fact that there appears to be an optimum ratio of the two components of the redox couple which gives rise to a maximum surface area. This maximum occurs when the ratio of the two components is approximately 0.1.

All of the redox initiated polymerisation reactions went to completion with conversion of monomer to polymer above 95% with very low levels of coagulum being produced.

#### **4.1.2.3 Oil Soluble Initiators**

Oil soluble initiators are favoured in suspension polymerisation and in the production of macroreticular resins are used to promote polymerisation within the monomer droplet.

The oil soluble initiators 2,2' azo-*bis*-isobutronitrile and benzoyl peroxide were examined for possible use in the production of porous latex nanoparticles, however all attempts to produce a latex with these two initiators failed. All of the reactions resulted in unstable dispersions with the production of large amounts of coagulum. The analysis of the conversion of monomer to polymer was difficult to measure and no satisfactory results were obtained. The reason for the failure of an oil soluble initiated system is possibly due to the difference in reaction loci between oil and water soluble initiators. As has been previously discussed water soluble initiators initiate polymerisation of the small amount of monomer soluble in the aqueous phase whereas oil soluble initiators initiate polymerisation in the monomer droplets and micelles. Surface active oligomers are known to have an important role in the stability of the nucleating particles formed during emulsion polymerisation. Oil soluble initiators do not contribute charge stabilising ionic end groups to the polymer which has to compete with other oil / water interfaces for the available surfactant.

### 4.1.3 Effect of surfactant concentration

#### 4.1.3.1 Polymerisation in the presence of Sodium Dodecylsulphate

In this series of experiments the concentration of the surfactant sodium dodecylsulphate was varied whilst all other ingredients were kept constant.

Fig. 4.3. shows the results obtained for this series of polymerisations. It was found that at a sodium dodecylsulphate concentration below its CMC (0.0086 mol dm<sup>-3</sup>)<sup>167</sup> conversion rates were slow and total conversion of

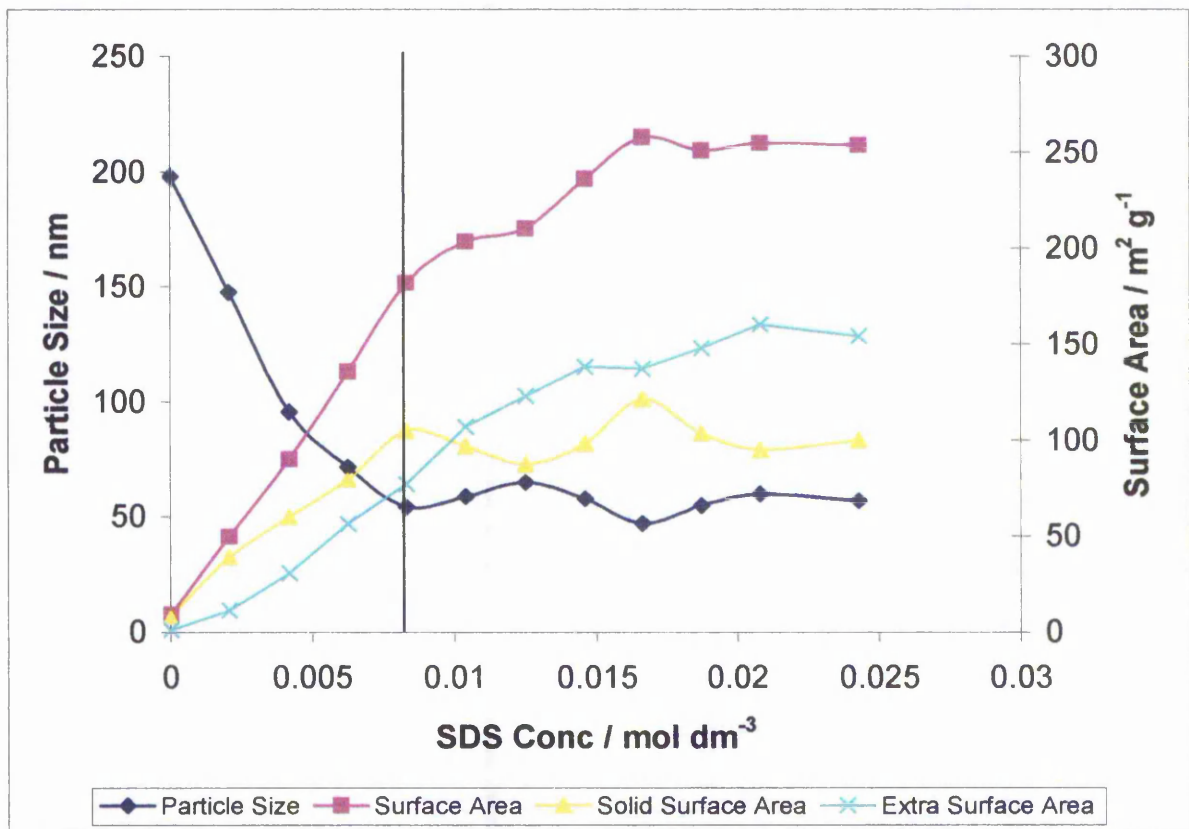


Fig. 4.3. Effect on particle size and surface area with change in concentration of sodium dodecylsulphate. Styrene/ divinylbenzene ratio = 1:1, monomer / porogen (toluene) ratio = 0.5, potassium persulphate concentration =  $7 \cdot 10^{-3}$  mol dm<sup>-3</sup>, Temperature = 80°C

monomer to polymer was difficult to assess due to high levels of coagulum produced. At concentrations above the CMC the rate of reaction increased and most noticeably the levels of coagulum dropped dramatically and degrees

of conversion of monomer to polymer in excess of 95% were achieved. The effect that the concentration of sodium dodecylsulphate has on the particle size can also be split into two regions that below the CMC and that above the CMC. At concentrations below the CMC there is a steady drop in particle size whilst at concentrations above the CMC the particle size decreases at a much reduced rate. The reason for the fall in particle size in the region below the CMC of sodium dodecylsulphate may be due to the fact that as the surfactant concentration is increased there are more aqueous phase nuclei becoming stabilised at the beginning of the reaction. With an increase in the number of growing particles competing for a fixed amount of monomer the rate of reaction will increase and there will be less monomer available to each growing particle, meaning that more smaller particles are formed. It can also be seen from Fig.4.3. that the amount of additional surface also increases as the concentration of sodium dodecylsulphate approaches its CMC, which would seem to reinforce the idea that the rate of reaction has a significant part to play in the development of porosity. Once the cmc of the surfactant has been reached, the reaction rate and the surface area continues to increase albeit at a reduced rate as the surfactant concentration is increased further up to a sodium dodecylsulphate concentration of around  $0.015 \text{ mol dm}^{-3}$ .

#### **4.1.3.2 Emulsifier Free Polymerisation**

As has been discussed earlier it is possible to produce model colloidal dispersions by performing an emulsion polymerisation in the absence of any stabilising surfactant, but it has been impossible so far to develop a method for the production of porous nanoparticles via a soap free polymerisation technique. Without surfactant in the system the rate of conversion is significantly reduced taking in some cases in excess of 24 hours for the reaction to reach completion in the case of monodisperse polystyrene and from the results discussed in section 3.1.3.1 when the rate of reaction is slow then the additional surface area introduced by the presence of a porogen is low. In the case of soap free polymerisation of a styrene / divinylbenzene copolymer at a monomer ratio of 1:1 with toluene as the porogen, at a monomer to porogen ratio of 1:0.5, initiated with potassium persulphate at a concentration of  $7 \times 10^{-3} \text{ mol dm}^{-3}$  after 24 hour the conversion of monomer to polymer was low in the region of 35% by weight. Analysis of the weak latex produced after filtering off the coagulum resulted in particles in the region of 700nm with a surface area of  $9 \text{ m}^2 \text{ g}^{-1}$ . Non-porous spheres of this diameter would yield a polymer with a surface area of  $8 \text{ m}^2 \text{ g}^{-1}$  giving a possible additional surface of only  $1 \text{ m}^2 \text{ g}^{-1}$  but the difference in values falls within expected experimental error based on repeated experiments. It is therefore unlikely that any porosity at all is developed in the soap free reaction.

#### **4.1.4 Effect of Porogen Concentration and Type**

As has already been discussed (section 1.4) in the production of macroreticular resins the choice of porogenic species has a significant effect on the final product. In the following section the effect of different porogens on the final particle size and surface area of porous nanoparticles produced via an emulsion cross-linking copolymerisation process will be examined.

##### **4.1.4.1 Toluene**

In this series of experiments the concentration of toluene used as a porogen was varied whilst all the other components within the reaction mixture were kept constant. The porogen ratio was determined as volume of porogen / total volume of monomers.

Toluene is a solvent for polystyrene and has been used and studied extensively in the production of coarse macroreticular resins used for chromatography and ion exchange.

The mechanism by which the porous network is produced in these resins is one of mechanical retention of the porogen. As the particles grow small pockets of the porogen are trapped inside the network structure, at the end of the polymerisation the porogen is extracted from the particle and these pockets remain as pores. More solvating the diluent, the fewer the pores.

Fig. 4.4. shows the results obtained for this series of experiments, it can clearly be seen that beyond an initial threshold concentration at a ratio around 0.1 where the effect of the non-polymerisable diluent in the organic

phase initially reduces particle size, further increase in the concentration of toluene has little effect on the particle size of the final product. This small decrease is thought to be due to an initial dilution of the monomer within the micelles, with no diluent added the micelle is fully converted to polymer however on introducing the diluent the organic phase is diluted leading to the production of smaller nuclei. There is an effect on the final surface area of the product, as the porogen concentration increases there is a steady increase in the surface area. As there is no significant change in the particle size, all of this increase in surface area is additional. This steady increase in additional surface area continues up to a ratio of approximately 0.6 toluene / monomer v/v, above this level no further additional surface is developed. This would suggest that at this concentration of solvating porogen the growing particles are expanded to their fullest extent and are thus incapable of incorporating any more toluene in the interior of the forming polymer. In macroreticular resin production the effect of the concentration of toluene used is much more dramatic than that found here and this may be explained by higher polymer concentrations within growing particles during emulsion polymerisation compared with suspension polymerisation. As the initial cross-linked nuclei grow they are fully solvated by toluene and monomer, the amount of both being dependant on the cross link density, thus adding more toluene to the system does not have a major effect on the swelling of the growing polymer particles.

All of the polymerisations were taken to completion reaching conversion of monomer to polymer above 95% with very low levels of coagulum produced.

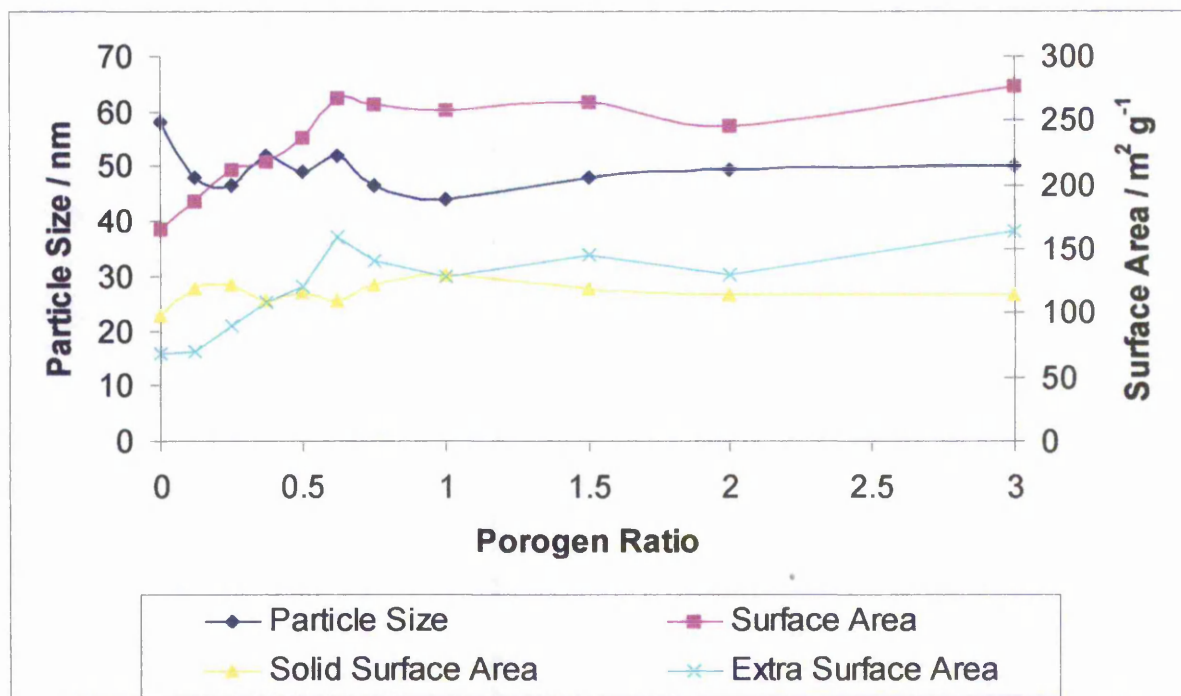


Fig. 4.4. Effect on particle size and surface area of porogen (toluene) concentration. Styrene / divinylbenzene ratio = 1:1, surfactant (sodium dodecylsulphate) =  $0.014 \text{ mol dm}^{-3}$ , initiator (potassium persulphate) =  $7.0 \times 10^{-3} \text{ mol dm}^{-3}$ , temperature =  $80^\circ\text{C}$

#### 4.1.4.2 Xylene

Xylene is a similar type of molecule to toluene and as such is also a solvent for styrene, it does however have a larger molecular radius and so this study was carried out to see if this increase in molecular radius had any effect on the characteristics of the final polymer produced.

In this series of polymerisations the concentration of xylene used as a porogen was varied whilst the concentrations of all other ingredients was kept constant.

From the results shown in Fig. 4.5 it can be seen that the effect of varying the xylene concentration has a very similar effect to that of varying the concentration of toluene. Again there is only a small effect on the final particle

size of the final polymer with an initial small decrease in the particle size. There is a steady increase in the surface area with increasing porogen concentration.

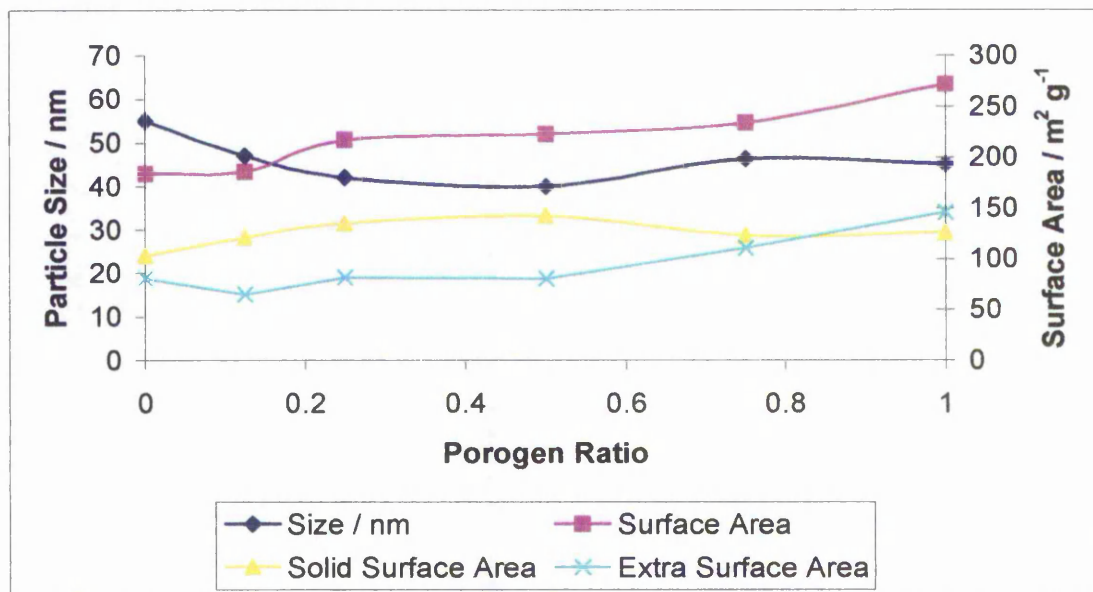


Fig. 4.5. Effect on particle size and surface area of porogen (xylene) concentration. Styrene / divinylbenzene ratio = 1:1, surfactant (sodium dodecylsulphate) =  $0.014 \text{ mol dm}^{-3}$ , initiator (potassium persulphate) =  $7.0 \times 10^{-3} \text{ mol dm}^{-3}$ .

Fig. 4.6. shows both plots of surface area for toluene and xylene on the same chart and it is quite clear that there is no significant difference between the surface area produced with the two porogens.

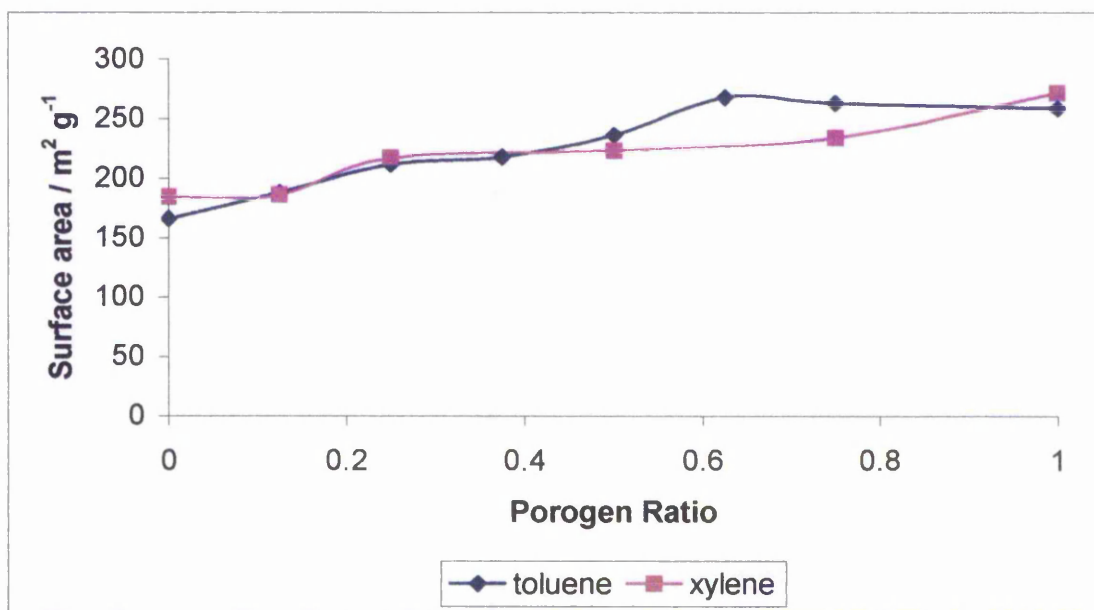


Fig. 4.6. Comparison of effect on the surface area of porous nanoparticles with change in porogen size. Styrene / divinylbenzene ratio 1:1, potassium persulphate concentration =  $7 \cdot 10^{-3} \text{ mol dm}^{-3}$ , sodium dodecylsulphate =  $0.014 \text{ mol dm}^{-3}$ , temperature =  $80^\circ\text{C}$

All of the polymerisations were taken to completion with conversion of monomer to polymer above 95% with low levels of coagulum produced.

#### 4.1.4.3 Heptane

In the formation of the porous structure of macroreticular resins a non solvent for the monomer is used to create a resin that has a high pore volume and a low specific surface area, in other words when a non-solvent is used the internal dimensions of the pores are larger than in resins where a solvent for the monomer is used. This leads to a decrease in total surface area as there are fewer pores contained within the resin. A suitable non-solvent for styrene / divinylbenzene copolymers is *n*-heptane.

In this series of experiments the concentration of *n*-heptane was varied whilst the concentration of the remaining ingredients was kept constant.

Fig. 4.7. shows the results for this series of polymerisations, it can be seen that the concentration of the porogen again has little effect on the particle size of the final polymer after an initial decrease, but there is an increase in surface area as the concentration of the porogen is increased, up to a ratio of approximately 1.0. After this point no further additional surface is developed. As there is no difference in particle size this increase in surface area is due to the creation of more internal surface area.

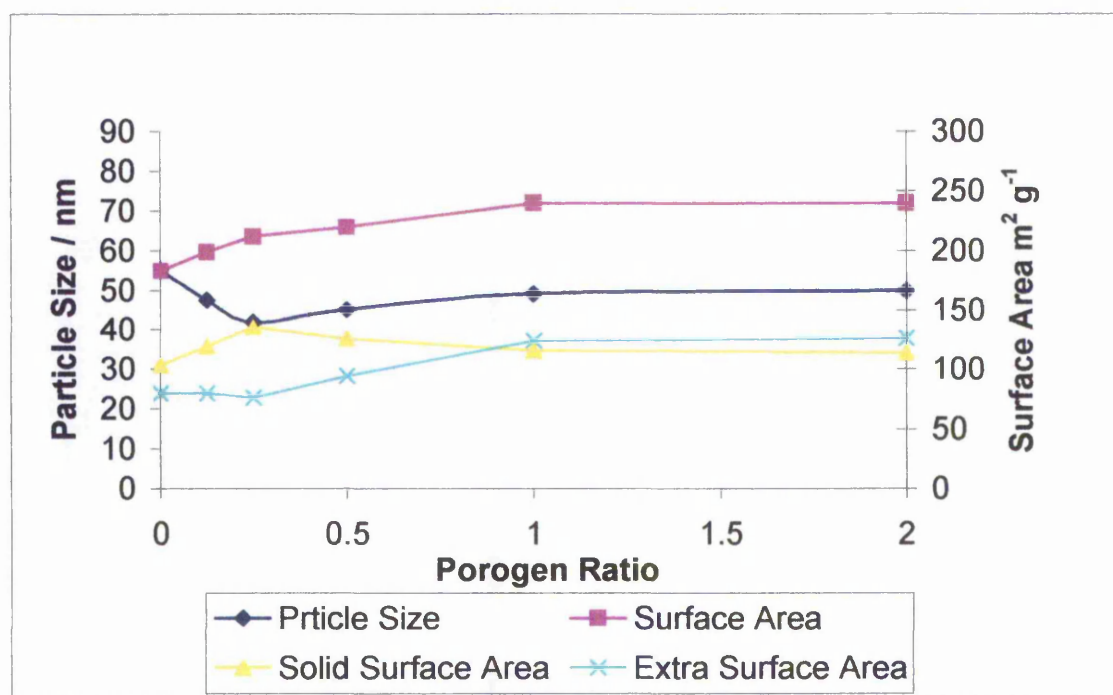


Fig. 4.7. Effect on particle size and surface area of porogen (xylene) concentration. Styrene / divinylbenzene ratio = 1:1, surfactant (sodium dodecylsulphate) =  $0.014 \text{ mol dm}^{-3}$ , initiator (potassium persulphate) =  $7.0 \times 10^{-3} \text{ mol dm}^{-3}$ , temperature =  $80^\circ\text{C}$

All of the polymerisations were taken to completion with conversion of monomer to polymer above 95% with low levels of coagulum being produced.

#### 4.1.4.4 Comparison Between Solvating and Non Solvating Porogen

As has been stated earlier (section 1.4) in the production of coarse macroreticular resin beads the pore structure is very dependant on the pore generating mechanism. This pore generating mechanism is controlled by selecting or blending together either solvating or non-solvating porogens to produce the desired pore structure. As a general rule solvating porogens lead to a resin with a high specific surface area and low pore volumes and a non-solvating porogen leads to a resin with a lower specific surface area but high pore volumes. Fig 4.8. shows the results obtained for solvating porogens (toluene and xylene) and a non-solvating porogen (*n*-heptane) for the production of porous latex nanoparticles via emulsion cross-linking copolymerisation.

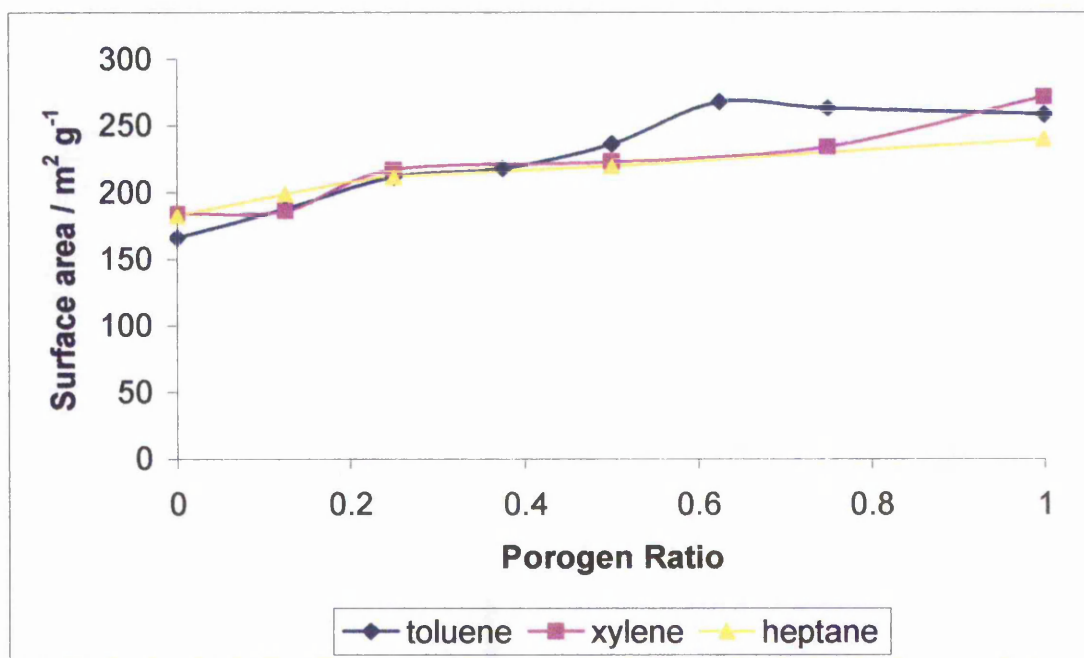


Fig. 4.8. Comparison of the effect of solvating and non-solvating porogen on the surface area of porous latex nanoparticles

It can be seen from the plot that there appears to be no difference between the two types of porogen on the final surface area of the latex, however these results give no indication of the pore structure within the particles (considered in section 4.1.7). It would seem that contrary to the effect that the different porogens have on macroreticular resin production, the solvating power of the porogen has little or no effect on the final product. This can be attributed to different mechanisms of pore formation between the two systems. In macroreticular resin synthesis the pores are thought to be formed as a result of agglomeration of nuclei, made up of agglomerated cross-linked polymer chains, to form microspheres that trap the porogen in the interstices between them, which then creates voids when the porogen is removed. In the case of porous nanoparticles produced via emulsion cross-linking copolymerisation the mechanism is likely to be different as the final product is not much bigger than the microspheres associated with suspension polymerisation and pore formation is therefore unlikely to be caused by trapping the porogen between agglomerating particles but rather that the porogen is trapped between polymer chains and the particle grows around these trapped pockets of porogen. It is an interesting and unexpected finding that the solvating power of the porogen has no influence over the surface area and porosity produced.

#### **4.1.4.5 Linear Polymeric Porogen**

The use of polymeric porogen is of interest in the production of macroreticular resins in which its use yields a resin with a low specific surface

area and a low pore volume. As the aim of the project is to maximise the surface area available it was decided not to study the effect of linear polymeric porogens which are known only to make a small contribution to pore volume and surface area.

#### **4.1.5 Monomer Ratio**

##### **4.1.5.1 Persulphate Initiated Porous Nanoparticles**

In the preparation of porous latex nanoparticles as well as in the formation of the porous structure within macroreticular resins the ratio between the vinyl and divinyl monomers will have an influence on the properties of the final polymer produced. As the percentage of divinyl monomer is increased then the degree of cross-linking will also increase leading to a polymer that is more rigid and less able to swell.

In this series of experiments the ratio between styrene (vinyl) and divinylbenzene (divinyl) monomers was altered whilst the concentration of the remaining ingredients was kept constant.

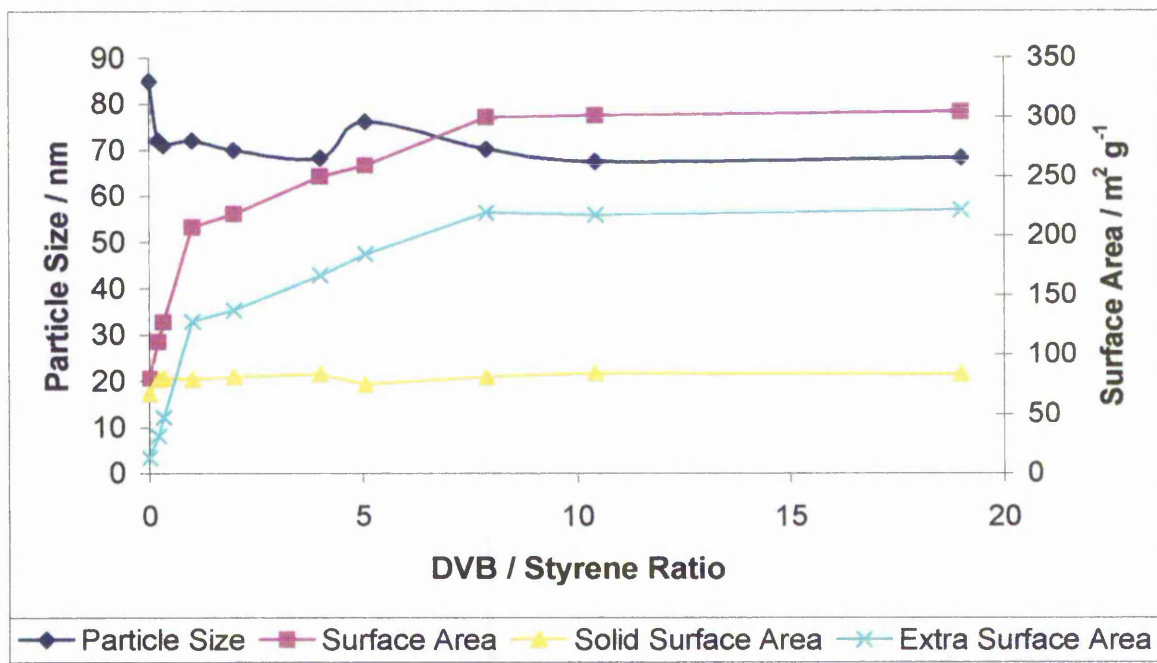


Fig. 4.9. Effect on particle size and surface area with monomer ratio. Potassium persulphate =  $7 \cdot 10^{-3} \text{ mol dm}^{-3}$ , sodium dodecylsulphate =  $0.014 \text{ mol dm}^{-3}$ , porogen ratio (toluene) = 1:0.5, temperature =  $80^\circ\text{C}$ .

Fig. 4.9 shows a plot of particle size and surface area against monomer ratio. It can be seen that at low amounts of divinylbenzene small increases lead to a rapid rise in the surface area but the rate of increase in the surface area slows as the composition of the polymer tends towards pure divinylbenzene.

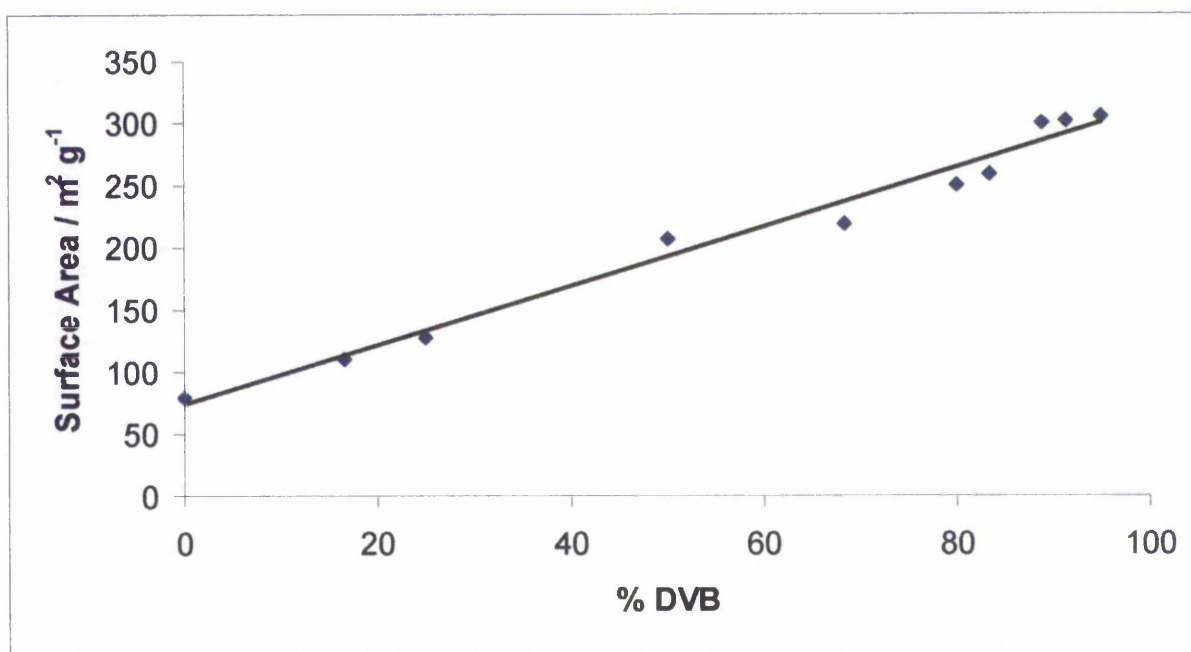


Fig. 4.10. Effect on surface area with increasing DVB content. Potassium persulphate =  $7 \cdot 10^{-3}$  mol dm<sup>-3</sup>, sodium dodecylsulphate = 0.014 mol dm<sup>-3</sup>, porogenratio (toluene) = 1:0.5

In Fig. 4.10. the results have been plotted in terms of percent divinylbenzene and it shows a linear relationship between the percentage divinylbenzene and surface area.

There is also a small decrease in particle size as the initial divinylbenzene content is increased but at reasonably low levels of divinylbenzene the particle size soon stabilises and becomes unaffected by further increases in the divinylbenzene content of the polymer. It may be expected that at low levels of divinylbenzene the cross-link density will be low and the final polymer would be able to swell in the toluene. Removal of the toluene may lead to collapse of the porous structure and show a corresponding drop in surface area due to pore closure and so the surface area results for polymers with low divinylbenzene content may be lower than expected. As the divinylbenzene content is increased the three dimensional structure formed should be more rigid and thus less susceptible to pore closure upon drying. The small

decrease in the particle size as the divinylbenzene content is raised may also be due to the increases in cross-link density. As the cross-link density increases monomer absorption into the growing polymer will be restricted, increasing the number of available loci for particle nucleation. This will in turn lead to an increase in the number of growing particles and thus more competition for available monomer and smaller particles are formed. Once a certain level of cross-link density has been achieved then monomer adsorption may be controlled by diffusion and thus becomes constant leading to particle size stabilisation.

All of the polymerisations were taken to completion, however there was a significant increase in the level of coagulum produced in the polymers with a divinylbenzene content greater than 1:1 (50% of the monomer phase). Also at divinylbenzene content greater than 1:1 when left in a sealed container after filtering a solid like gel formed. The onset of this phenomenon was seen to be dependant on the level of divinylbenzene in the final polymer, steadily becoming more rapid as the divinylbenzene content increased. Reasons for this occurrence were not obvious as there was no sign of destabilisation of the dispersion as associated with sedimentation (settling out at the bottom of the container leaving a clear aqueous phase above the polymer) or creaming (rising to the surface of the aqueous phase), even after several months of storage there was no change in the appearance of the dispersion. If the latex was diluted by 100% with double distilled water immediately after being removed from the reaction vessel then the thickening of the dispersion was not observed and the dispersion remained stable. Also at the low level of solids content used to produce these dispersions at around 7.5% this

thickening of the dispersion would not be expected. Samples of the thickened dispersion were cleaned in the same way as the diluted dispersions and upon drying and testing for surface area gave comparable results. TEM examination of the two dispersions gave good correlation in particle size and shape.

In order to investigate whether the observed behaviour was due to instability of the final latex dispersion a series of polymers with high divinylbenzene to styrene ratio were prepared with increasing surfactant concentrations, the results from these experiments are given in Table 4.1.

SDS Concentration / mol dm <sup>-3</sup>	Particle Size / nm	Gel Formed (Yes / No)
8*0-3	60.7	Yes 24 Hrs
1.4*10 <sup>-2</sup>	58.1	Yes 48 Hrs
6.5*10 <sup>-2</sup>	54.2	Yes 2 weeks
8*10 <sup>-2</sup>	54.9	Yes 4 weeks

Table 4.1. Onset of gelation with increasing surfactant concentration

The results shown in table 4.1. would suggest that the thickening of the dispersion was due to some form of instability of the dispersion as with increased amounts of surfactant the onset of the thickening could be delayed. A possible reason for the onset of this thickening could be that some form of weak attraction between the particles in the dispersion occurs although TEM results do not show aggregates. The sheer thinning of the dispersion that

occurs upon stirring is in agreement with weak aggregates. The density of the porous polymer is very close to that of water so that the particles neither sediment nor cream but remain suspended. These two factors could account for the thickening of the dispersion whilst the dried polymer shows properties that correlate with polymers produced at lower divinylbenzene to styrene ratios.

#### **4.1.5.2 Redox Imitated Porous Nanoparticles**

As the monomer ratio appeared to have the most significant effect on the final surface area and the next most significant effect was that of initiation, a series of polymers were produced in the same manner as above but including sodium metabisulphite to give redox initiation. These polymers showed similar behaviour to the polymers produced with just potassium persulphate as initiator, with the dispersions produced using high levels of divinylbenzene showing the thickening properties as discussed. Fig. 4.12. shows a comparison plot of surface area against percent divinylbenzene content. Again the relationship is linear but the surface area is higher in each case for the polymers produced using the redox couple. This would also suggest that the rate of reaction plays an important role in the formation of the porous structure indicating that more porogen is trapped in the faster reactions or that in the slower reactions the porogen is able to diffuse from the interior of the particle allowing fresh monomer to diffuse into the interior and thus close up some of the pores by polymerising within available sites inside the growing particle.

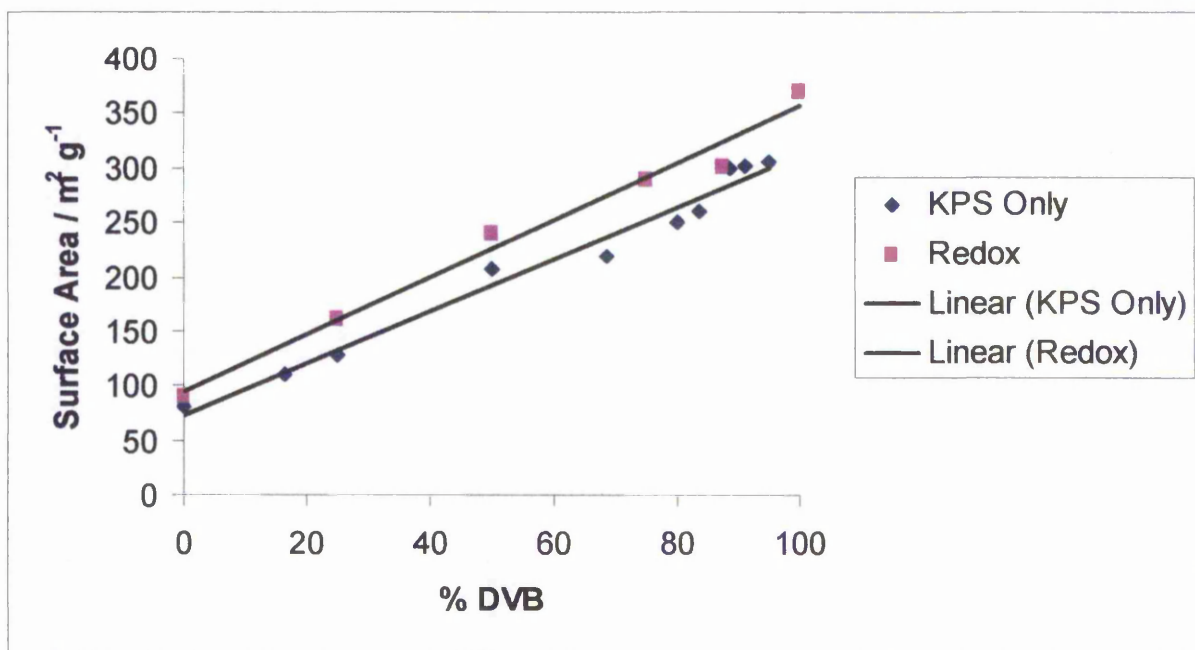


Fig. 4.12. Comparison plot of surface area against DVB content with initiator system. Potassium persulphate =  $7 \cdot 10^{-3} \text{ mol dm}^{-3}$ , sodium dodecylsulphate =  $0.014 \text{ mol dm}^{-3}$ , porogen ratio (monomer / toluene) = 1:0.5

The polymerisations with the redox couple also showed the increase in coagulum as the divinylbenzene content is increased, although to a noticeably lesser extent.

All polymerisations were taken to completion with conversion of monomer to polymer greater than 95% allowing for the weight of coagulated polymer

#### 4.1.6 Effect of Temperature

Temperature is of course a major factor in the rate at which chemical reactions proceed. In this series of experiments the effect of monomer ratio was examined at a reduced temperature of  $50^\circ\text{C}$  for comparison with the results obtained at  $80^\circ\text{C}$ . Fig. 4.13. and Fig. 4.14 show comparison charts for surface area and particle size against increasing divinylbenzene concentration for polymerisations carried out at  $80^\circ\text{C}$  and  $50^\circ\text{C}$ .

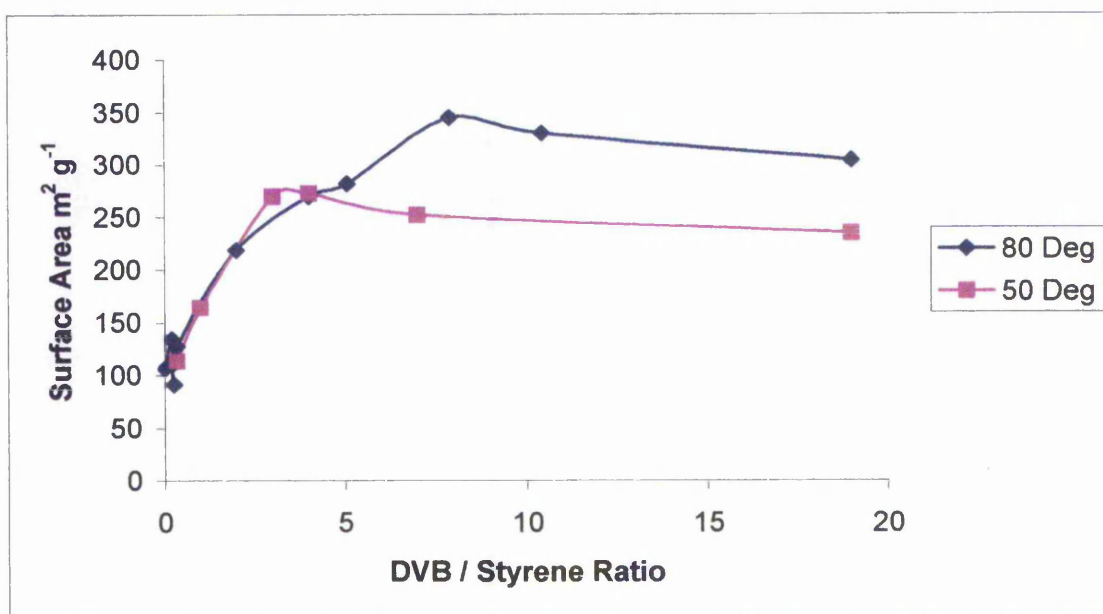


Fig. 4.13. Effect on surface area with change in temperature and DVB / styrene ratio Potassium persulphate =  $7 \cdot 10^{-3}$  mol dm<sup>-3</sup>, sodium dodecylsulphate = 0.014 mol dm<sup>-3</sup>, porogenratio (toluene) = 1:0.5, temperature = 80°C

From Fig. 4.13. it can be seen that the surface area for polymerisations carried out at 50°C follow the same profile as those produced at the higher temperature showing at low DVB content a similar degree of surface area that increases at a similar rate, however at higher DVB concentrations the final particles produced at 80°C have a significantly higher surface area than those produced at 50°C with the same starting ingredients This result would seem to confirm earlier speculation that the rate of reaction plays a significant role in the production of porosity in latex nanoparticles.

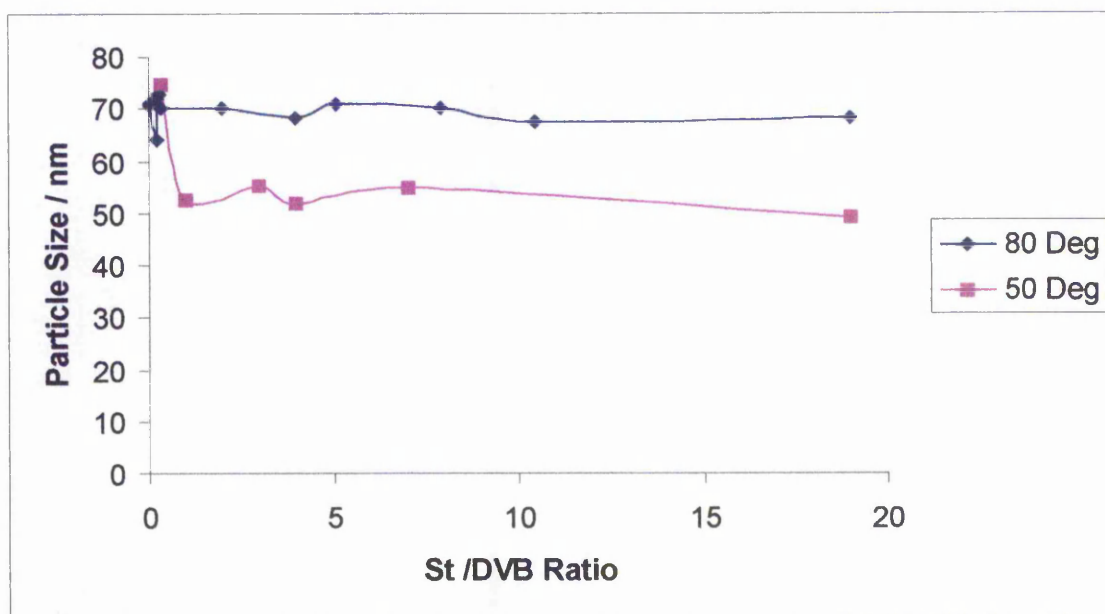


Fig. 4.14. Effect on particle size with change in temperature and DVB / styrene ratio potassium persulphate =  $7 \cdot 10^{-3} \text{ mol dm}^{-3}$ , sodium dodecylsulphate =  $0.014 \text{ mol dm}^{-3}$ , porogen ratio (toluene) = 1:0.5

From Fig. 4.14. it can be seen that temperature also has a significant effect on particle size, polymers produced at the lower temperature having smaller particle size than those produced at  $80^{\circ}\text{C}$ . This would suggest that polymers produced at  $50^{\circ}\text{C}$  have a more compact structure. At  $50^{\circ}\text{C}$  the polymerisations took significantly longer to reach completion and it is thought that the porogen is able to diffuse from the inside of the growing particle faster than it can be trapped inside resulting in a more compact particle. As surface area is inversely proportional to particle size the smaller particles produced at  $50^{\circ}\text{C}$  will have a larger non-porous external surface and therefore the particles produced at  $80^{\circ}\text{C}$  having a greater surface area must have significantly more internal surface area.

#### **4.1.7 Effect on Surface Area of Cleaning Technique**

The method of cleaning the final polymer latex has a significant effect on the final surface area. Adsorbed surfactant, oligomer and low molecular weight polymer will be present at the end of the polymerisation process and must be removed for the full surface area to be available. Dialysis will remove any soluble salts and surfactant molecules from the particles, steam distilling will remove the volatile porogenic species and any unreacted monomer. Continuous liquid/liquid extraction with 2,2,4 trimethylpentane (iso-octane) was carried out to remove any low molecular weight polymer that may be left over at the end of the polymerisation. To assess the effect that the cleaning methods had on the final surface area a porous polymer was produced and divided into portions. Each portion was then subjected to a different cleaning process or series of processes and the final specific surface area calculated. Table 4.2 gives the results for the different cleaning systems employed.

Cleaning Method	Specific Surface Area / m <sup>2</sup> g <sup>-1</sup>
Freeze Dried Only	203
Steam Distilled + Freeze Dried	216
Dialysed + Steam Distilled + Freeze Dried	224
Dialysed + Steam Distilled + Liquid Liquid Extraction (6 Hours) + Freeze Dried	322
Dialysed + Steam Distilled + Liquid Liquid Extraction (9 Hours) + Freeze Dried	326
Steam Distilled + Oven Dried	205
Flocculated + Centrifuged + Freeze Dried	272
Flocculated + Centrifuged + Oven Dried	254
Flocculated + Centrifuge + Liquid Liquid Extraction (6 Hours) + Freeze Dried	396
Flocculated + Centrifuge + Liquid Liquid Extraction (9 Hours) + Freeze Dried	406

Table 4.2 Effect of cleaning method on the final specific surface area of porous nanoparticles.

From Table 4.2 it can be seen that the method of cleaning the porous nanoparticles has a major impact on the final specific surface area. The best result was for a system incorporating dialysis, steam distillation, liquid / liquid extraction (9 Hours) and freeze drying, but as the difference between the result of extraction for 6 hour to that of 9 hours was small it was decided to standardise the method with a six hour extraction. All the results so far discussed were treated using this method of cleaning.

## **4.1.8 Pore Size Analysis**

### **4.1.8.1 Introduction**

Porous materials can be classified into three distinct types.

- Microporous – These materials contain pores in the region below 20 Å
- Mesoporous – These materials contain pores in the region 20 Å - 500 Å
- Macroporous – These materials contain pores in the region greater than 500 Å

Pore size analysis was achieved by deriving the nitrogen adsorption isotherms for the polymer under study and applying the BJH equation to give a pore size distribution. The BJH equation is not very accurate for the pore size range in the micropore region and so comparison of the micropore volume was achieved by applying the Dubinin-Radushkevich equation. Whilst this does not reveal any information about the pore size distribution within the micropore region the total volume of the pores within this region can be calculated. Nonane preadsorption was also applied to some of the samples as *n*-nonane has been shown to have a very slow rate of removal from pores in the micropore region.

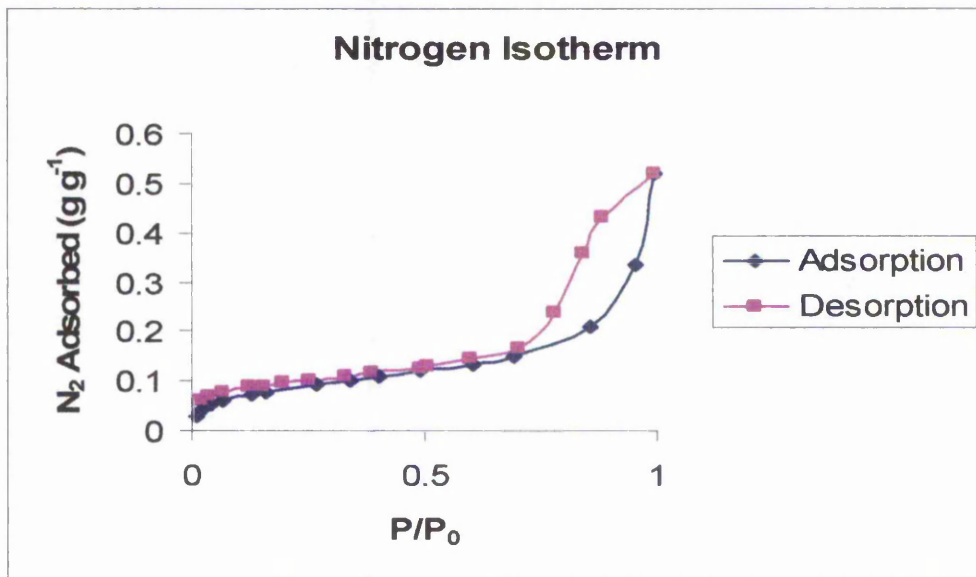


Fig. 4.15. Typical Nitrogen Adsorption / Desorption Isotherm

Fig. 4.15. shows a typical nitrogen adsorption isotherm produced by the polymers under study. It can be seen that the adsorption branch of the isotherm complies with a type II isotherm normally associated with non-porous solids, however the desorption isotherm shows hysteresis along the full range of  $P/P_0$  values. This hysteresis is not indicative of mesopores as the hysteresis produced by the different processes of pore filling and pore emptying in mesopores always closes before a value of  $P/P_0$  of 0.42 is reached for  $N_2$  and at values below  $P/P_0$  0.42 the desorption branch of the isotherm coincides with the adsorption branch. The low pressure hysteresis shown here is attributed to the presence of micropores in the sample.

#### **4.1.8.2 Pore Size Distribution – Effect of Porogen**

In this series of experiments the pore size distribution for the samples produced using the porogens examined previously were determined.

### 4.1.8.2.1 Toluene

The nitrogen adsorption / desorption isotherms for the polymers produced using toluene as porogen were generated. Fig 4.16. shows the nitrogen adsorption isotherms for several of the samples at different ratios of toluene to monomer.

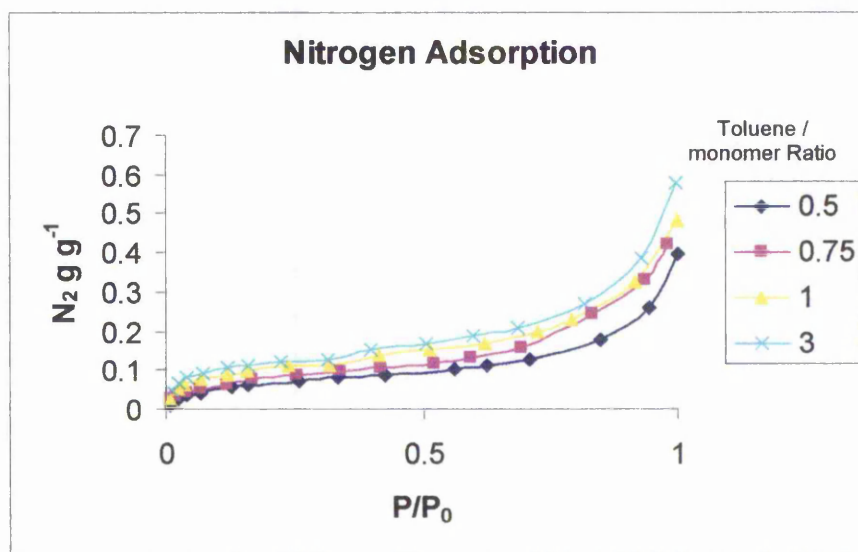


Fig. 4.16 Nitrogen adsorption isotherms for polymers produced using toluene as the porogen. Styrene / DVB ratio = 1:1, surfactant (sodium dodecylsulphate) =  $0.014 \text{ mol dm}^{-3}$ , potassium persulphate initiator,  $7 \cdot 10^{-3} \text{ mol dm}^{-3}$ , temperature =  $80^\circ\text{C}$ .

It can be seen that as the toluene content is increased the quantity of nitrogen adsorbed also increases. This is as expected as it has already been shown that although particle size does not change the surface area of the polymers increase as the toluene level is increased.

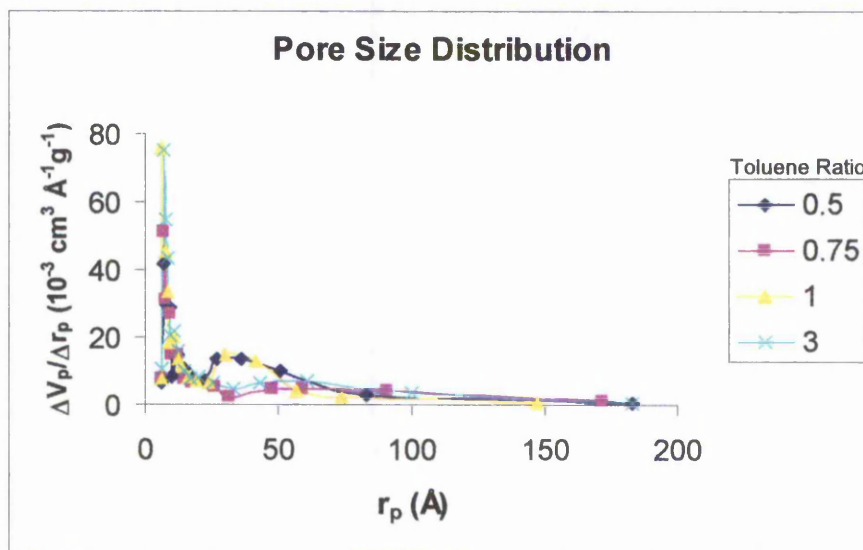


Fig. 4.17. Pore size distribution for porous polymers produced using toluene as the progen at different toluene to monomer ratios.

Fig 4.17 shows the pore size distribution according to the BJH equation. It can be seen that there is a negligible contribution from pores above 50 Å radius. It was speculated that due to the packing of the polymer particles within the sample holder a small contribution to the pore size distribution in the macropore range may have occurred due to adsorption in the interstices between the particles. Fig. 4.18 shows the same chart as in Fig. 4.17 but with the pore radius axis expanded.

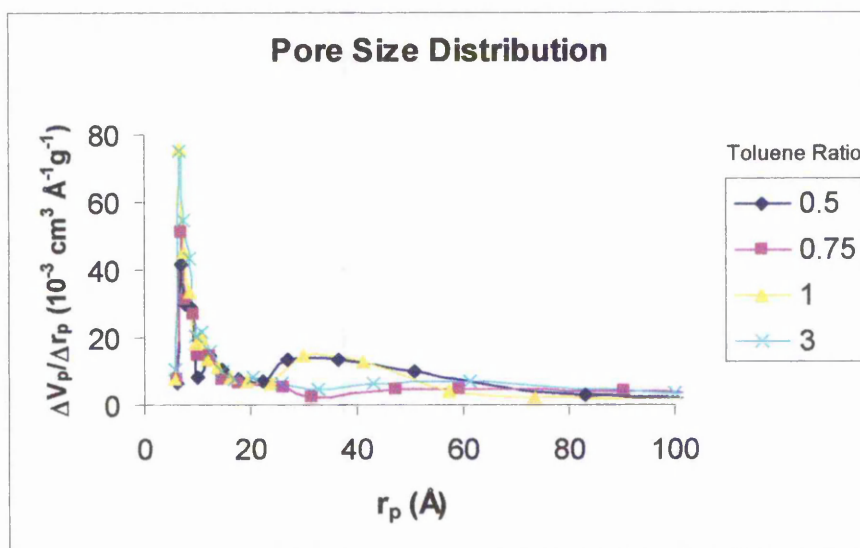


Fig. 4.18. Pore Size Distribution for Polymers Produced using Toluene as the Porogen (expanded axis).

It can be seen from this chart that there is a small contribution from pores in the mesopore range but the bulk of the pores lie within the micropore region.

Table 4.2. gives the Dubinin-Radushkevich micropore volume for the samples shown.

Toluene / Monomer Ratio	DR Micropore Volume $\text{cm}^3 \text{g}^{-1}$
0.5	0.088
0.75	0.100
1	0.137
3	0.152

Table 4.3. DR micropore volume

It can clearly be seen from table 4.3. that as the toluene concentration in the reaction mixture is increased there is a significant increase in the Dubinin-Radushkevich micropore volume.

#### 4.1.8.2.2 Xylene

The nitrogen adsorption / desorption isotherms for the polymers produced using xylene as the porogen were generated. Fig. 4.19. shows the adsorption isotherms for several of the samples at various xylene to monomer ratios.

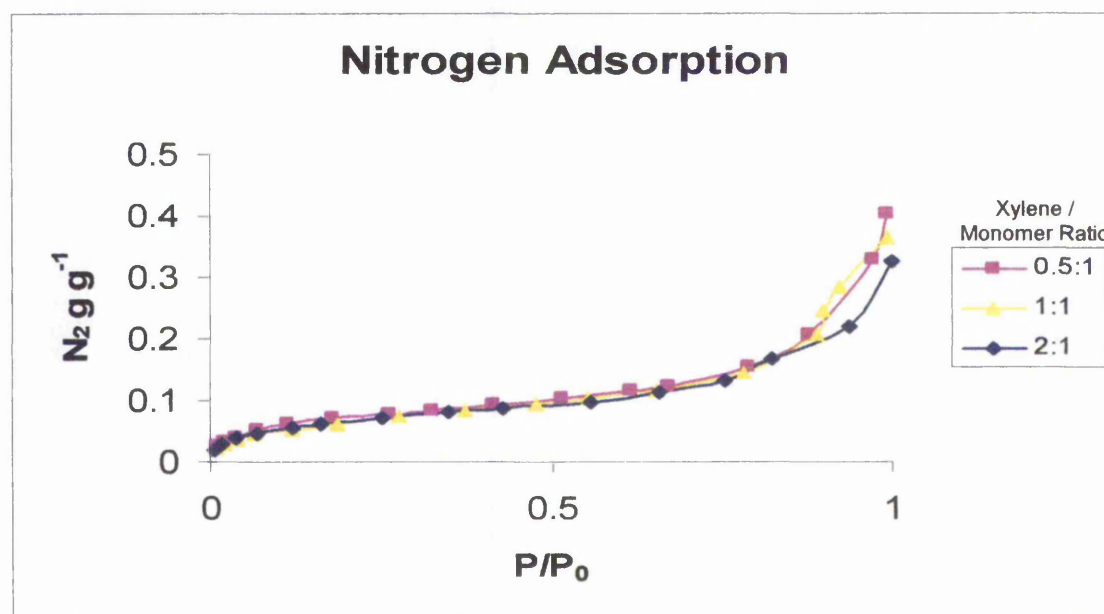


Fig 4.19 Nitrogen adsorption isotherms for porous polymers produced with xylene as porogen.

It can be seen from Fig. 4.19. that the adsorption isotherms for the polymers produced with xylene do not show such a marked trend as those produced with toluene (Fig. 4.17) yet the increase in surface area has already been shown to be similar for both porogens. Fig. 4.20. shows the pore size distribution calculated from the isotherms.

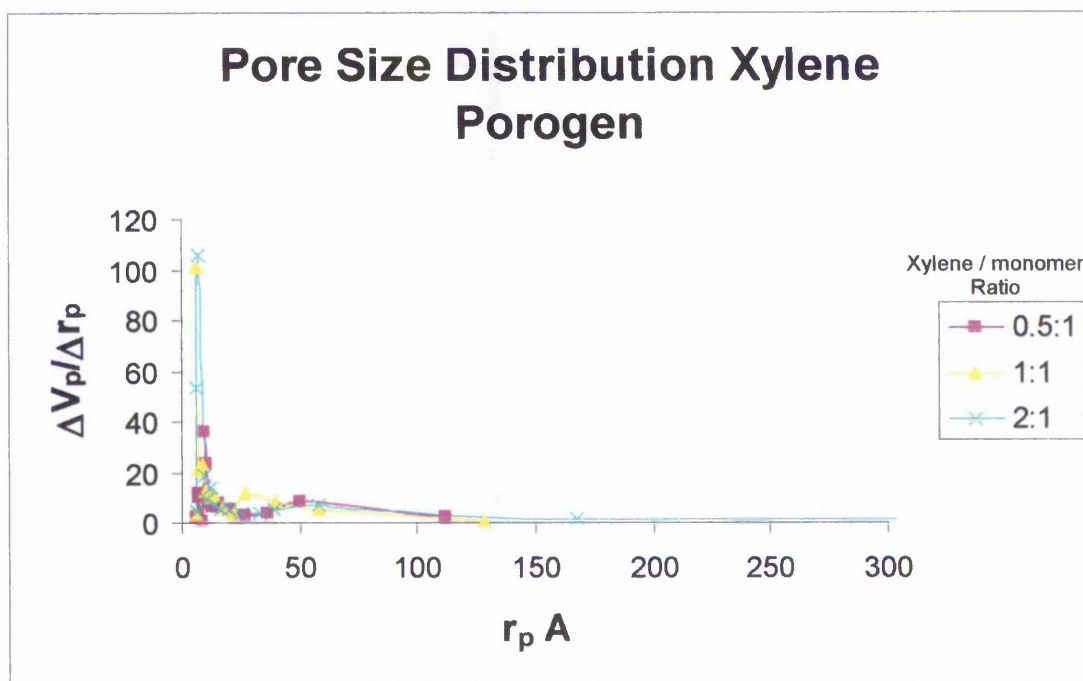


Fig. 4.20. Pore Size Distribution for Polymers Produced with Xylene as Porogen

From the chart shown in Fig. 4.20. it can be seen that there is no contribution from macropores. Fig. 4.21. shows the chart from Fig. 4.20 but with the axis expanded. Again there is a small contribution to the overall pore volume from mesopores but the bulk of the pore volume is made up of micropores, with an increase in the micropore volume with increasing xylene content. Table 4.3. gives the values of the Dubinin-Radushkevich micropore volume.

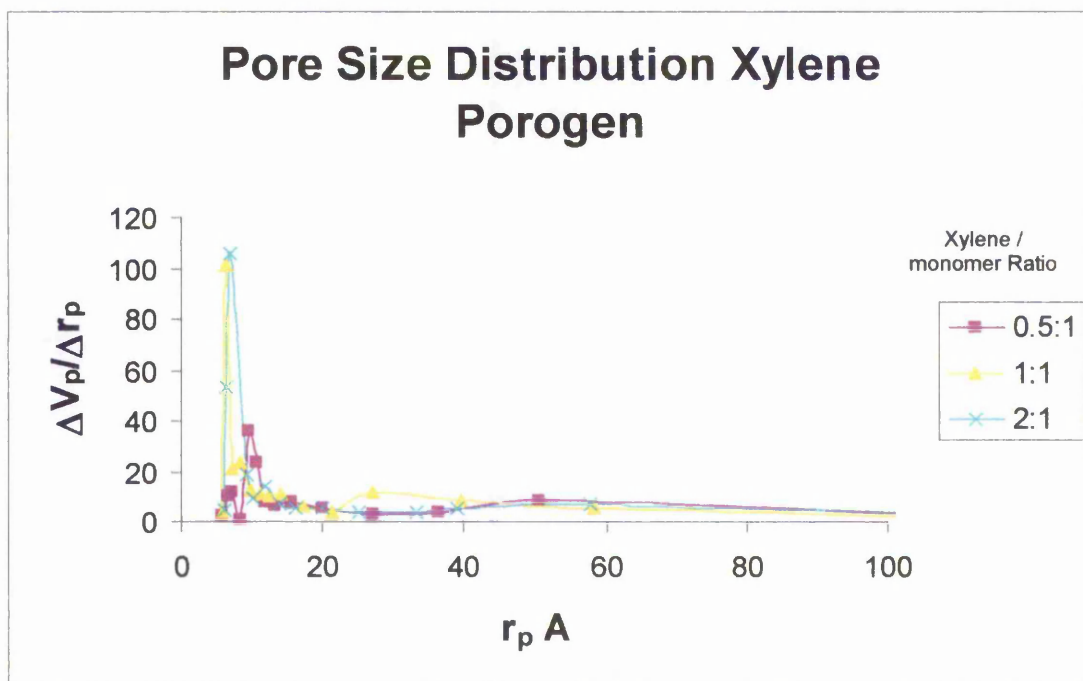


Fig. 4.21. Expanded Plot of Pore size Distribution for Polymers Produced Using Xylene as Porogen (expanded axis)

Xylene / Monomer Ratio	DR Micropore Volume $\text{cm}^3 \text{g}^{-1}$
0.5	0.075
0.75	0.095
1.0	0.1
2.0	0.107

Table 4.3. DR Micropore Volume For Polymers Produced with Xylene as Porogen

It can be seen that there is again an increase in the micropore volume as the amount of xylene used in the reaction mixture is increased.

#### 4.1.8.2.3 *n*-Heptane

In this series of experiments the effect on pore size and pore size distribution of polymers using *n*-heptane as a non-solvating porogen was examined. The nitrogen adsorption / desorption isotherms were generated and are shown in Fig. 4.22.

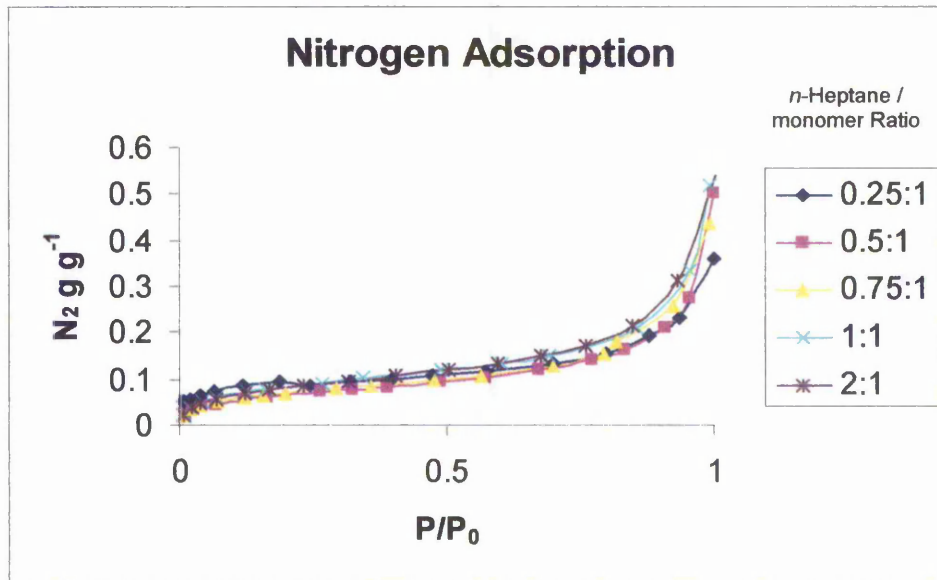


Fig. 4.22. Nitrogen Adsorption isotherms for polymer produced using *n*-heptane as porogen at various *n*-heptane / monomer ratio.

It can be seen from Fig. 4.22. that polymers produced with *n*-heptane as a non-solvating porogen leads to polymers that show a similar adsorption profile to those produced with solvating porogens. The pore size distributions calculated from the desorption branch of the isotherms are given in Fig. 4.23.

Again as with the solvating porogen there is an increase in the micropore volume as the porogen concentration increased, with a small contribution to the total pore volume from pores in the mesopore range and no macropores. Fig. 4.24 shows the results from Fig. 4.23 with the axis expanded.

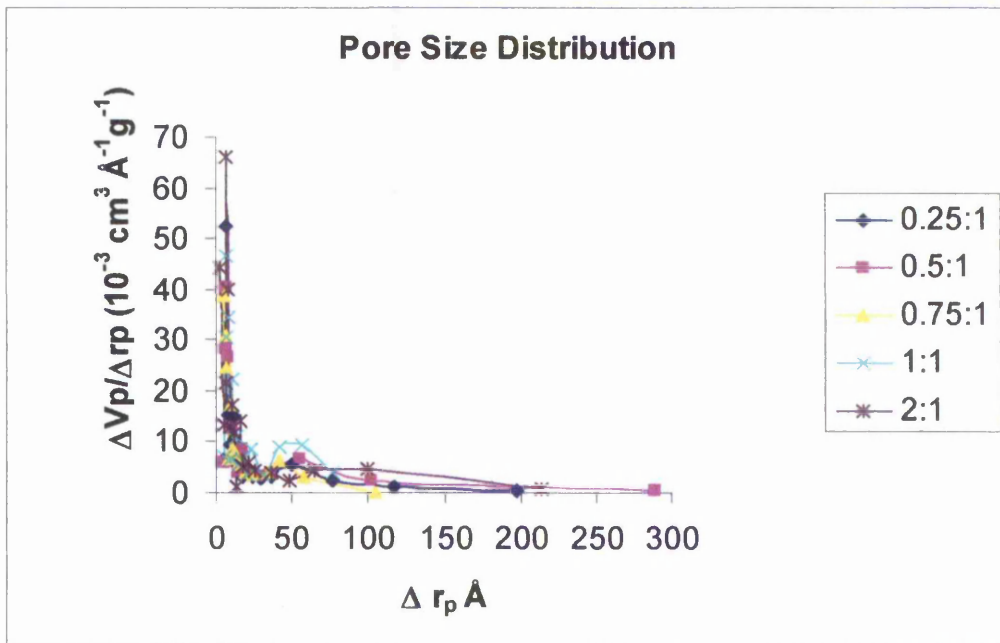


Fig.4.23. Pore size distribution for porous polymers produced using *n*-heptane as porogen.

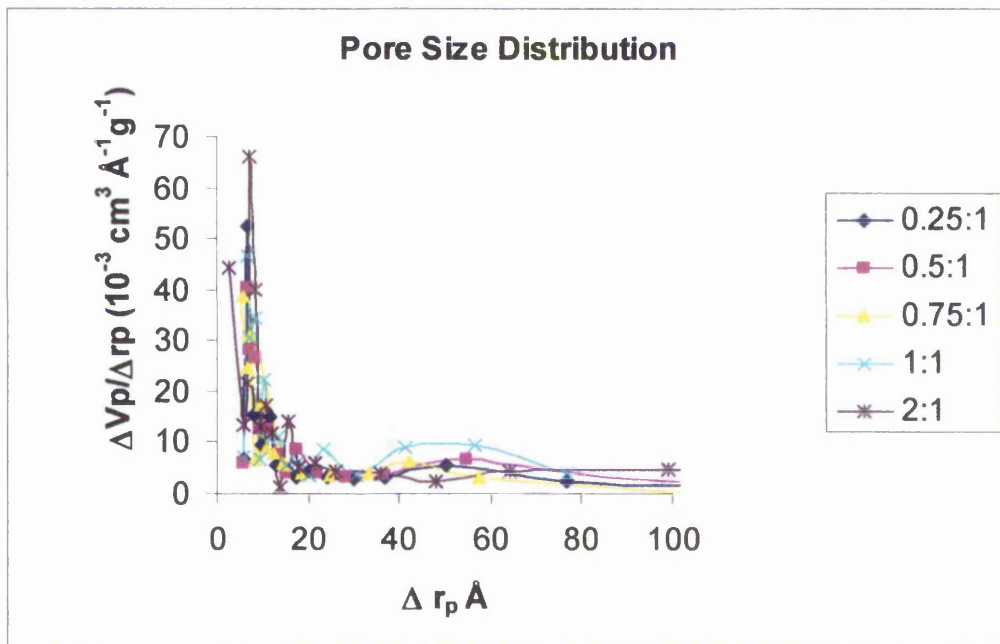


Fig. 4.24. Pore size distribution for porous polymers produced using *n*-heptane as porogen. Axis expanded to show more clearly the micropore region.

Table 4.4 shows the values of the Dubinin-Radushkevich micropore volume for this series of polymers.

<i>n</i> -heptane Ratio	DR Micropore Volume cm <sup>3</sup> g <sup>-1</sup>
0.25:1	0.084
0.5:1	0.096
0.75:1	0.1
1:1	0.105
2:1	0.118

Table 4.4. DR micropore volume for porous polymers produced using *n*-heptane as porogen.

The results given in Table 4.4 show a similar micropore volume to those achieved with the solvating porogens. This is quite different to results obtained for the production of macroreticular resins where non-solvating porogens give rise to a significantly different pore structure than resins produced with a solvating porogen.

#### **4.1.8.3 Pore Size Distribution – Effect of Cross-Linker Concentration**

As has been shown earlier the level of cross-linker included in the reaction mixture has a major effect on the final surface area of the latex. In the following section the effect that the concentration of cross-linker has on the pore size distribution will be examined.

#### 4.1.8.3.1 Persulphate Only Porous Nanoparticles

In this series of experiments the effect on the pore size distribution and Dubinin-Radushkevich micropore volume for porous nanoparticles produced using a persulphate initiator but with varying amounts of divinyl cross-linker have been examined.

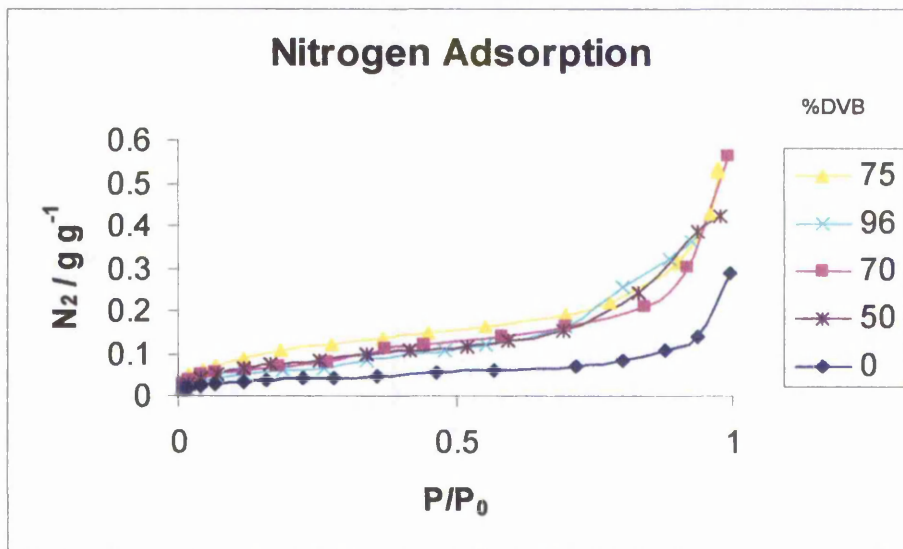


Fig. 4.25. Nitrogen adsorption isotherms for porous nanoparticles with increasing divinylbenzene concentration

Fig. 4.25 shows the nitrogen adsorption isotherms for some of the porous nanoparticles with increasing cross-linker concentration. It can be seen that as the cross-linker concentration is increased then the volume of nitrogen adsorbed by the sample also increases. Fig. 4.26. and Fig. 4.27. again show the pore size distribution for the samples shown in Fig. 4.25. with the axis expanded in Fig. 4.27 to show more clearly the pore size distribution in the mesopore / micropore region. It can be seen from Figs. 4.26. and 4.27. that as the cross-linker concentration is increased then the contribution to the total pore volume of pores in the mesopore range decreases and the

contribution of pores in the micropore range increases. As was seen in the trend of results for total surface area (section 4.1.5) the effect on the pore size distribution by varying the initial cross-linker concentration has a greater effect than by varying the concentration of the porogenic species.

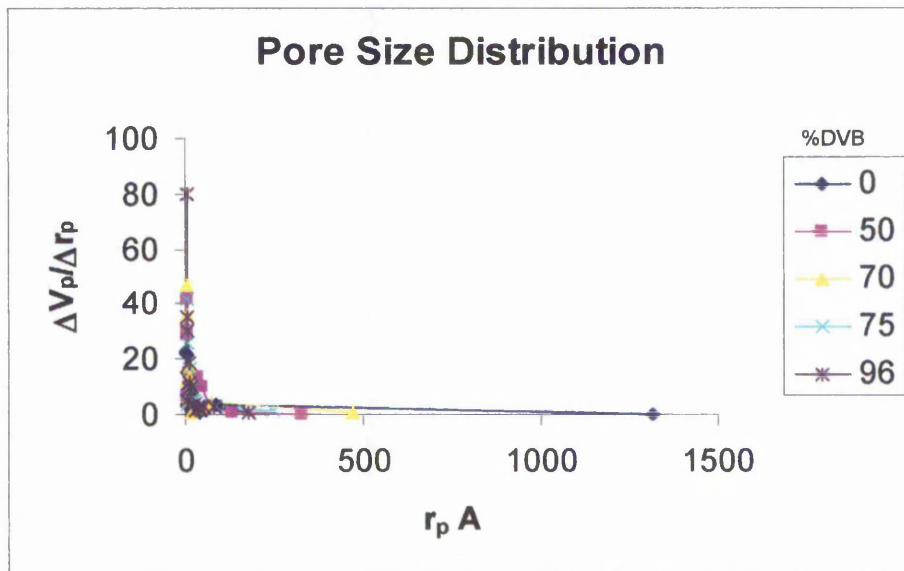


Fig. 4.25. Pore size distribution for porous nanoparticles with increasing divinylbenzene concentration

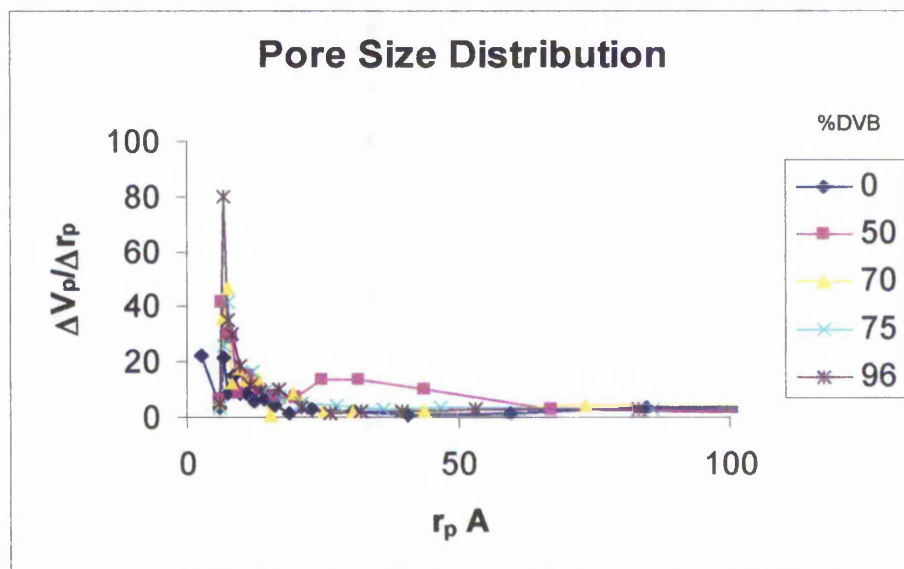


Fig. 4.26. Pore size distribution for porous nanoparticles with increasing divinylbenzene concentration.

Table 4.5 gives the Dubinin-Radushkevich micropore volume for porous nanoparticles produced with increasing divinylbenzene concentration

DVB %	DR Micropore Volume / cm <sup>3</sup> g <sup>-1</sup>
0	0.038
50	0.098
70	0.11
75	0.12
96	0.14

Table 4.5 DR micropore volume for porous nanoparticles with increasing DVB concentration

From table 4.5 it can be seen that the Dubinin-Radushkevich micropore volume increases with an increase in the divinylbenzene concentration.

#### **4.1.8.3.2 Redox Initiated Porous Nanoparticles**

As has previously been shown (section 4.1.2.2) the use of a redox couple gives rise to porous nanoparticles with a higher specific surface area than those produced using a persulphate only system. It has also been shown previously that the ratio of the two components in the redox couple has a significant effect on the final specific surface area of the final polymer. In the following section results for pore size distribution and Dubinin-Radushkevich micropore volume for porous nanoparticles produced with both differing ratios of the redox couple and for porous nanoparticles produced at the optimum

ratio of the redox couple but with increasing divinylbenzene concentration will be examined.

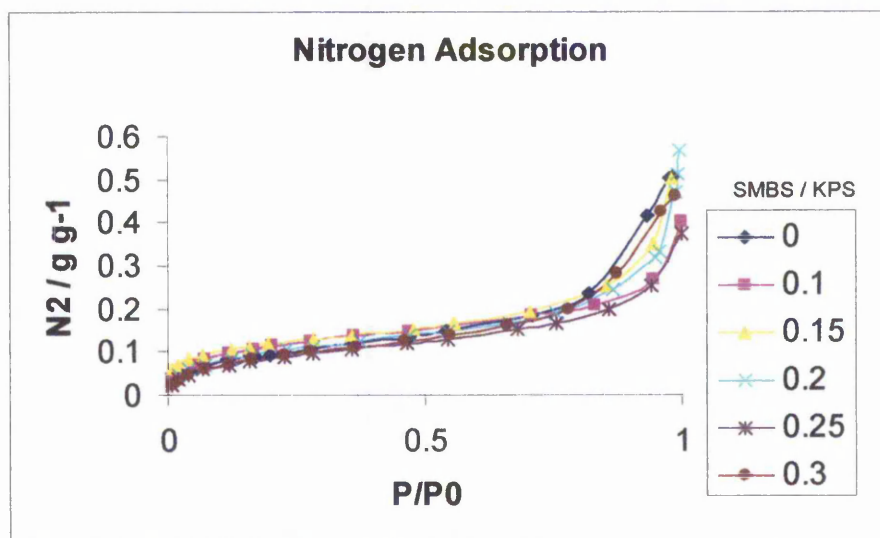


Fig 4.27 Nitrogen adsorption isotherms for porous nanoparticles produced with varying redox couple ratio.

From Fig. 4.27 it can be seen that as the redox couple ratio is changed then there is initially an increase in the nitrogen adsorption up to a sodium metabisulphite / potassium persulphate ratio of 0.1. After this point the quantity of nitrogen adsorbed by the porous nanoparticles begins to decrease.

Figs. 4.28 and 4.29 show the BJH pore size distribution for the porous nanoparticles shown in Fig. 4.27.

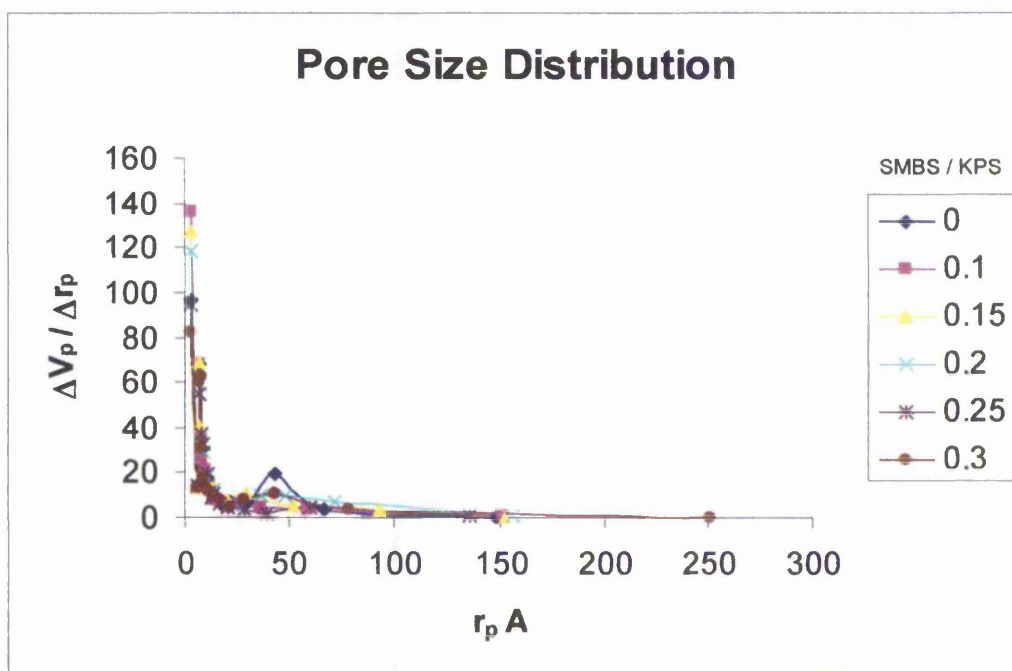


Fig. 4.28. Pore size distribution for porous nanoparticles produced with varying redox couple ratio

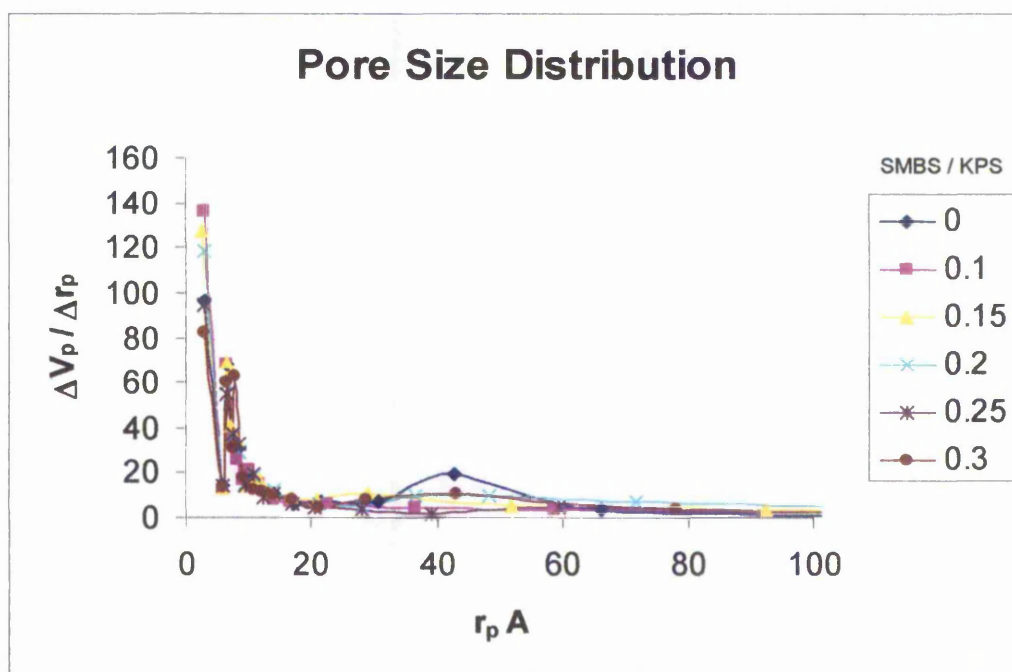


Fig. 4.29. Pore size distribution for porous nanoparticles produced with varying redox couple ratio. Expanded axis

It can be seen from figs. 4.28 and 4.29 that there is a small contribution to the overall pore volume from pores in the mesopore range for the porous nanoparticles produced with a redox couple ratio of 0 and 0.3, but those

produced within the range 0.1-0.25 do not show any major contribution from pores in this area. Porous nanoparticles produced with a redox ratio from 0.1 – 0.25 also show a higher pore volume in the micropore region.

Table 4.6 gives the Dubinin-Radushkevich micropore volume for the porous nanoparticles shown in fig 4.27.

SMBS:KPS Ratio	DR Micropore Volume / cm <sup>3</sup> g <sup>-1</sup>
0	0.137
0.1	0.152
0:15	0.148
0.2	0.149
0.25	0.126
0.3	0.12

Table 4.6 Dubinin-Radushkevich micropore volume for porous nanoparticles produced with varying redox initiator ratio

From table 4.6 it can be seen that there is an optimum micropore volume at the redox ratio 0.1 and after this point then the micropore volume begins to decrease and at a redox ratio of 0.25 and above the micropore volume is less than that achieved with persulphate alone.

### 4.1.8.3.3 Pore Size Distribution of Porous Nanoparticles Produced With a Redox couple – Effect of Monomer Ratio

From previous results it has been shown that varying the monomer ratio in the reaction mixture has a major effect on the final polymer produced (section 4.1.5). Following the results for redox initiated porous nanoparticles a series of polymers were produced at a redox ratio of 0.1 but with varying amounts of divinylbenzene in the reaction mixture.

Fig. 4.30. shows the nitrogen adsorption isotherms for the series of polymers.

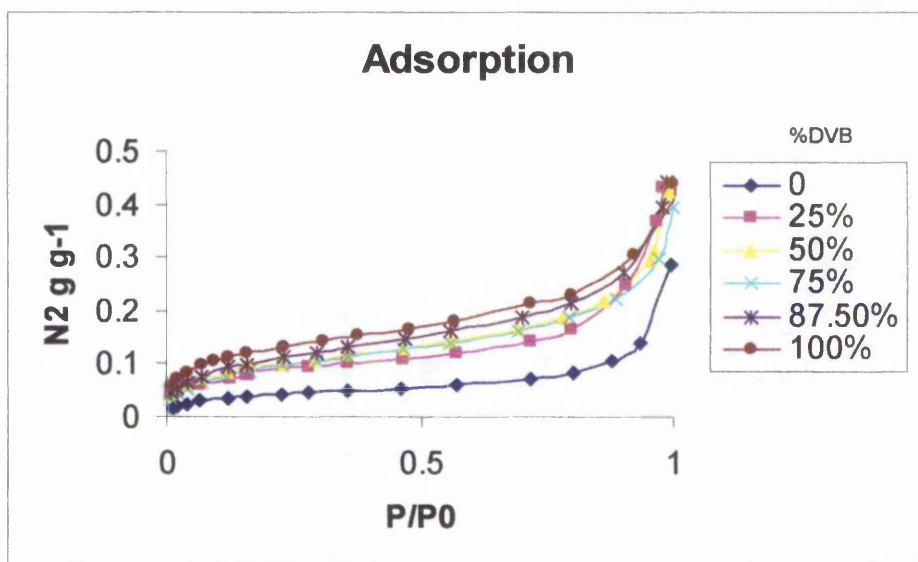


Fig. 4.30. Nitrogen Adsorption Isotherms for porous nanoparticles produced with redox initiator ratio of 0.1 with increasing DVB content.

It can be seen from Fig. 4.30 that as the divinylbenzene content of the reaction mixture is increased there is an increase in the amount of nitrogen adsorbed by the polymer. Figs. 4.31 and 4.32. show the pore size distributions for this series of polymers.

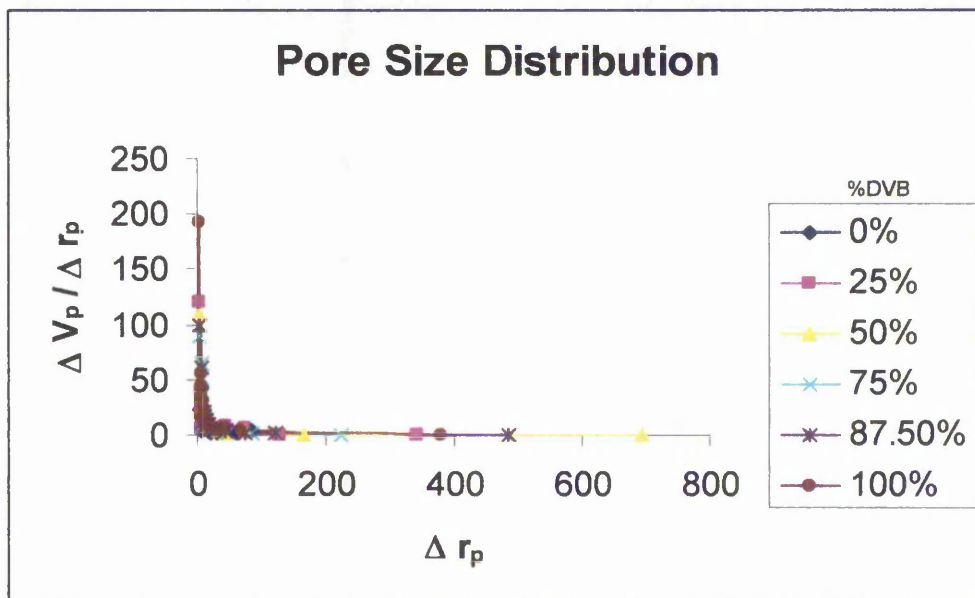


Fig 4.31. Pore size distribution for porous nanoparticles produced with a redox couple with varying DVB concentration

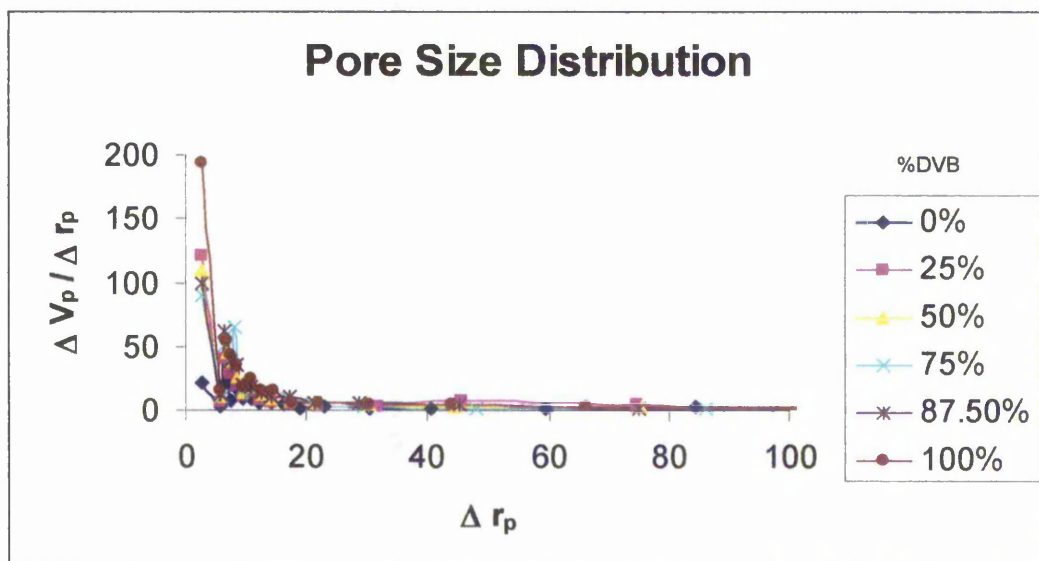


Fig. 4.32 Pore size distribution for porous nanoparticles produced with a redox couple with varying DVB concentration. Expanded axis

From figs 4.31 and 4.32 it can be seen that there is almost no contribution to the total pore volume from pores within the mesopore range, and also that as the divinylbenzene concentration is increased there is an increase in the pore volume in the micropore range. Table 4.7 gives the Dubinin-Radushkevich micropore volume for the porous nanoparticles shown in fig 4.30.

% DVB	DR Micropore Volume / cm <sup>3</sup> g <sup>-1</sup>
0	0.03
25	0.116
50	0.123
75	0.119
87.5	0.131
100	0.185

Table 4.7 DR micropore volume for porous nanoparticles produced with a redox couple with varying DVB content

#### 4.1.8.3.4 XAD-4

XAD-4 is a commercially available styrene / divinylbenzene macroreticular resin with a particle size in the region of 550  $\mu\text{m}$  and a specific surface area of about 800  $\text{m}^2 \text{g}^{-1}$ . The large size of the resin beads make them unsuitable for inclusion in thin films. A sample of XAD-4 was ground in a hammer mill to reduce particle size. After the beads had been milled the resulting rough particles were in the region of 2-3  $\mu\text{m}$ , Fig. 4.33 and 4.34 show the size distribution obtained from a Coulter multi-sizer. Fig 4.33 shows the distribution with edit on, eliminating mis-shapen peaks, which gives the best result for size distribution and Fig. 4.34 shows the result for the same sample with edit off which takes into account the full weight of the sample.

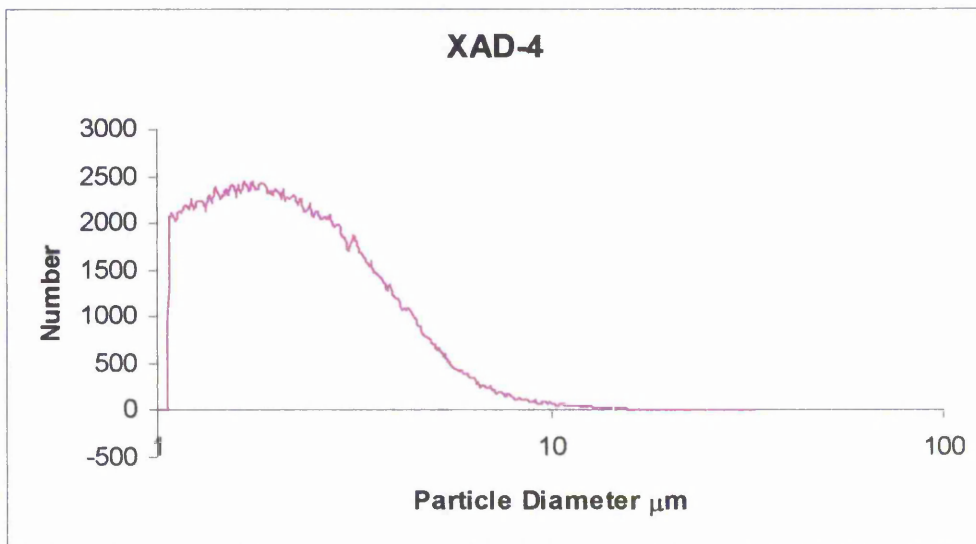


Fig. 4.33. XAD-4 size distribution, edit on.

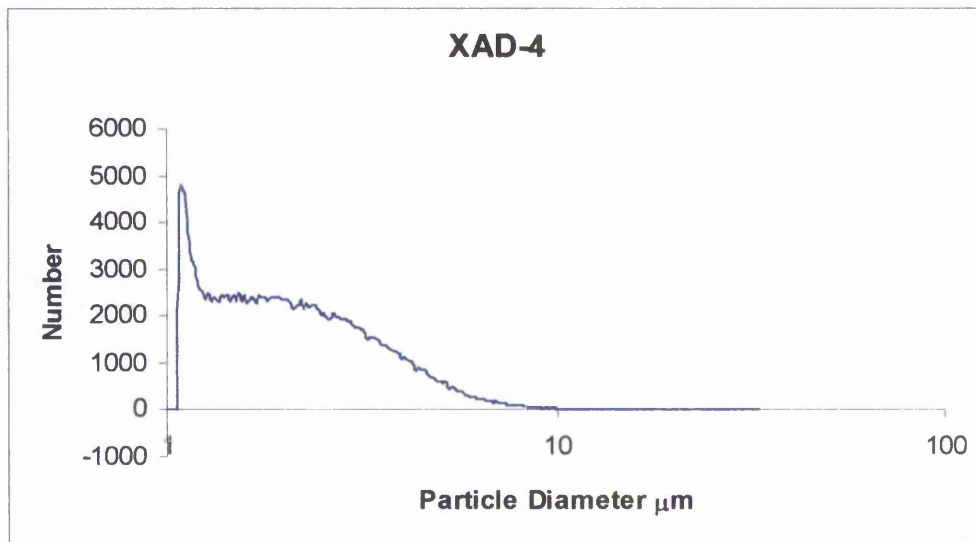


Fig. 4.34. XAD-4 size distribution, edit off.

Nitrogen adsorption gave a BET surface area of  $700 \text{ m}^2 \text{ g}^{-1}$  and the pore size distribution is shown in Fig 4.35. The DR micropore volume is  $0.25 \text{ cm}^3 \text{ g}^{-1}$ .

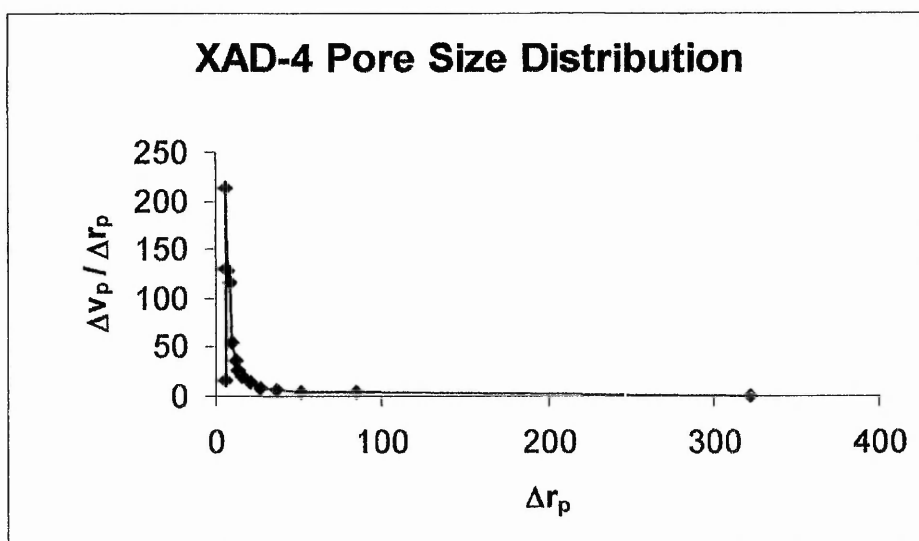


Fig 4.35. Pore size distribution for milled XAD-4

This ground XAD-4 was used in the vapour adsorption experiments as a comparison with the porous nanoparticles.

#### **4.1.8.4 Nonane Preadsorption**

Nonane pre-adsorption is a method used to evaluate the microporosity of a sample. Gregg and Langford<sup>168</sup> showed that the rate at which *n*-nonane could be removed from micropores was very slow, but that the rate at which it leaves mesopores, macropores and the external surface is much faster. A sample of porous nanoparticles was exposed to *n*-nonane vapour and the specific surface area determined by nitrogen adsorption. The results are given in table 4.8.

	Surface Area m <sup>2</sup> g <sup>-1</sup>
Before Nonane Preadsorption	214
After Nonane Preadsorption	153
120 min @ 50°C	153
120 min @ 100°C	154
120 min @ 150°C	169
120 min @ 250°C	207

Table 4.8. Nonane pre-adsorption by styrene/divinylbenzene co-polymers

It can be seen from Table 4.8 that *n*-nonane is adsorbed by the porous nanoparticles that leads to a decrease in the total specific surface area to a level that closely corresponds to that of a solid particle of equal size, it can also be seen that a high temperature must be employed to drive off the nonane in any significant amount. This would indicate that the additional surface area of the latex particles is due almost completely to micropores and not to mesopores, macropores or surface roughness.

#### **4.1.9 Vapour Adsorption by Porous Nanoparticles.**

Activated carbon has been used as an adsorbent for vapours for many years. The microporous network developed within activated carbons has seen use in a variety of applications most notably in the development of personal protective equipment supplied to the military in the form of gas masks and protective clothing, going back to the first use of poison gas during the First World War. To date no superior alternative to activated carbon has been found and hence activated carbons are still widely deployed as the adsorbent species in protective equipment. Carbon performance deteriorates in the presence of water vapour however and a more hydrophobic adsorbent could have advantages for use at higher humidities. In the following series of experiments the porous nanoparticles produced with the different porogenic species were exposed to different vapours having different vapour pressures and their performance compared to carbon BPL, an activated carbon used extensively in personal protective equipment as well as XAD4 a commercially available styrene / divinylbenzene macroreticular resin.

All of the adsorption isotherms were measured at 25°C and the saturated vapour pressure for each of the adsorbents was calculated using the Antoine equation.

$$\text{Log}_{10} (P) = A - (B/(T+C)) \quad 4.1$$

Where

P = Vapour pressure (Bar)

T = Temperature (K)

The parameters A, B and C have been taken from the literature values, for methanol<sup>169</sup> and pentane and toluene<sup>170</sup> (Section 3.6). These sorbates were chosen for their varying boiling points.

#### 4.1.9.1 Methanol Adsorption

In this series of experiments the porous nanoparticles produced with the three porogenic species previously examined were exposed to methanol vapour and their adsorption performance compared to that of carbon BPL and XAD4.

Figs. 4.36 to 4.38 show the methanol adsorption isotherms for porous nanoparticles produced with the three porogenic species previously discussed along with those for carbon BPL and XAD4.

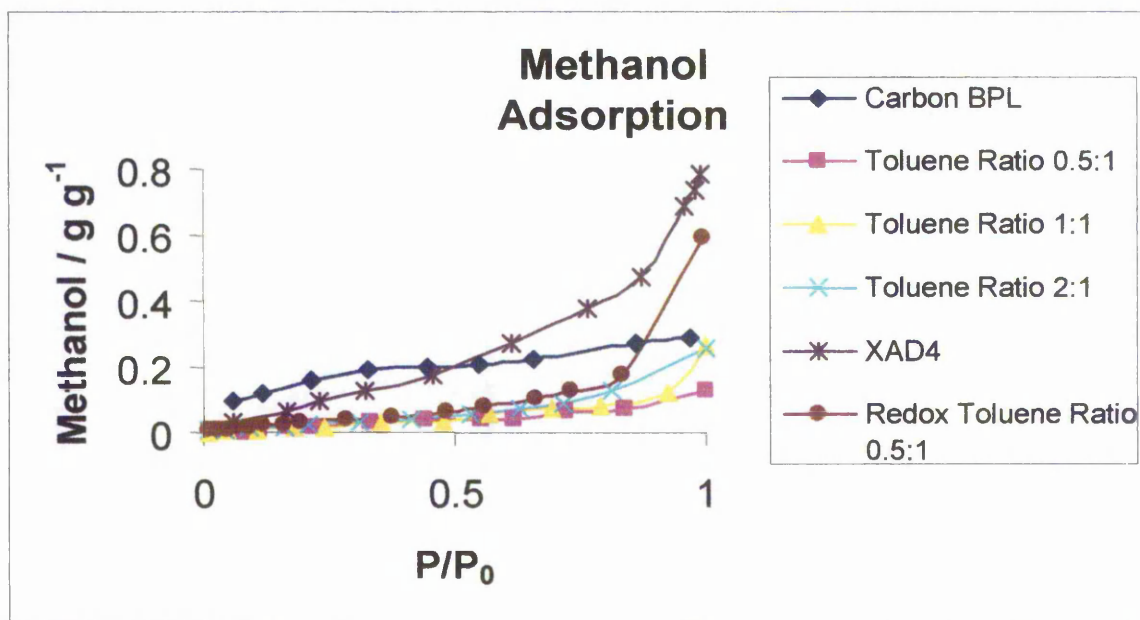


Fig. 4.36 Methanol adsorption isotherm for porous nanoparticles produced with toluene as porogenic species

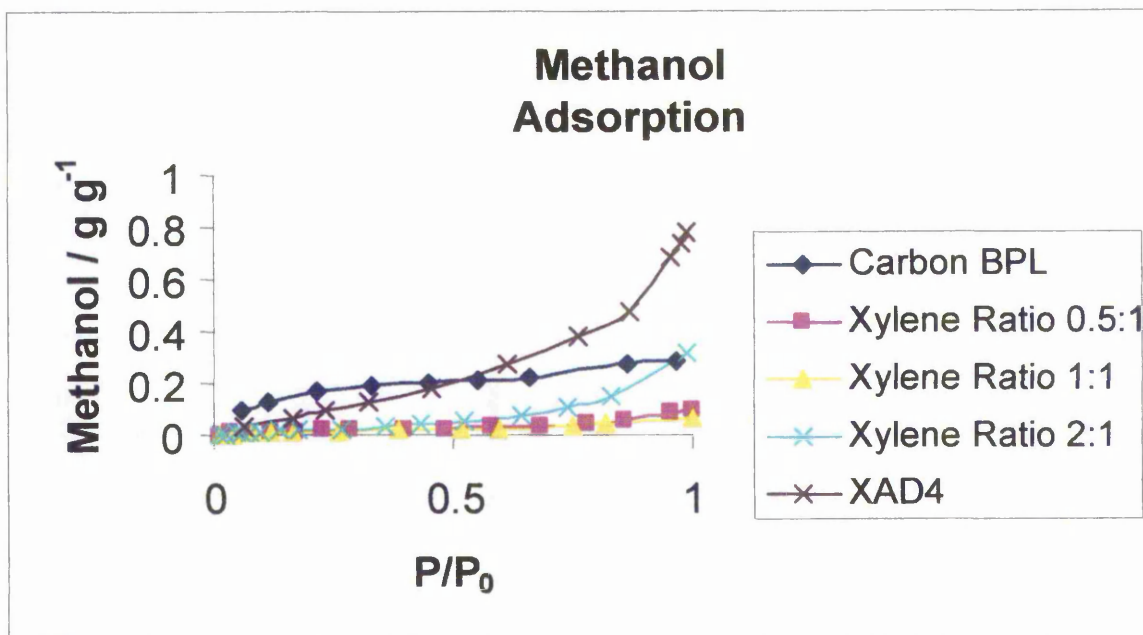


Fig. 4.37 Methanol adsorption isotherm for porous nanoparticles produced with xylene as porogenic species.

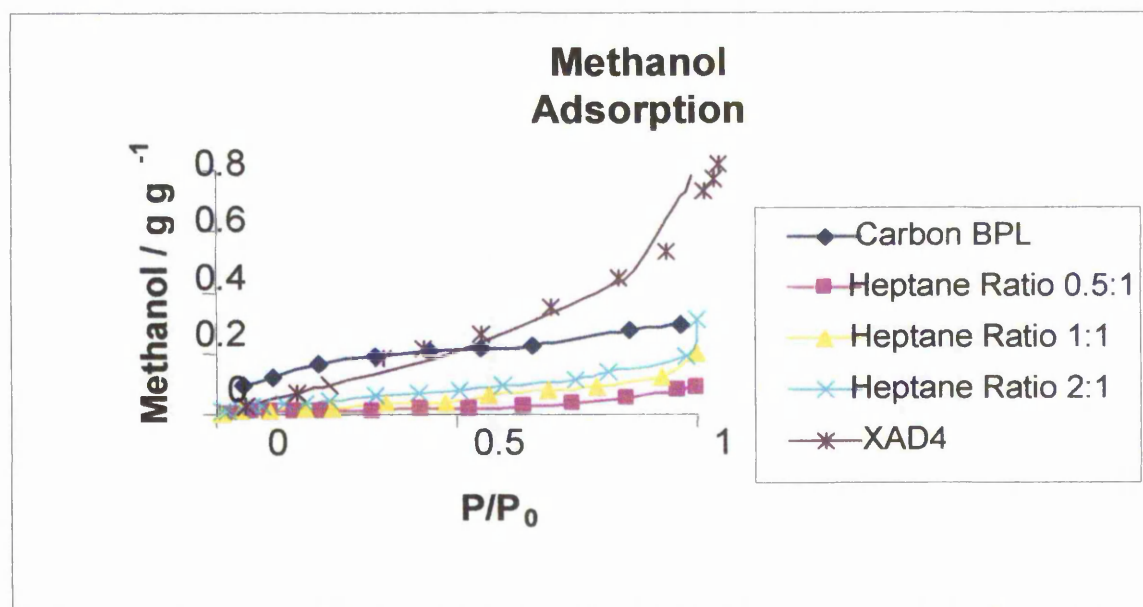


Fig. 4.38. Methanol adsorption isotherm for porous nanoparticles produced with heptane as porogenic species.

From Figs 4.34, 4.35 and 4.36 it can be seen that there is a significant difference in the type of adsorption isotherm produced by the styrene / divinylbenzene copolymers compared to that produced by the activated carbon BPL. Carbon BPL results in a typical type I adsorption isotherm where

the bulk of the adsorption takes place at low value of  $P/P_0$ , whereas the adsorption isotherms derived for the styrene / divinylbenzene copolymers result in a type II adsorption isotherm. It can also be seen that at low values of  $P/P_0$  the total amount of methanol adsorbed by the sample is much lower for the copolymers than for the carbon sample, however as the relative pressure is increased then the total amount of methanol adsorbed approaches that of carbon BPL, indeed for XAD 4 and the porous nanoparticles produced via a redox couple the total amount of methanol adsorbed at high relative pressures exceed that of carbon BPL, with XAD 4 having the highest methanol adsorption as  $P/P_0$  tends to 1.

From the figures it can also be seen that the performance of the porous nanoparticles is very similar regardless of the porogenic species used to create the porous network. This would again suggest that unlike in the production of macroreticular resins where the choice of porogenic species has a major impact on the porous structure, the porosity associated with porous nanoparticles produced via direct emulsion cross-linking copolymerisation is not influenced by the choice of porogenic species.

	Toluene	Xylene	Heptane
Carbon BPL	0.2	0.2	0.2
XAD-4	0.17	0.17	0.17
0.5	0.03	0.024	0.01
1	0.04	0.027	0.035
2	0.07	0.03	0.08

Table 4.9. Methanol Adsorption at  $P/P_0 = 0.5$

Table 4.9 shows the methanol adsorption at  $P/P_0 = 0.5$ . From the table it can be seen that the porous nanoparticles produced with toluene adsorb the most methanol at this relative pressure.

In Figs 4.39 and 4.40 the methanol adsorption / desorption isotherms for carbon BPL and porous nanoparticles produced with toluene at a porogen to monomer ratio of 2:1 are shown.

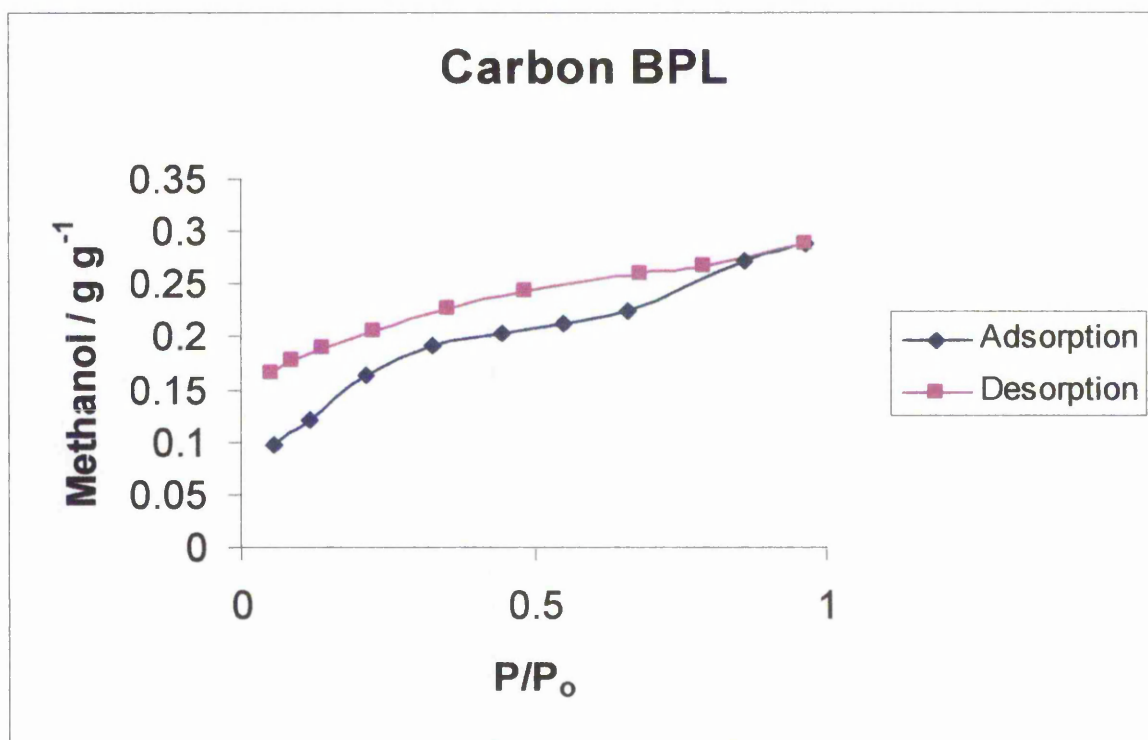


Fig. 4.39. Methanol adsorption / desorption isotherm for carbon BPL.

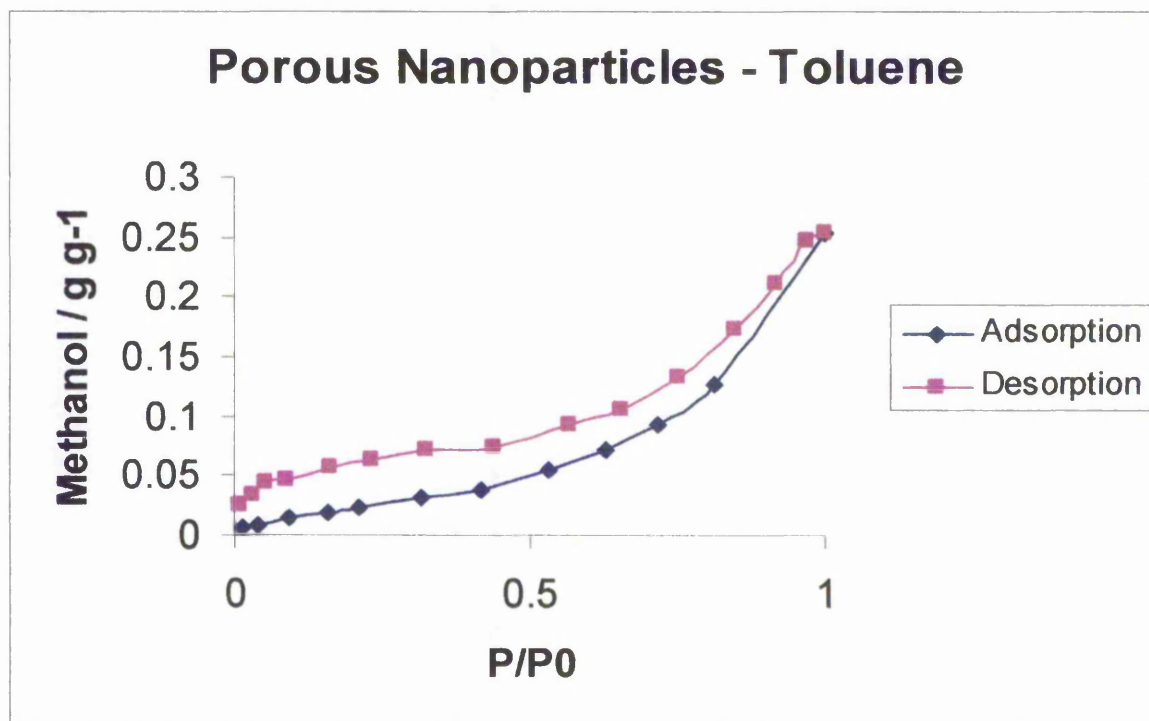


Fig 4.40. Methanol adsorption / desorption isotherm for porous nanoparticles produced with toluene as porogen, porogen to monomer = 2:1.

From Figs 4.38 and 4.40 it can be seen that carbon BPL is much more effective at retaining methanol at lower  $P/P_0$  values within the porous network than the porous nanoparticles, even though the amount of methanol adsorbed at  $P/P_0 = 1$  is similar.

#### 4.1.9.2 Pentane Adsorption.

In this series of experiments the porous nanoparticles produced with three porogenic species previously examined were exposed to pentane vapour and their adsorption performance compared to that of carbon BPL and XAD 4.

Figs. 4.41, 4.42 and 4.43 show the pentane adsorption isotherms for porous nanoparticles produced with the three porogenic species previously discussed.

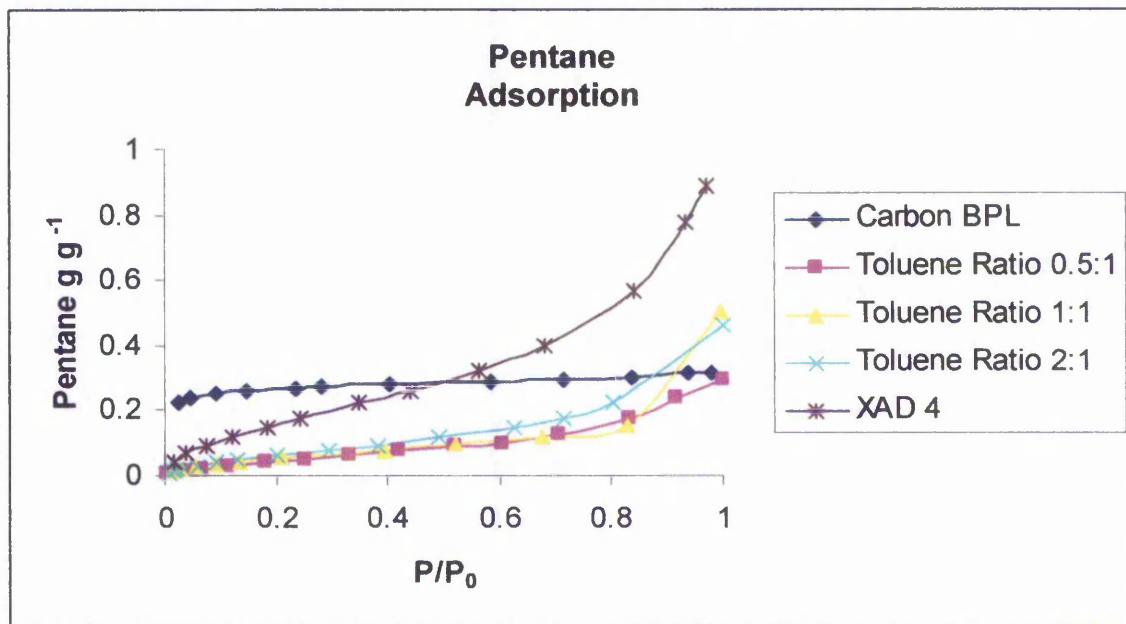


Fig 4.40 Pentane Adsorption Isotherm for porous nanoparticles produced with toluene as porogen

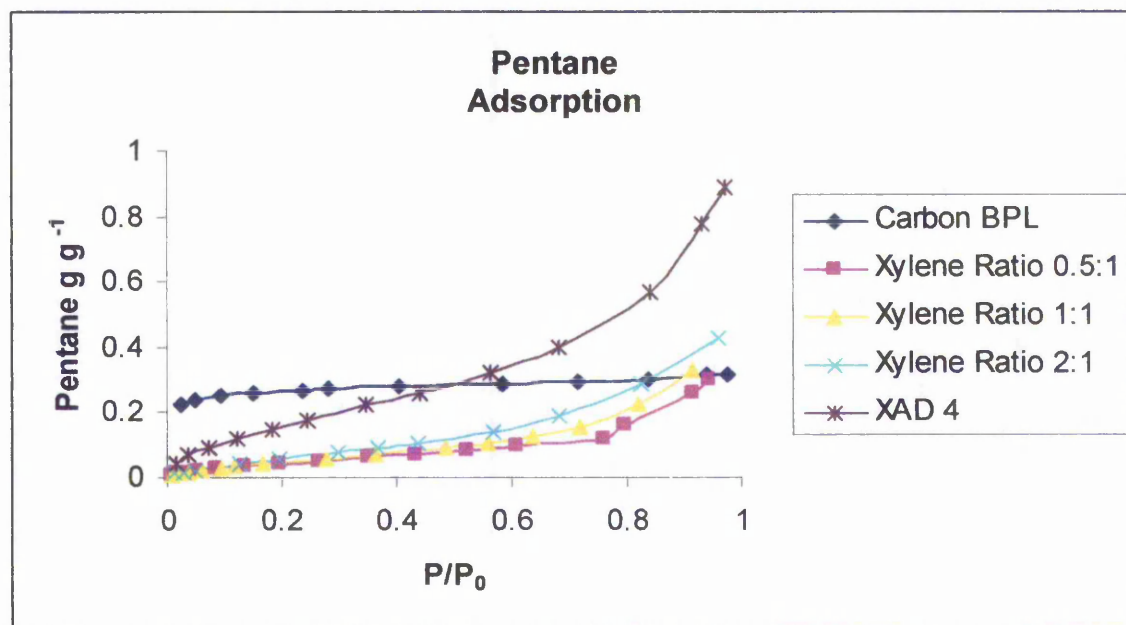


Fig 4.42 Pentane adsorption isotherm for porous nanoparticles produced with xylene as porogen

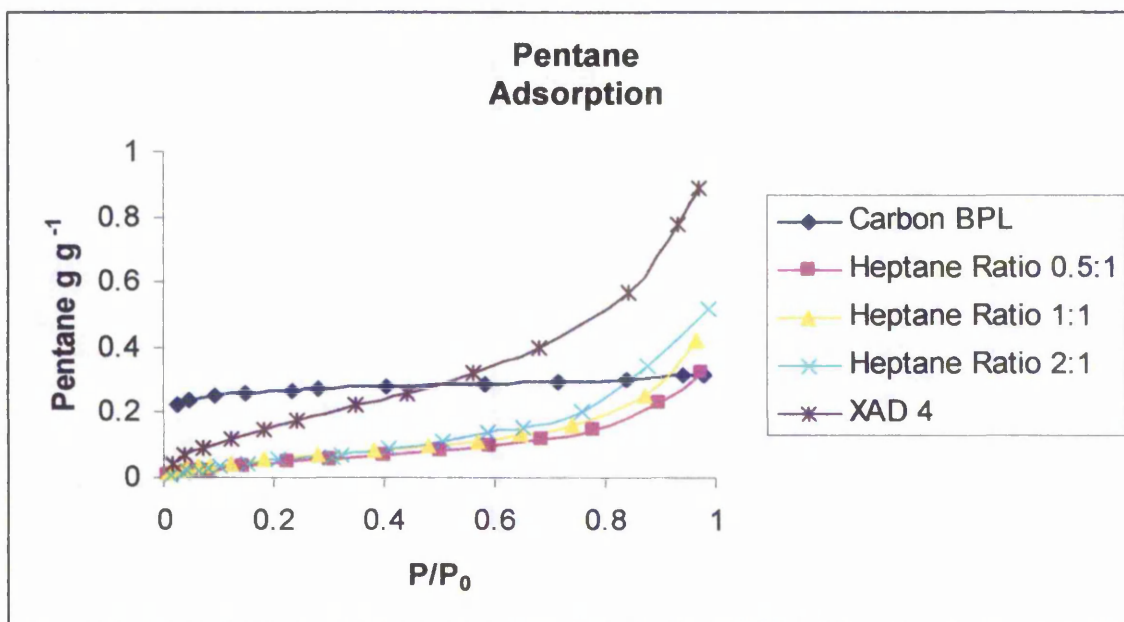


Fig. 4.43 Pentane adsorption isotherm for porous nanoparticles produced with heptane as porogen

From the figures it can be seen that as with methanol adsorption the pentane adsorption isotherm for carbon BPL conforms to a typical type I isotherm, whereas those for the styrene / divinylbenzene copolymers produce a typical type II. As with methanol adsorption there is no significant difference in the performance of the porous nanoparticles produced with the three porogenic species under study.

In the case of pentane adsorption the total amount of pentane adsorbed at high values of  $P/P_0$  is greater for the porous nanoparticles than for carbon BPL, however at lower values of  $P/P_0$  carbon BPL adsorbs significantly more pentane.

Table 4.10 shows the pentane adsorption at  $P/P_0 = 0.5$ . From the table it can be seen that the porous nanoparticles produced with toluene adsorb the most pentane at this relative pressure.

	Toluene	Xylene	Heptane
Carbon BPL	0.28	0.28	0.28
XAD-4	0.28	0.28	0.28
0.5:1	0.09	0.08	0.09
1	0.12	0.09	0.11
2	0.16	0.1	0.14

Table 4.10. Pentane adsorption at  $P/P_0 = 0.5$

### **4.1.9.3. Toluene Adsorption**

In this series of experiments the porous nanoparticles produced with the three porogenic species previously studied were exposed to toluene vapour and their adsorption performance compared to that of carbon BPL and XAD 4. Toluene is a solvent for polystyrene and it was expected that the ability of the porous nanoparticles to adsorb toluene might be enhanced by a certain amount of swelling of the particles.

Figs. 4.44, 4.45 and 4.46 show the toluene adsorption isotherms for porous nanoparticles produced with the three porogenic species previously discussed.

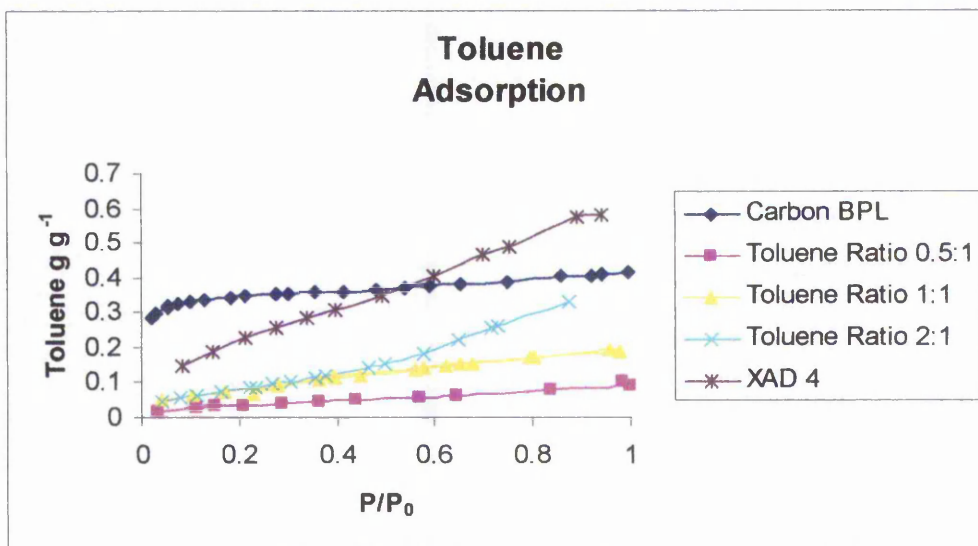


Fig. 4.44 Toluene adsorption isotherm for porous nanoparticles produced with toluene as porogen.

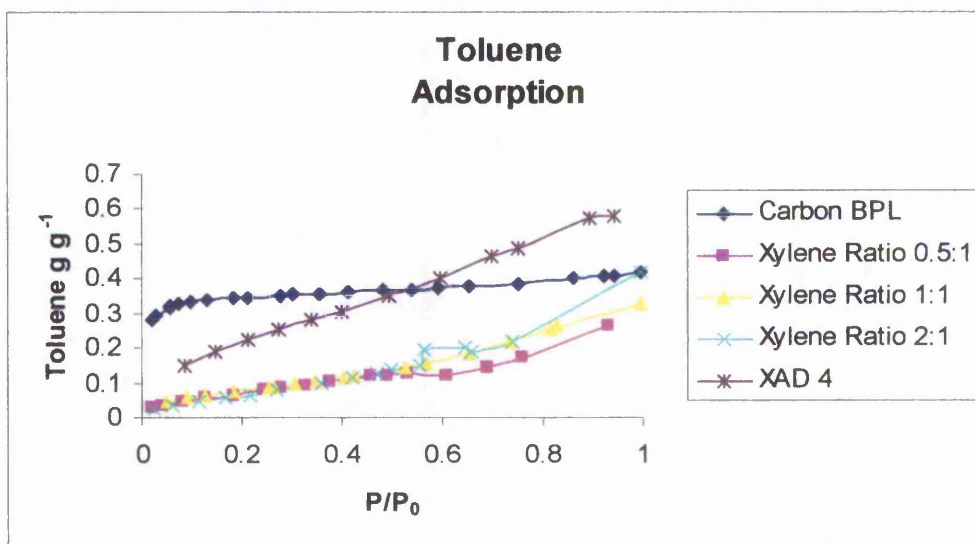


Fig. 4.45 Toluene adsorption isotherm for porous nanoparticles produced with xylene as porogen.

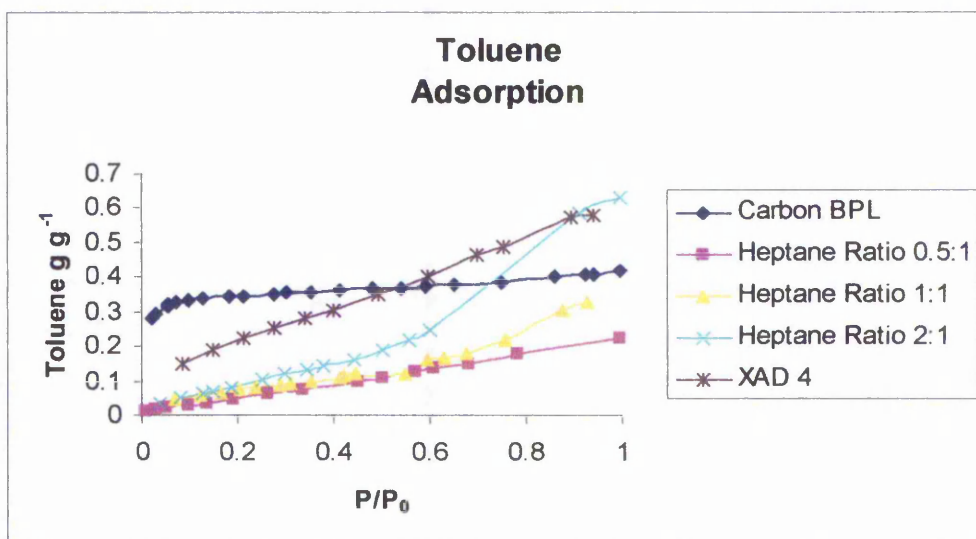


Fig. 4.46 Toluene adsorption isotherm for porous nanoparticles produced with heptane as porogen.

From the isotherms produced for toluene adsorption it can be seen that there is a noticeable difference compared to those produced for methanol and pentane in that the isotherms for toluene adsorption result in a near linear plot. Again as with methanol and pentane adsorption XAD 4 performs best out of the styrene / divinylbenzene copolymers and the adsorption of toluene by carbon BPL again shows better adsorption at low  $P/P_0$  values, but total adsorption as  $P/P_0$  tends toward unity is better for both XAD 4 and the porous nanoparticles produced with the highest ratio of heptane.

Table 4.11 shows the toluene adsorption at  $P/P_0 = 0.5$ . From the table it can be seen that there is no real difference between the porogens.

	Toluene	Xylene	Heptane
Carbon BPL	0.36	0.36	0.36
XAD-4	0.34	0.34	0.34
0.5:1	0.06	0.12	0.11
1	0.12	0.13	0.13
2	0.15	0.14	0.18

Table 4.11 Toluene adsorption at  $P/P_0 = 0.5$

No additional uptake of toluene is apparent as a consequence of biomimetic templating<sup>171</sup> which might have occurred when toluene was used as the porogen.

## 4.2 Kinetics of Polymerisation

### 4.2.1 Kinetics of Styrene Polymerisation Using a Redox Couple Initiator

The kinetics of the polymerisation of styrene using the redox couple of potassium persulphate and sodium metabisulphite initiator was studied as a precursor to a more detailed kinetic study of the styrene/divinylbenzene copolymer system. Although this system of initiating emulsion polymerisation was patented as early as 1940<sup>172</sup>, there are still aspects of the system which are not fully understood<sup>40</sup>.

Smith-Ewart case 2 interval II kinetics are independent of radical production rate provided that the average number of radicals per particle ( $\bar{n}$ ) can be maintained at 0.5. In a conversion against time plot interval II is at a constant rate because  $R_p = K_p[M]\bar{n}N$ , and all the quantities on the right hand side of the equation are constant. The overall rate of reaction is affected by the value of  $N$ , which will depend on the efficiency of particle nucleation in interval I. To verify if the reaction complies with classical Smith-Ewart case 2 kinetics, the observed rate can be inserted and the equation solved for  $\bar{n}$

The reaction was followed using dilatometry, the change in density over time being proportional to the rate of conversion of the monomer to polymer. The rate of polymerisation  $R_p$  was determined for a series of reactions at constant temperature with different sodium metabisulphite / potassium persulphate ratios.

### 4.2.1.1 Sodium Dodecylsulphate

In this series of experiments styrene was polymerised in the presence of sodium dodecylsulphate as surfactant and with increasing sodium metabisulphite / potassium persulphate ratio. The reaction were carried out at three temperatures 50°C, 40°C and 30°C, the conversion against time plots are shown in Figs. 4.47, 4.48 and 4.49.

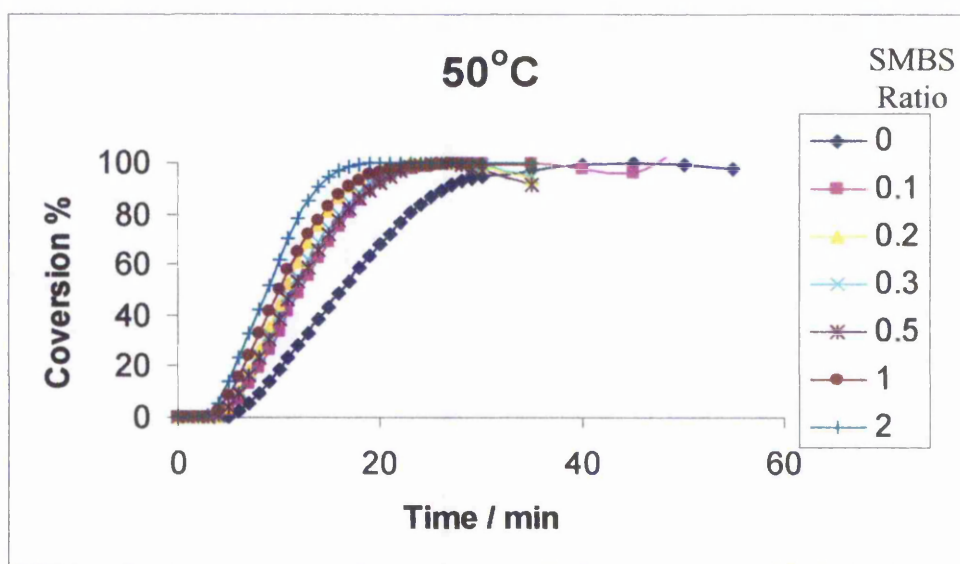


Fig. 4.47 Conversion against time plots for polystyrene with varying sodium metabisulphite / potassium persulphate ratio at 50°C

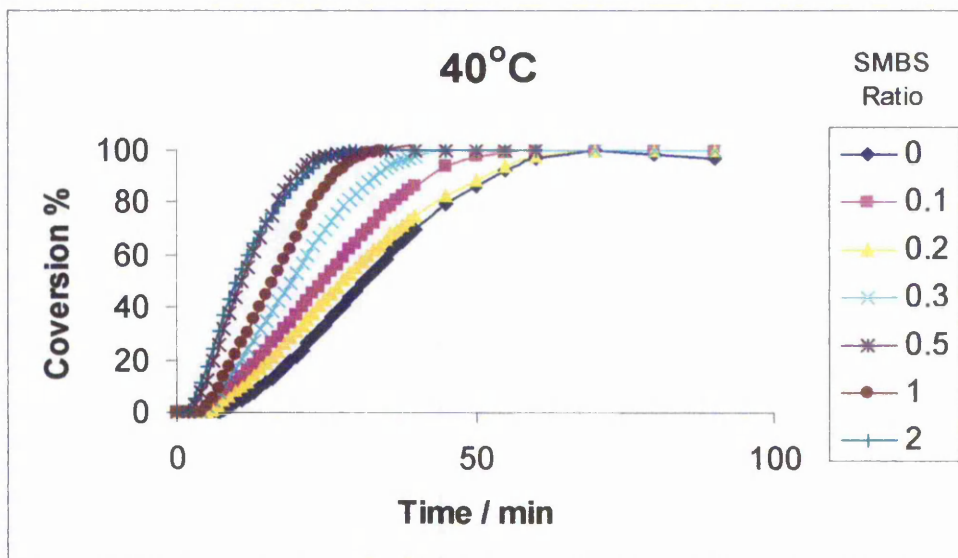


Fig. 4.48 Conversion against time plots for polystyrene with varying sodium metabisulphite / potassium persulphate ratio at 40°C

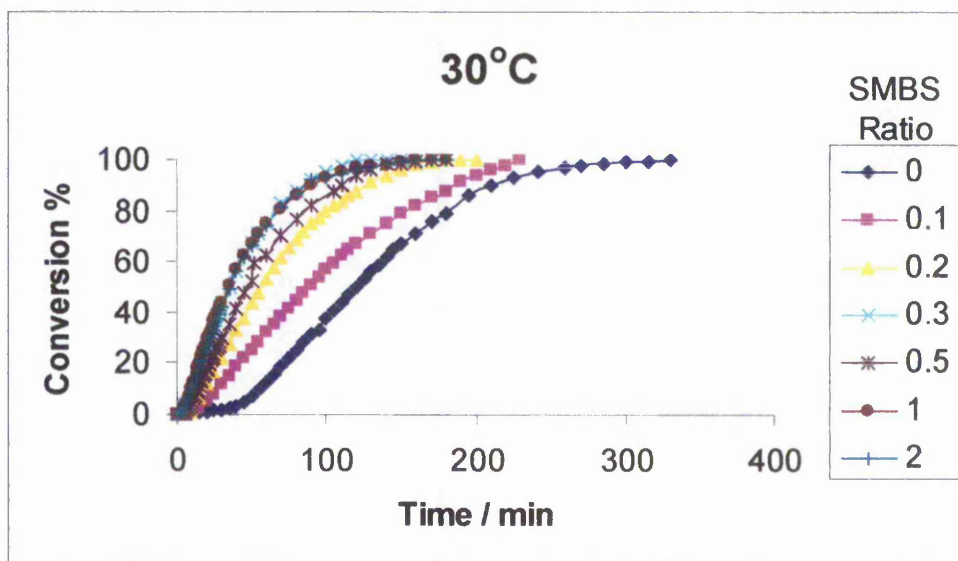


Fig. 4.49 Conversion against time plots for polystyrene with varying sodium metabisulphite / potassium persulphate ratio at 30°C

From Figs. 4.47, 4.48 and 4.49 It can be seen that as the sodium metabisulphite is introduced into the system the rate of conversion increases, also as expected as the temperature is reduced for the same sodium metabisulphite / potassium persulphate ratio the rate of conversion decreases.

From interval II of the conversion against time charts the rate of polymerisation in  $\text{mol min}^{-1}$  can be calculated, Fig. 4.50 shows a plot of  $R_p$  against sodium metabisulphite / potassium persulphate ratio for the three temperatures studied.

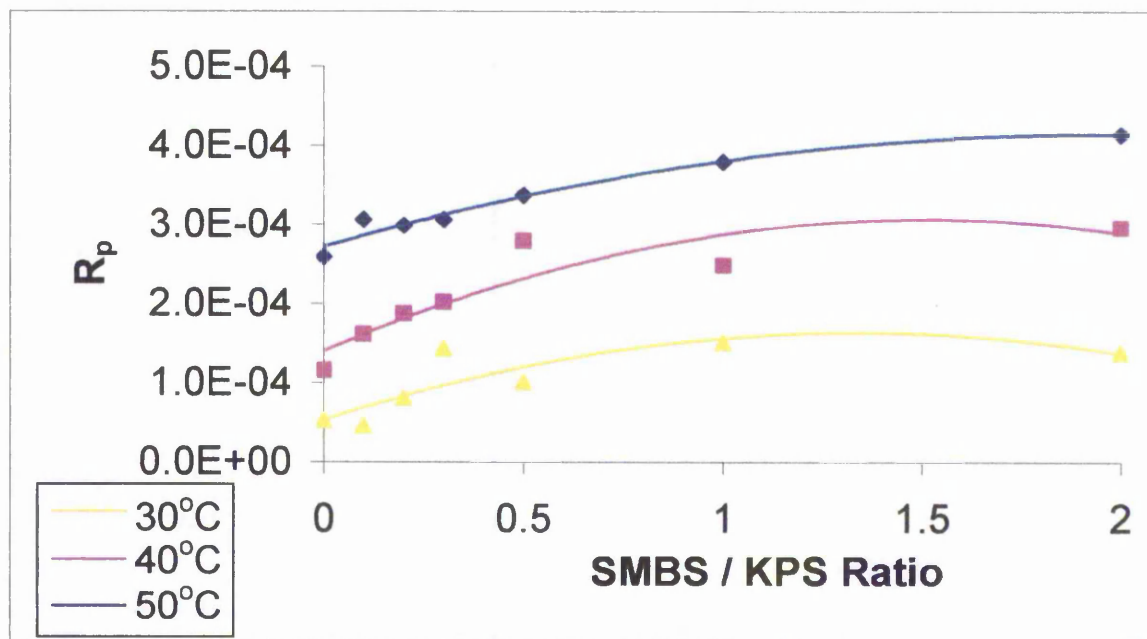


Fig. 4.50 change in rate of polymerisation,  $R_p$ , with change in redox ratio for the conversion of styrene to polystyrene with SDS surfactant

Fig. 4.50 more clearly shows that as the reducing agent is introduced into the system the rate of reaction increases. There is an increase in the rate as the ratio of the two components change to higher sodium metabisulphite concentrations. There is as expected a significant difference in the rate of reaction at lower temperatures but it can be seen that the rate of reaction could be doubled at each temperature with the use of the redox couple.

Tables 4.12, 4.13 and 4.14 show the kinetic data for the polymerisations at 50°C, 40 °C. and 30°C respectively with sodium dodecylsulphate as emulsifier. For all the polymerisations at the three temperatures studied, the values of  $\bar{n}$  from the Smith-Ewart equation are all

approximately 0.5 implying that all the runs regardless of redox ratio or temperature comply to Smith-Ewart case 2 kinetics. The only difference can be seen in Table 4.14 for the runs at 30°C, when at low redox ratios the particle size is much larger. It is therefore possible to produce stable polystyrene latices at very low temperatures using a redox couple, although polymerisation times are significantly greater at low temperatures.

KPS/SMBS	$R_p / 10^{-4} \text{ mol dm}^{-3} \text{ s}^{-1}$	Particle Size / nm	Number Density $N / 10^{14} \text{ ml}^{-1}$	$\bar{n}$
0	2.59	77.9	2.57	0.62
0.1	3.06	78.2	2.54	0.74
0.2	2.99	64.7	4.49	0.41
0.3	3.06	76.4	2.72	0.69
0.5	3.37	69	3.71	0.56
1	3.79	65.4	4.35	0.54
2	4.15	64	4.64	0.55

Table 4.12. Kinetic data for the polymerisation of styrene at 50°C with increasing sodium metabisulphite concentration with sodium dodecyl sulphate as surfactant.

KPS/SMBS	$R_p / 10^{-4} \text{ mol dm}^{-3} \text{ s}^{-1}$	Particle Size / nm	Number Density $N / 10^{14} \text{ ml}^{-1}$	$\bar{n}$
0	1.53	70.3	3.5	0.29
0.1	1.6	75.9	2.78	0.54
0.2	1.87	82.1	2.2	0.72
0.3	2.02	77.4	2.63	0.67
0.5	2.79	57.5	6.4027	0.36
1	2.48	75.5	2.828	0.73
2	2.96	70	3.5487	0.69

Table 4.13. Kinetic data for the polymerisation of styrene at 40°C with increasing sodium metabisulphite concentration with sodium dodecyl sulphate as surfactant.

KPS/SMBS	$R_p / 10^{-4} \text{ mol dm}^{-3} \text{ s}^{-1}$	Particle Size / nm	Number Density $N / 10^{14} \text{ ml}^{-1}$	$\bar{n}$
0	0.52	106.2	1.016	0.59
0.1	0.46	99.8	1.224	0.43
0.2	0.8	83	2.1287	0.44
0.3	1.43	74.9	2.8968	0.57
0.5	1.0	83.2	2.1134	0.55
1	1.5	74	3.0038	0.58
2	1.37	70	3.5487	0.45

Table 4.14 Kinetic data for the polymerisation of styrene at 30°C with increasing sodium metabisulphite concentration with sodium dodecyl sulphate as surfactant.

### 4.2.1.2 Aerosol OT

In this series of experiments the polymerisation of styrene was carried out using a redox couple but the surfactant was changed from sodium dodecyl sulphate to Aerosol OT. Fig 4.51 shows the change in  $R_p$  against redox ratio for Aerosol OT stabilised polystyrene lattices at a series of temperatures.

From Fig. 4.51 it can be seen that there is a significant difference in the change in  $R_p$  as the ratio of the redox couple is changed compared to that shown in Fig. 4.48 for sodium dodecylsulphate, in that as the ratio of the sodium metabisulphite component in the redox couple is increased there is an initial increase in the value of  $R_p$  similar to that encountered with sodium dodecylsulphate, however at higher sodium metabisulphite ratios there is a marked decrease in the value of  $R_p$ .

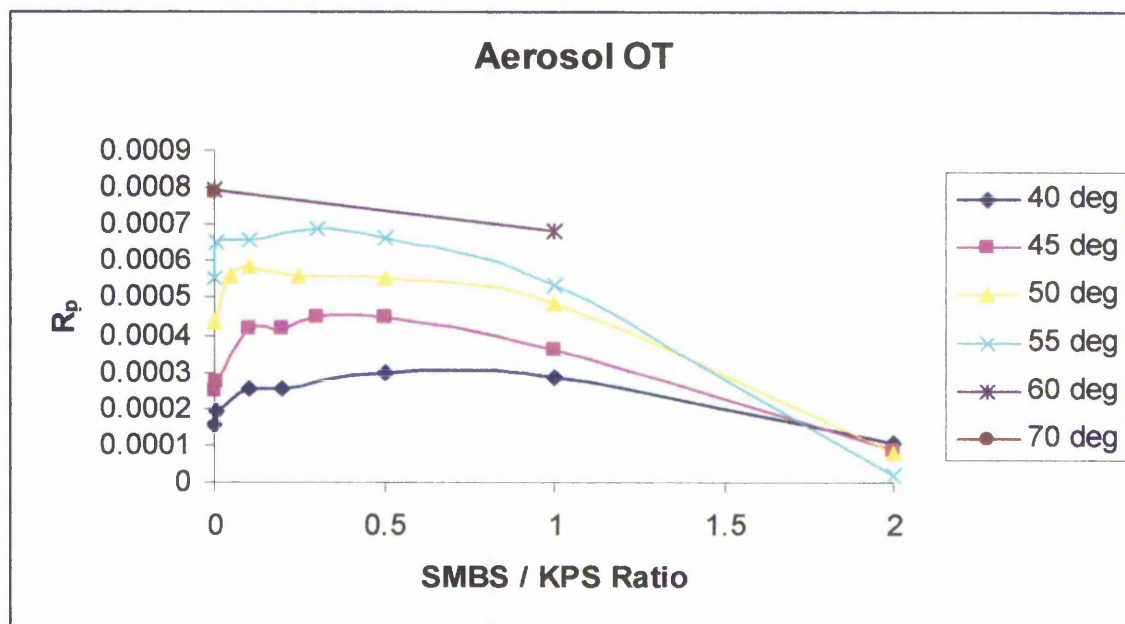


Fig 4.51 change in  $R_p$  with change in redox ratio for the conversion of styrene to polystyrene with Aerosol OT surfactant.

A more detailed study on the effect of the redox ratio on both  $R_p$  and  $\bar{n}$  was carried out at 50°C and the results are given in Fig. 4.52 and table 4.15.

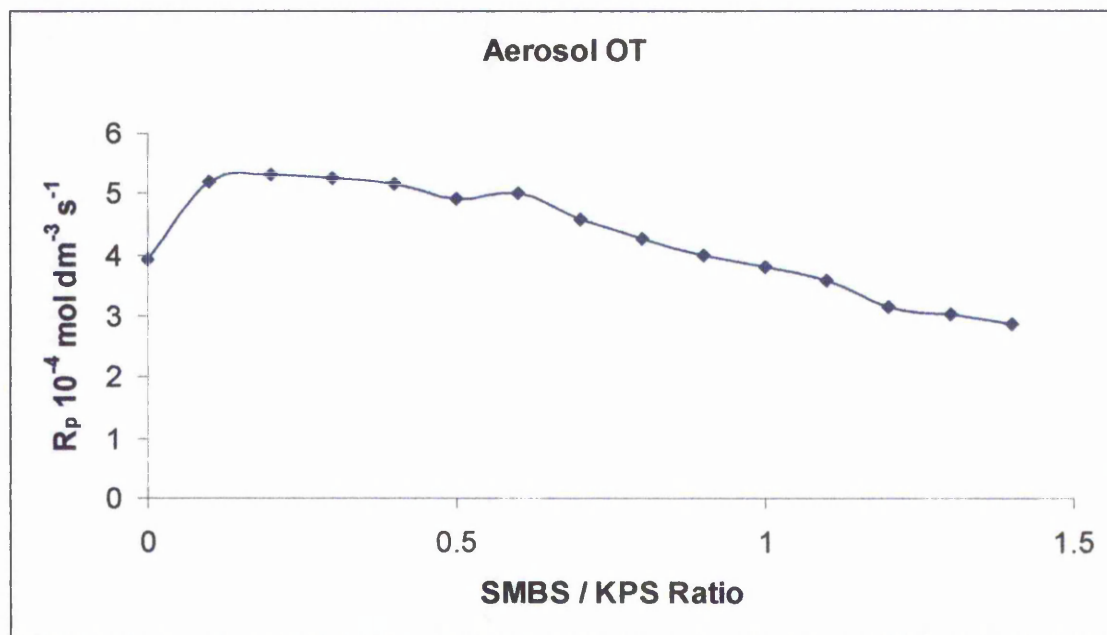


Fig. 4.52 Change in  $R_p$  with change in redox ratio for the conversion of styrene to polystyrene with Aerosol OT surfactant at 50°C.

KPS/SMBS	$R_p / 10^{-4} \text{ mol dm}^{-3} \text{ s}^{-1}$	Particle Size / nm	Number Density $N / 10^{14} \text{ mol}^{-1}$	$\bar{n}$
0	3.915	70.2	3.58	0.45
0.1	5.19	59.2	5.96	0.36
0.2	5.325	63.2	4.9	0.44
0.3	5.25	64.8	4.5	0.48
0.4	5.16	65.3	5.2	0.4
0.5	4.905	66.1	4.2	0.48
0.6	5.025	64.1	4.7	0.44
0.7	4.575	68.6	3.8	0.49
0.8	4.26	70	3.6	0.48
0.9	3.975	71.4	3.4	0.48
1	3.795	75.7	2.85	0.55
1.1	3.6	85.6	1.97	0.75
1.2	3.15	91.7	1.6	0.8
1.3	3.045	104.7	1.08	1.15
1.4	2.88	113.6	0.84	1.4

Table 4.15 Kinetic data for the polymerisation of styrene at 50°C with increasing sodium metabisulphite concentration with Aerosol OT as surfactant.

From table 4.15 it can be seen that as the ratio of sodium metabisulphite is increased there is an initial increase in the value of  $R_p$  with a maximum value at a ratio of 0.2:1 after this point there is a steady decrease in the value of  $R_p$ . however the value of  $\bar{n}$  remains within the region of 0.5 which corresponds to the value expected for Smith-Ewart case 2 kinetics until a ratio of 1:1 after which the value of  $\bar{n}$  tends toward 1 which corresponds to Smith-Ewart case 3 kinetics. This trend is thought to be due to particle destabilisation caused by an increase in the ionic strength within the system; this destabilisation causes a reduction in  $N$  the particle number density which corresponds to an increase in the particle size. The surfactant having a branched tail will pack less efficiently at the particle surface and contribute less charge density than would a surfactant with a linear tail. The particles will therefore be more susceptible to the effects of ionic strength.

#### **4.2.1.3 Igepal**

A further examination of the kinetics of the polymerisation of styrene using the non-ionic surfactant Igepal CO720. Fig. 4.53. shows the change in  $R_p$  with changing redox couple ratio.

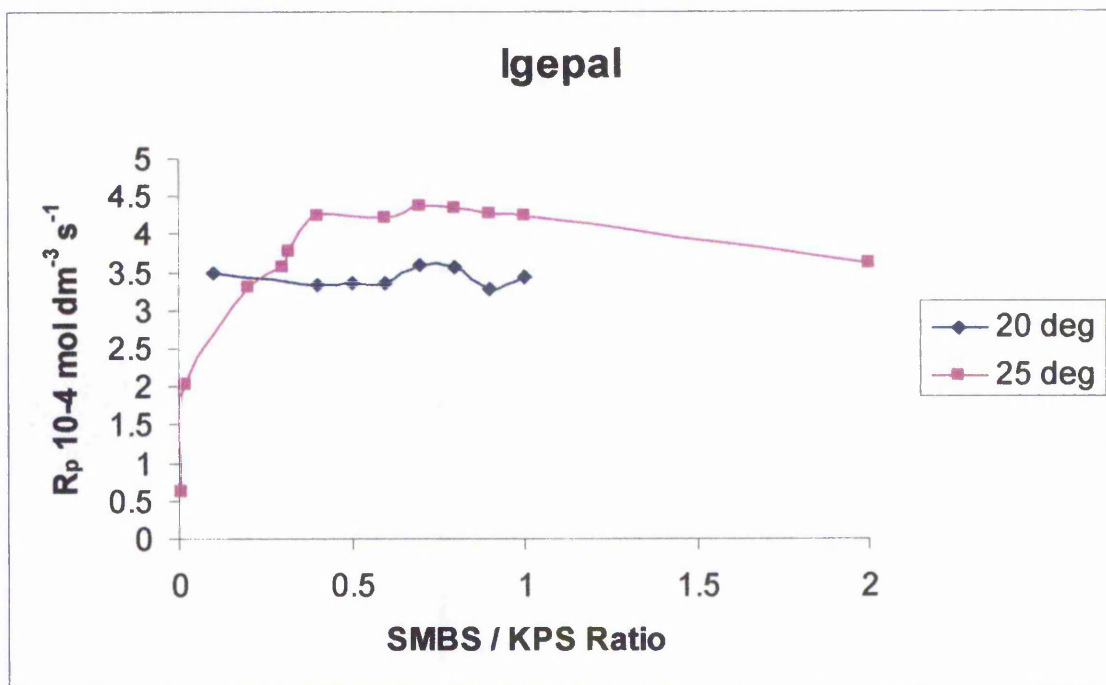


Fig. 4.53. Change in  $R_p$  with changing redox couple ratio for the conversion of styrene to polystyrene using Igepal as surfactant.

From the figure it can be seen that at 25°C there is a dramatic change in the value of  $R_p$  with the introduction of the sodium metabisulphite. Tables 4.16 and 4.17 give the kinetic data for the two temperatures.

KPS/SMBS	$R_p / 10^{-4} \text{ mol dm}^{-3} \text{ s}^{-1}$	Particle Size / nm	Number Density $N / 10^{14} \text{ mol}^{-1}$	$\bar{n}$
0.008	0.62	81	2.34	0.32
0.016	2.02	62	5.14	0.54
0.2	3.32	55.3	7.37	0.61
0.3	3.58	56.7	6.79	0.71
0.32	3.78	50	9.84	0.52
0.4	4.24	50.4	9.67	0.59
0.6	4.22	49.3	10.37	0.56
0.7	4.38	47.8	10.99	0.53
0.8	4.34	51.7	8.97	0.66
0.9	4.27	50.3	9.78	0.61
1	4.24	50.6	9.56	0.61
2	3.61	55.3	7.34	0.674

Table 4.16 Kinetic data for the polymerisation of styrene at 25°C with increasing sodium metabisulphite concentration with Igepal as surfactant.

KPS/SMBS	$R_p / 10^{-4} \text{ mol dm}^{-3} \text{ s}^{-1}$	Particle Size / nm	Number Density $N / 10^{14} \text{ mol}^{-1}$	$\bar{n}$
0.1	3.48	51.7	8.98	0.52
0.4	3.33	53.4	8.14	0.66
0.5	3.35	52.5	8.55	0.64
0.6	3.36	55.2	7.37	0.743
0.7	3.6	49.5	10.2	0.57
0.8	3.57	50.4	9.61	0.6
0.9	3.29	54.2	7.79	0.69
1	3.45	55.4	7.27	0.78

Table 4.17 Kinetic data for the polymerisation of styrene at 20°C with increasing sodium metabisulphite concentration with Igepal as surfactant.

From the tables it can be seen that at both temperatures the value of  $\bar{n}$  does not show the same tendency towards Smith-Ewart case 3 kinetics displayed using Aerosol OT, but rather shows Smith-Ewart case 2 kinetics across the range of ratios studied.

## **4.2.2 Porous Nanoparticles**

### **4.2.2.1 Kinetic Study By Dilatometry**

The above experiment was repeated for porous nanoparticles, however there were problems involved in monitoring the progress of the polymerisations via dilatometry. Cavitation within the dilatometer bulb caused gas bubbles to be generated within the dilatometer stem which meant accurate readings were not possible. This initial problem was partially solved by applying a freeze / thaw technique proposed by Pashley *et al.*<sup>173, 174, 175</sup> who studied forming stable soap free emulsions by extracting all dissolved atmospheric gases from the system.

Applying this technique removed the problem of cavitation however further problems were encountered with the polymerisation process itself. When styrene converts to polystyrene there is a change in density which results in volume decrease as mass remains constant, with porous nanoparticles however the change in density shows a distinct two stage process. Figs. 4.54 and 4.55 show the change in relative density for a styrene homopolymer and porous nanoparticles respectively. The relative density was determined by dividing the change in height within the capillary by the initial height at the start of the polymerisation.

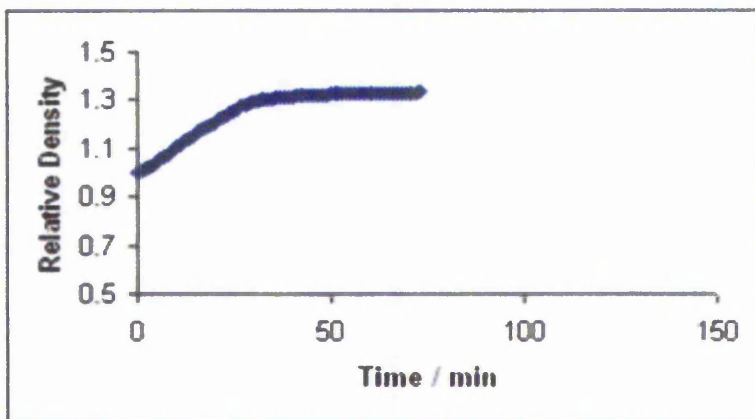


Fig. 4.54 Change in relative density with time for polystyrene homopolymer

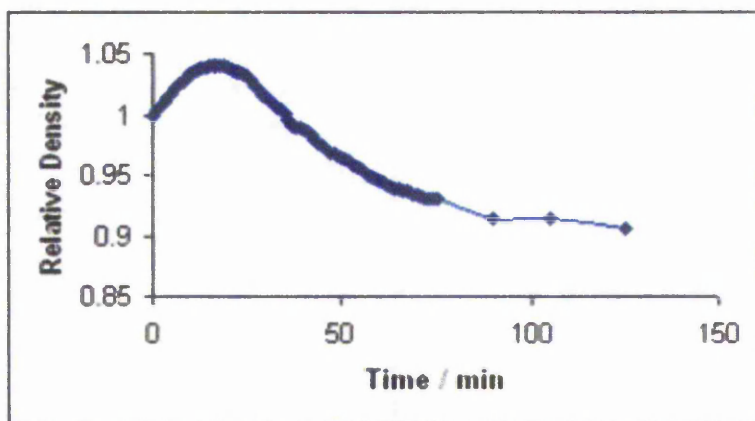


Fig. 4.55 Change in relative density with time for porous nanoparticles

From the relative density against time plots the difference between the two density profiles can clearly be seen. In the case of styrene homopolymer the change in relative density increases until a maximum is reached after this point the density of the product remains constant, this plateau is reached when all of the monomer has been converted to polymer. In the case of porous nanoparticles in the early stage of polymerisation there is an increase in the relative density, however as conversion from monomer to polymer proceeds then a maximum is reached and after this point there is a decrease in the relative density of the final polymer product. It is thought that at the point where the relative density begins to decrease is the point at which the

porous network begins to form i.e. gel point. It should also be noted that the time to completion for styrene homopolymer is more rapid than that for conversion for the porous nanoparticles, presumably due to the effect of porogen dilution of the reaction medium.

#### **4.2.2.2 Kinetic Study By Gravimetric Method**

Due to the difficulties of studying the kinetics of the polymerisation of porous nanoparticles by dilatometry a gravimetric method of analysis was employed. This method involves the removal of small aliquots of the polymerisation mixture at timed intervals and the % conversion calculated by mass. Previous work by Steward<sup>176</sup> has shown that any residual unreacted monomer in the sample will not effect the gravimetric determination of the degree of conversion. Monomer deliberately added to samples removed from the reaction vessel was shown to evaporate off in the oven rather than polymerise.

Fig 4.56 shows the conversion against time plot for porous nanoparticles with increasing potassium persulphate initiator concentration with sodium dodecylsulphate as surfactant at a constant concentration of 0.0138 mol l<sup>-1</sup>. From the chart it can be seen that as the concentration of potassium persulphate is increased the rate of conversion also increases.

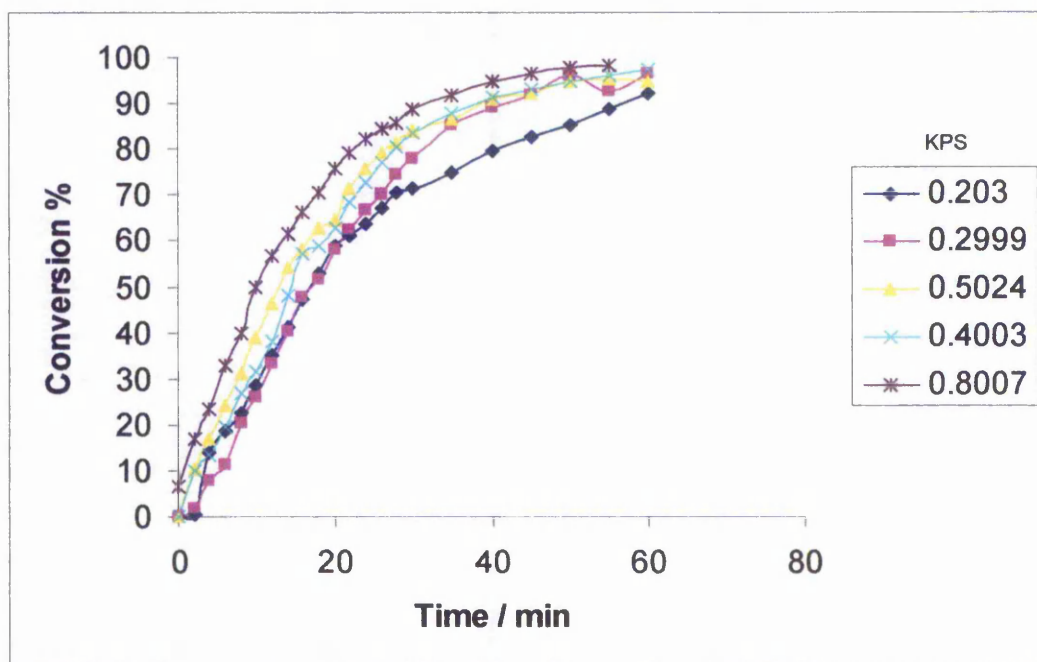


Fig. 4.56 Conversion against time plot for porous nanoparticles with change in potassium persulphate initiator concentration with SDS as surfactant, monomer ratio 1:1.

This increase in rate can be more clearly seen in Fig. 4.57 which shows the slope of the linear stage II portion of the conversion against time chart against the concentration of potassium persulphate initiator.

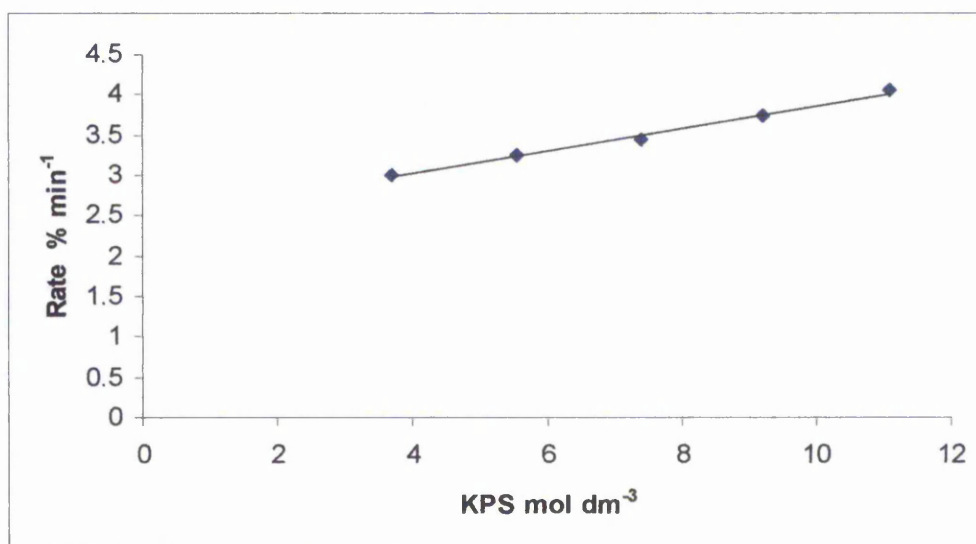


Fig. 4.57 Slope of linear stage II portion of conversion against time chart against molar concentration of potassium persulphate initiator.

The other major influence on the rate of polymerisation is the surfactant concentration. Fig. 4.58 shows the conversion against time plot for porous nanoparticles with changing sodium dodecylsulphate surfactant concentration with a constant potassium persulphate initiator concentration of  $0.4 \text{ g l}^{-1}$ .

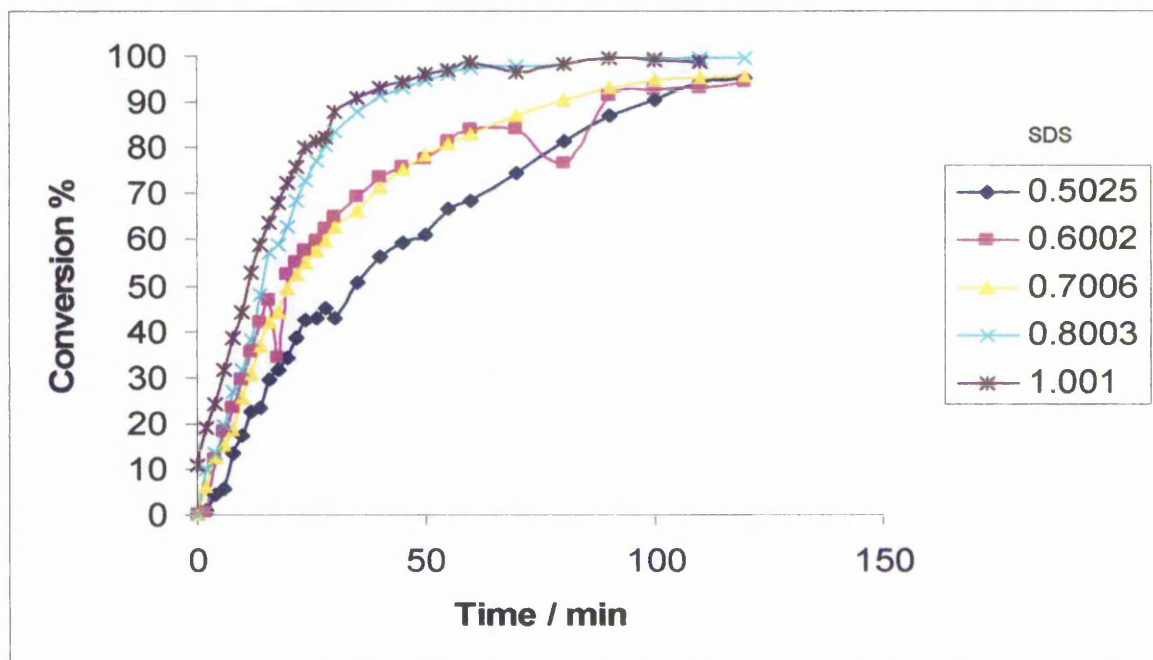


Fig. 4.56 Conversion against time plot for porous nanoparticles with change in sodium dodecylsulphate surfactant with constant potassium persulphate initiator concentration.

From Fig. 4.58 it can be seen that as the concentration of surfactant is increased the rate of polymerisation also increases. This increase in rate can more clearly be seen in Fig. 4.59 which shows the slope of the linear stage II portion of the conversion against time plot against molar concentration of sodium dodecylsulphate surfactant.

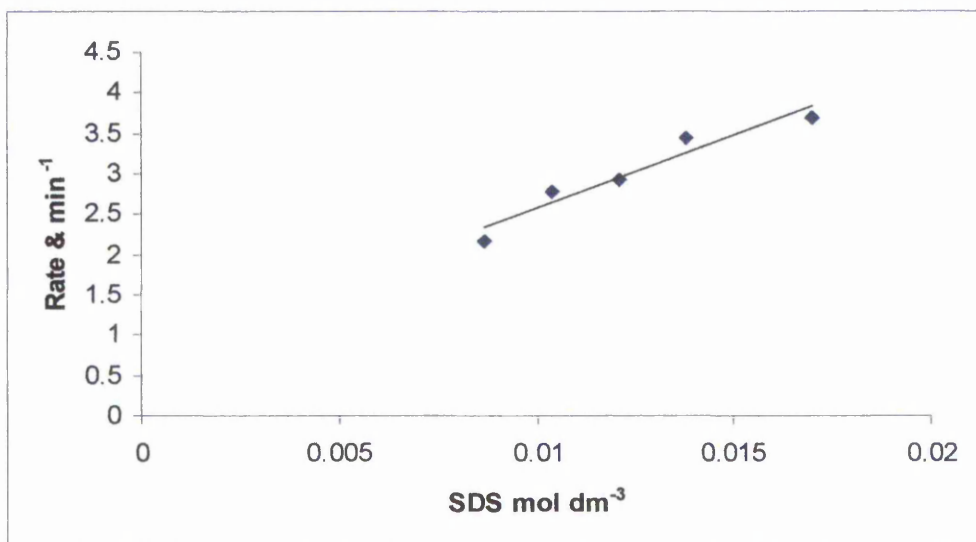


Fig. 4.59 Slope of linear stage II portion of conversion against time plot against sodium dodecylsulphate concentration.

From the log rate / log initiator concentration Fig 4.60 and log rate / log surfactant concentration Fig 4.61, it was possible to determine the rate dependence on these two variables.

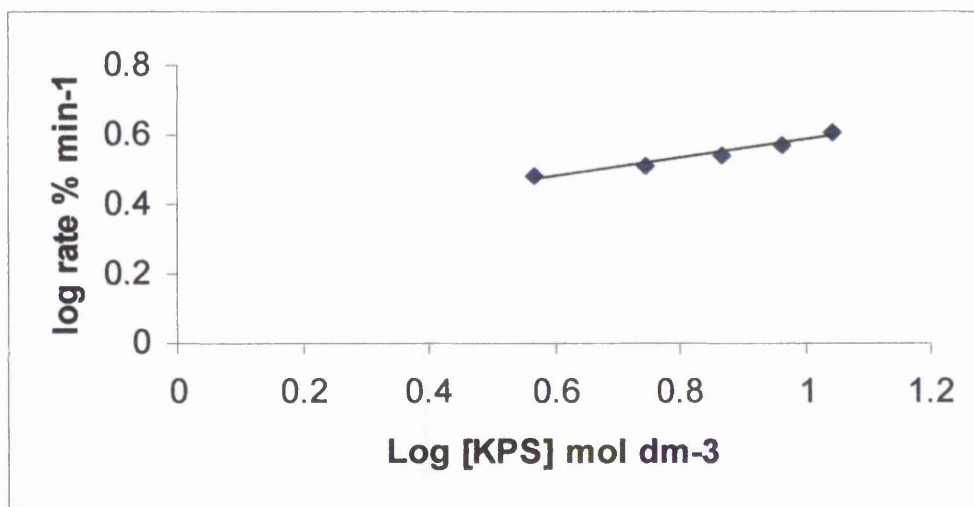


Fig. 4.60 log rate against log initiator concentration

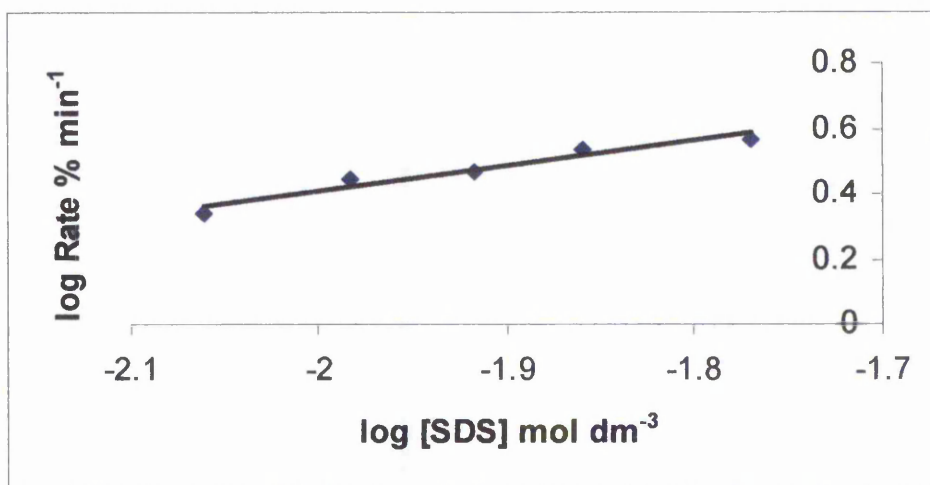


Fig. 4.61 log rate against log surfactant concentration

This dependence was found to be  $[\text{SDS}]^{0.78}$  and  $[\text{KPS}]^{0.26}$ , this compares to a figure of  $[\text{SDS}]^{0.6}$  and  $[\text{KPS}]^{0.4}$  from the results obtained by Smith-Ewart<sup>29</sup> for the polymerisation of styrene.

#### **4.2.2.3 Rate Dependence on Divinylbenzene Concentration**

A further gravimetric study was carried out on the effect of the divinylbenzene concentration on the rate of reaction. Fig. 4.62 shows the conversion against time plots for a series of porous nanoparticles produced with varying concentration of divinylbenzene.

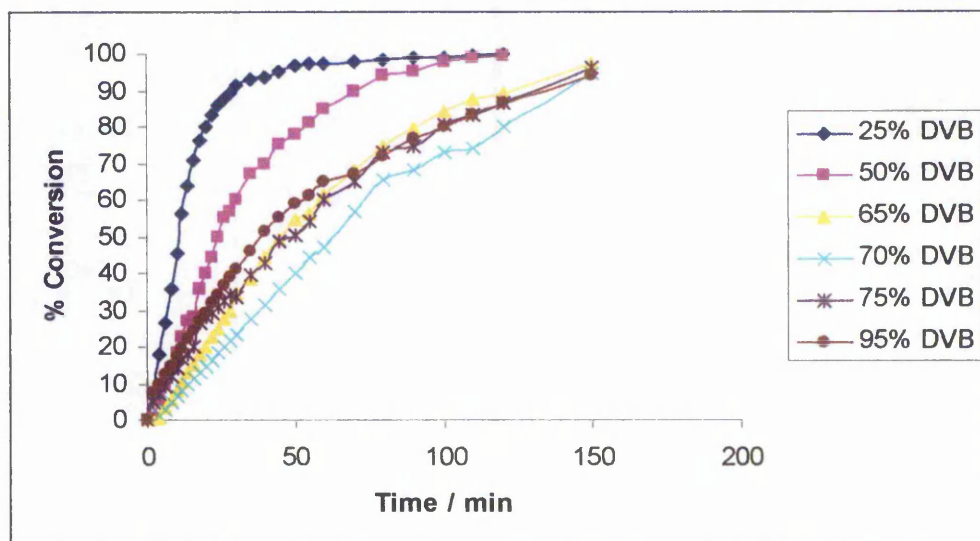


Fig. 4.62 Conversion against time plots for porous nanoparticles produced with varying divinylbenzene concentration. KPS =  $7 \cdot 10^{-3}$  mol dm<sup>3</sup>, SDS = 0.014 mol dm<sup>3</sup>, porogen ratio (toluene) = 0.5:1

From Fig. 4.62 it can be seen that as the divinylbenzene concentration increases there is an initial decrease in the rate of polymerisation, however after a divinylbenzene concentration of 70% there is an increase in the rate of reaction. Table 4.18 shows the slopes of the linear interval II section of the conversion against time plot with divinylbenzene concentration. At low divinylbenzene concentrations the particles are more able to swell with monomer to maintain a faster growth rate.

Divinylbenzene Concentration (%)	Slope / % conversion min <sup>-1</sup>
25	4.65
50	2.17
65	1.22
70	0.84
75	1.02
95	1.29

Table 4.18 Change in slope of linear interval II with divinylbenzene concentration

## **4.3 Reactive particles**

### **4.3.1 Introduction**

Styrene / divinylbenzene copolymers have found applications in a wide range of situations from chromatography to ion exchange, and it should be possible for the functionality normally associated with these applications such as sulphonate and amine to be imparted onto porous nanoparticles by harsh chemical treatments such as the use oleum. For the purpose of this study however it was decided to examine the possibility of producing functionalised particles by using a redox initiation system to leave reactive initiator fragments at the surface and also to investigate the possibility of incorporating chitosan into the polymer matrix to give functional amine groups.

### **4.3.2 Redox Initiated Porous Nanoparticles**

The potential of using a redox initiator system to impart functionality to porous nanoparticles was examined by conductometric titration. The latex was first protonated with HCl to ensure all available reactive sites were functionalised and then titrated. All of the samples when titrated resulted in a titration curve similar to that shown in Fig. 4.63.

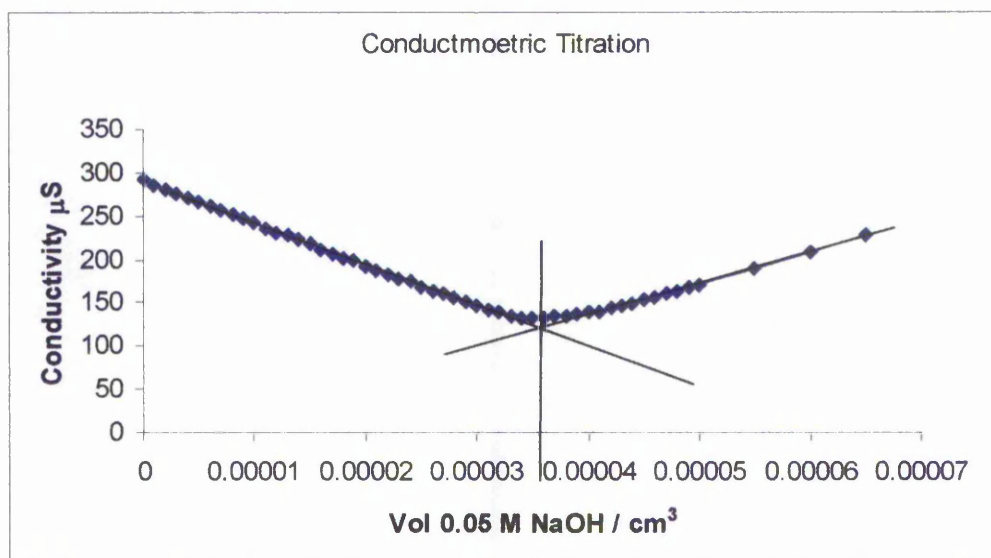


Fig. 4.63. Titration curve for porous nanoparticles produced with redox initiator

The series of porous nanoparticles produced with varying sodium metabisulphate / potassium persulphate ratios (section 4.1.2.2) were examined and the results are given in table 4.19.

SMBS / KPS Ratio	Surface Charge $\text{mol g}^{-1}$
0	1.05E-04
0.1	1.72E-04
0.15	1.39E-04
0.2	1.14E-04
0.25	1.01E-04
0.3	8.46E-05

Table 4.19. Surface charge in  $\text{mol g}^{-1}$  for porous nanoparticles with varying redox ratio

From table 4.19 it can be seen that the surface charge shows an initial increase as the sodium metabisulphite is introduced into the system but this soon decreases upon further increase in the metabisulphite concentration. This is a similar trend to that shown by the surface area of these particles as discussed in section 4.1.2.2 and Fig. 4.64 shows a plot of surface charge and surface area against sodium metabisulphite / potassium persulphate ratio.

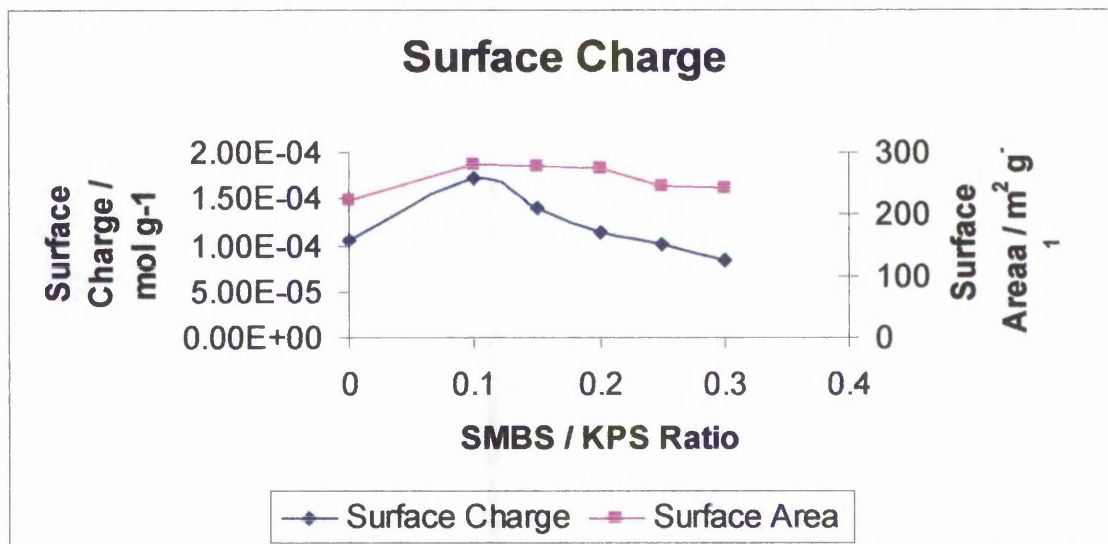


Fig. 4.64 Change in surface charge and surface area with varying sodium metabisulphite potassium persulphate ratio.

This would suggest that as the porous network increases more reactive sites become available within the porous network, but as the surface area decreases upon increasing the sodium metabisulphite concentration then some of the reactive sites are lost inside the particles with no access from the surface.

### 4.3.3 Catalysis of Ethyl Formate by Redox Initiated Porous Nanoparticles

The reactive sites made available via redox initiation may be suitable to act as a catalyst in the hydrolysis of ethyl formate. A polybutylmethacrylate film impregnated with redox initiated porous nanoparticles on a glass slide was used to evaluate the potential for this application. A blank run using a PBMA film only was carried out and then the experiment was repeated with the active film. After the first run the active film was rinsed and a repeat experiment carried out.

Fig. 4.65 shows a plot of conductance against time for the blank run and the two runs with the active film. It can be seen from the chart that with the PBMA film only the rate of hydrolysis of the ethylformate is negligible, but with the film activated with porous nanoparticles the rate of hydrolysis is much faster. Also it can be seen that the second run with the same piece of film shows a similar rate of hydrolysis as the first suggesting true catalytic activity.

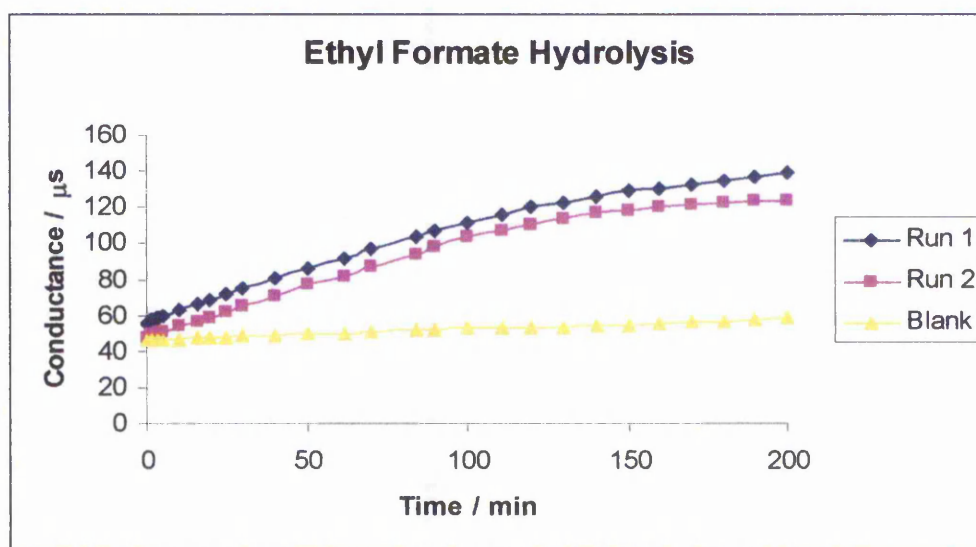


Fig. 4.65. Rate of ethylformate hydrolysis with redox initiated porous nanoparticles.

A plot of  $\ln(n_{inf}-n_0)$  gives a straight line whose gradient is equal to  $-k$ , fig 4.66 shows the plot for the two runs. It can be seen from the chart that both runs result in straight lines with a gradient of  $-0.01$  and a rate constant of  $0.01 \text{ min}^{-1}$  at  $25 \text{ }^\circ\text{C}$ .

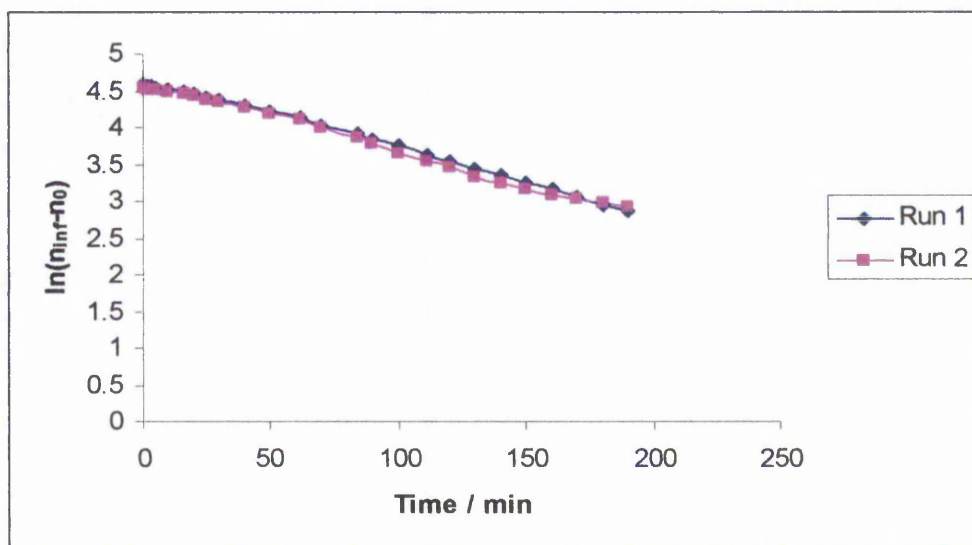


Fig. 4.66 Plot of  $\ln(n_{inf}-n_0)$  against time for the hydrolysis of ethyl formate with functional porous nanoparticles as catalyst.

#### **4.4 Chitosan Functionalisation**

As has previously discussed chitosan is rich in amine groups. These groups are of interest because of their ability to form metal complexes with transition metals.

#### **4.4.1 Chitosan Functionalised Solid Polystyrene**

In this series of experiments solid polystyrene microspheres were produced with chitosan functionality by incorporating the chitosan into the reaction mixture at the beginning of the polymerisation.

The incorporation of Jeffamine D2000 was tried as previous workers had shown that by incorporating a low molecular weight flexible amine allowed the chitosan to attach more easily to the polymer chain<sup>177</sup>



Fig 4.67. Jeffamine D2000

Chitosan tends to adsorb in a very flat conformation which Jeffamine, by competing for some of the available anionic sites, prevents and so the chitosan chains tend to be more extended into the aqueous phase making it a better steric stabiliser.

#### **4.4.2 Chitosan Functionalised Spheres Produced Using Jeffamine D2000**

In this series of experiments solid polystyrene spheres were produced with increasing amounts of chitosan incorporated in the reaction mixture, all the other ingredients were kept at a constant concentration.

All the polymerisations were taken to completion with conversion of monomer to polymer above 95%, levels of coagulum were low. One of the

most noticeable changes that occurred was a change in the solution viscosity of the polymers produced in the presence of high levels of chitosan. All the polymerisations were carried out in 0.1 M acetic acid to ensure full dissolution of the chitosan but as the chitosan concentration was increased there was a significant increase in the solution viscosity, indeed it was not possible to perform polymerisations with a chitosan solution concentration greater than 1% as the solution was too viscous and the resulting polymer was formed as large lumps of coagulum. At chitosan solution concentrations less than 1% then the solution viscosity dropped to near water viscosity as the polymerisation proceeded and a stable latex was produced.

Fig. 4.68 shows a chart of the acid orange 7 uptake of the final polymer spheres against the initial chitosan concentration in the reaction mixture.

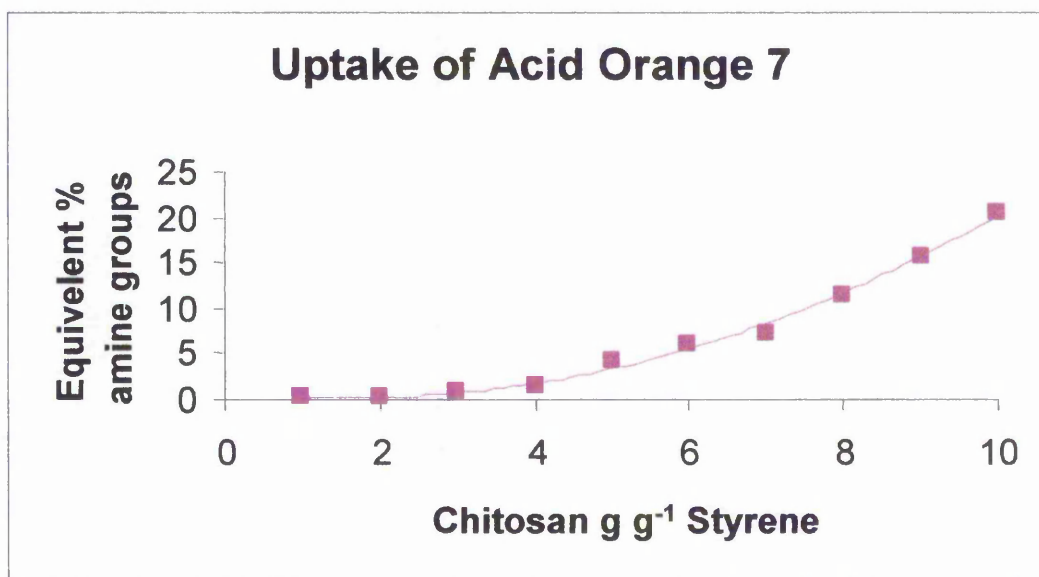


Fig. 4.68 Acid Orange 7 uptake by chitosan functionalised solid polystyrene spheres incorporating Jeffamine D2000 in the reaction mixture

It can be seen that as the concentration of the chitosan in the initial reaction mixture is increased there is a steady increase in the amount of acid orange 7 adsorbed by the spheres.

Fig. 4.69 shows a TEM image of one of the samples from the series. It can be seen that the spheres are very spherical however there does appear to be a bimodal distribution, most of the spheres are in the 100 nm size range but there is a significant number of much larger spheres in the 200 nm size range. This bi-modal size distribution was observed on several of the samples most noticeably on those with higher concentrations of chitosan incorporated in the reaction mixture. This would seem to suggest that although chitosan can be successfully incorporated into solid polystyrene spheres, as the concentration of the chitosan is increased then there is a shift towards a less monodisperse size distribution of the particles. This decrease in monodispersity may be linked to the solution viscosity at the start of polymerisation.

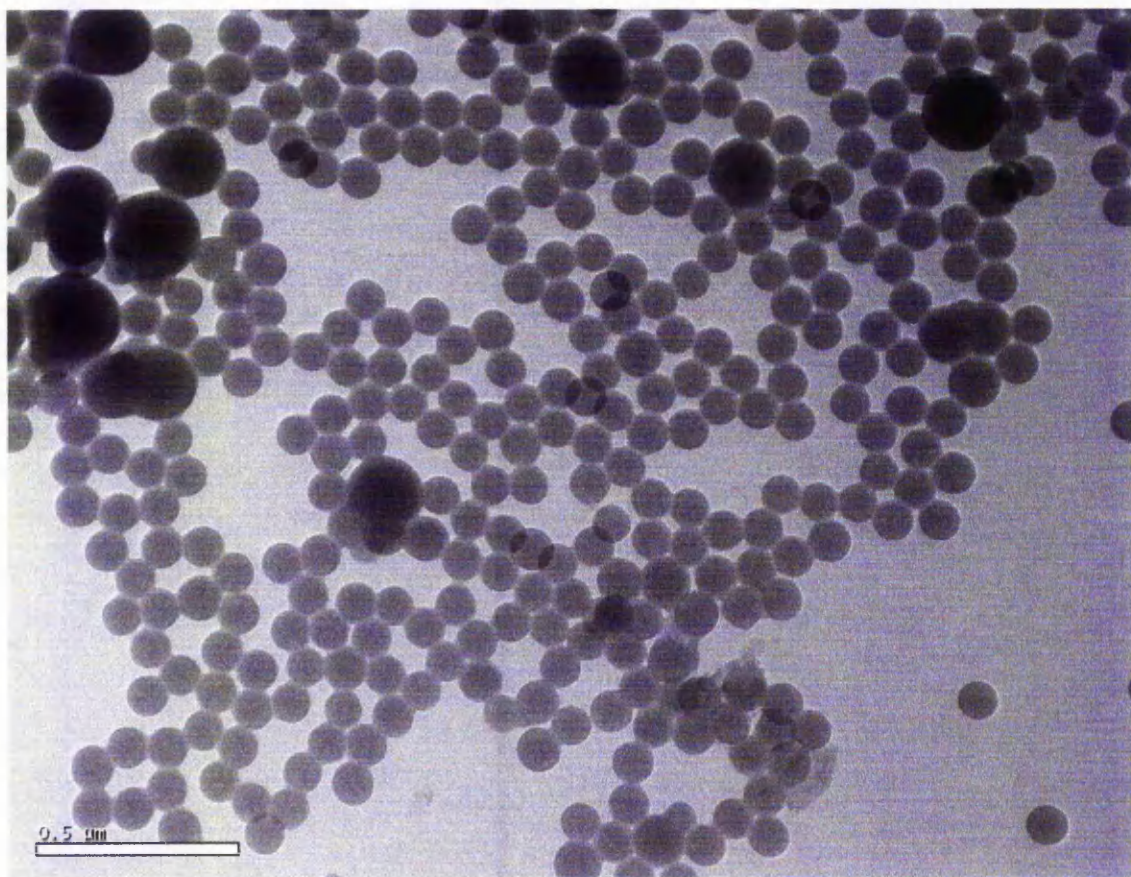


Fig 4.69. TEM of chitosan activated polystyrene

To assess the stability of the binding of the chitosan to the polymer beads samples of the dried latex were washed in water and 0.1 M acetic acid. Fig. 4.70 shows the acid orange 7 uptake for the series after treatment compared to the untreated samples. From the figure it shows that with water there is almost no change in the uptake of acid orange 7, this is not surprising as water is not a solvent for chitosan and would not be expected to remove any of the chitosan from the polymer, however for the samples washed in 0.1 M acetic acid there is a small drop in the acid orange 7 uptake across the whole range suggesting that there is a small amount of chitosan that has just been deposited on the surface of the beads and is not rigidly bound to the polymer.

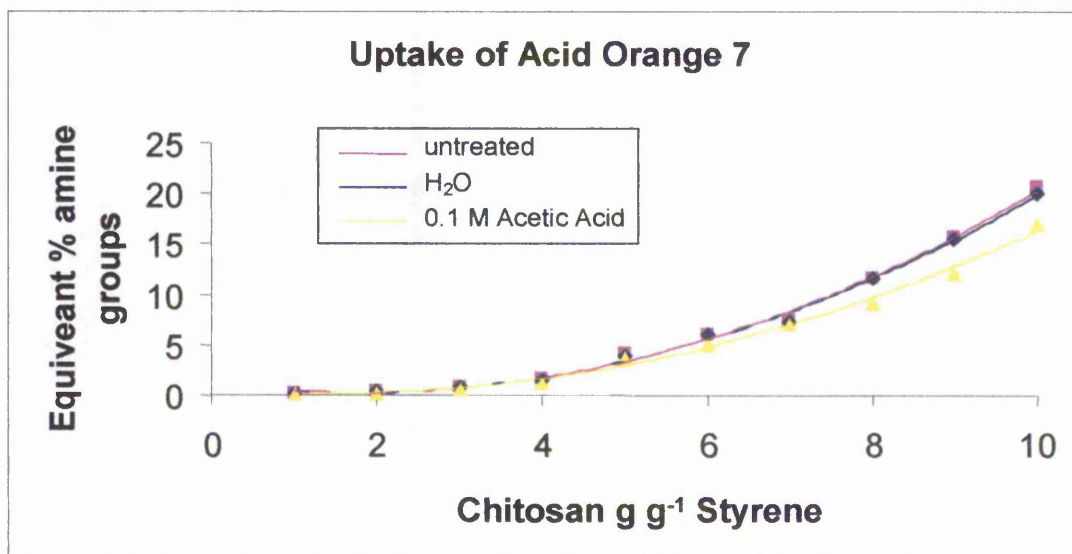


Fig. 4.70 Acid Orange 7 uptake by chitosan functionalised solid polystyrene spheres incorporating Jeffamine D2000 in the reaction mixture

FTIR results for the samples show a significant peak in the 3100 –3600  $\text{cm}^{-1}$  region associated with amine groups but for a latex produced without any chitosan no peak in this region was observed.

It has been suggested<sup>178</sup> that in the presence of potassium persulphate at 70°C a free radical degradation of chitosan takes place by attack of the anionic radicals on the C-4 carbon abstracting hydrogen and forming a chitosan radical. Chitosan could thus become covalently bound to the polymer surface which may help to explain the substantive nature of the attachment when chitosan is not removed by extraction in acetic acid.

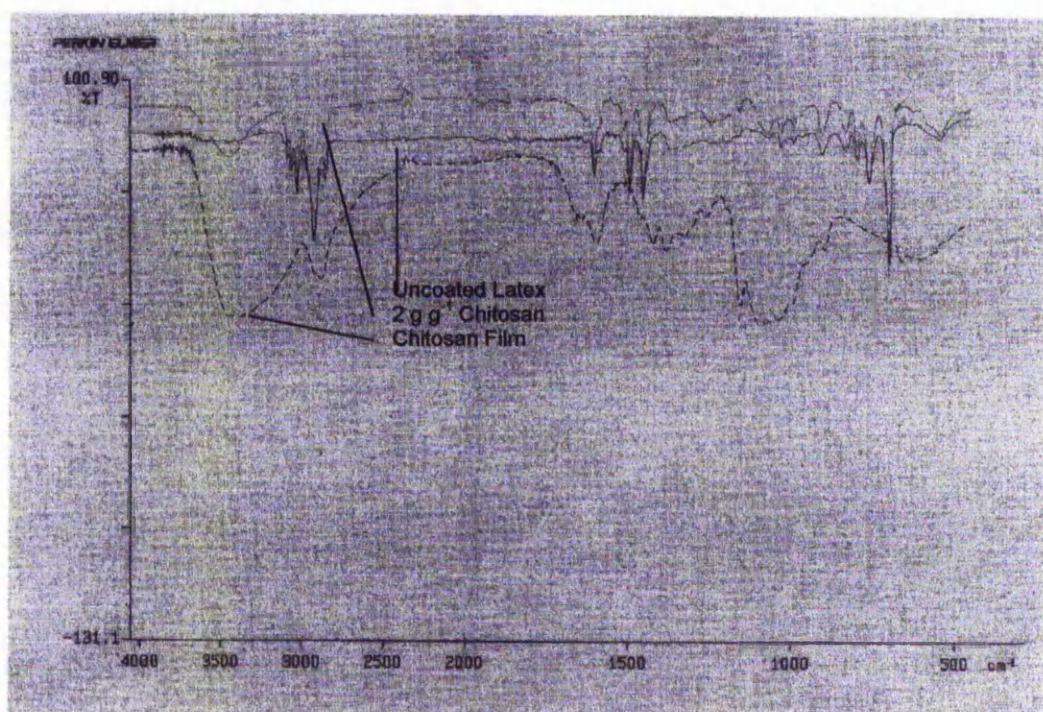


Fig 4.71. FTIR spectrum for uncoated latex, 2 g g<sup>-1</sup> chitosan coated latex and chitosan film.

#### **4.4.3 Chitosan Functionalised Solid Polystyrene Without Jeffamine**

##### **D2000**

The polymerisations were repeated without incorporating the Jeffamine D2000. In this case the polymerisation was not successful. Large amounts of coagulum were formed and the viscosity of the supernatant was high

indicating that the chitosan was still dissolved in the acidified aqueous phase and not incorporated into the polymer. Acid orange 7 analysis of the final polymer showed that only a small amount of chitosan was incorporated.

#### **4.4.4 Chitosan Functionalised Porous Nanoparticles**

The method for functionalising solid polystyrene was applied to the production of porous nanoparticles. Unfortunately the addition of a porogen to the reaction mixture at the start of polymerisation caused the system to break down. The final product was very high in coagulum and no stable latex was achieved. An alternative method of functionalising porous nanoparticles was thus tried.

It has already been shown that porous nanoparticles can be produced using a redox couple of potassium persulphate and sodium metabisulphite, this system of initiation will leave initiator fragments attached to the polymer that carries a negative charge. It was proposed to utilise this to post functionalise the porous nanoparticles with chitosan that will be protonated due to dissolution in a dilute organic acid.

Samples of previously prepared porous nanoparticles with a specific surface area of  $256 \text{ m}^2 \text{ g}^{-1}$ , were immersed in a chitosan solution for differing periods of time. The latices were then centrifuged and washed to ensure that any residual chitosan was removed before analysis.

Table 4.20 shows the results for surface area and acid orange 7 uptake for the samples treated with a 1% chitosan solution at different mixing times. The concentration of 1% was chosen as this was the maximum concentration that could be used to produce solid polystyrene spheres due to viscosity.

Sample	Surface Area $\text{m}^2 \text{g}^{-1}$	% Amine groups
Untreated	256	0.63
6 hours	244	4.54
24 hours	244	5.17
72 hours	198	6.83

Table 4.20. Surface area and % available amine groups for porous nanoparticles treated with chitosan at a concentration of 1% over differing time periods

From table 4.20 it can be seen that the amount of chitosan adsorbed by the porous nanoparticles increases as the time of mixing increased. It is also of interest that the untreated particles will adsorb a small amount of acid orange 7 presumably trapped within the porous network. It is also clear that the chitosan is being adsorbed into the pores of the nanoparticles as the surface area decreases with increasing mixing time.

A further experiment was performed in which the concentration of the initial chitosan solution was altered. All the samples were treated for 72 hours Table 4.21 shows the results for this series of experiments.

Chitosan Concentration	Surface Area $\text{m}^2 \text{g}^{-1}$	% Amine Groups
Untreated	256	0.63
0.25%	254	2.33
0.5%	244	2.5
0.75%	214	5.43
1.0%	193	7.13

Table 4.21 Change in surface area and amine group concentration with varying chitosan concentration.

From the table it can be seen that there is an increase in the acid orange 7 uptake with increasing concentration of the initial chitosan solution and a corresponding decrease in the specific surface area.

## **5.0 Conclusions**

The preparation of porous latex nanoparticles has been studied by varying the quantities of the initiator, monomer ratio, surfactant and inert diluent present in the reaction mixture. The results obtained show that the most significant aspect of the formation of porous latex particles is the ratio between the monomers, the best results obtained with a high degree of cross-linking divinylbenzene being present. The level of the porogen compared to the monomers also has an effect of increasing the surface area as the porogen content increases but this increase is only small. The surfactant concentration does not appear to have any significant effect on either surface area or particle size once the cmc value is reached, however below the cmc the surfactant concentration does effect both surface area and particle size. It is not possible to produce porous latices with any significant surface area using a soap free polymerisation technique. The initiator concentration also does not have any major influence on surface area or particle size above a concentration of  $3 \cdot 10^{-3} \text{ mol dm}^{-3}$  of potassium persulphate.

Unlike in the formation of macroreticular resins the type of progen (whether solvating or non solvating) does not appear to make any significant difference to the particle size or surface area of porous nanoparticles and thus to the final porous network formed.

The use of a redox couple for the initiator has a significant impact on the final surface area of the porous nanoparticles. A significant increase being seen when sodium metabisulphite was introduced.

Pore size analysis from nitrogen adsorption / desorption isotherms shows that the porous network contains mostly micropores. Analysis of the desorption isotherms showed an increase in the micropore volume following a similar trend to that for surface area with varying the ingredients and reaction conditions.

From the dilatometry studies it would appear that the formation of the porous structure is a two stage process, the initial stage shows an increase in the density of the forming polymer compared to that of the monomers and the latter stage shows a decrease in density compared to that of the monomers. It is thought that the second stage relates to the formation of the three dimensional network in which the porogen is entrapped.

Vapour adsorption studies have shown that porous nanoparticles are able to adsorb a variety of vapours but their performance in comparison to activated carbon was poor at low  $P/P_0$  values. However the small size of porous nanoparticles make them much more attractive for incorporation into thin films than the large particle size of the activated carbon or macroreticular resins.

Kinetic studies on the polymerisation of styrene using a redox initiation system showed that for the case of sodium dodecylsulphate the rate of polymerisation increases with the introduction of the reducing agent over the range of concentration studied and that the polymerisations followed Smith-Ewart case 2 kinetics, however for Aerosol OT surfactant after an initial steep rise in the rate of polymerisation a maximum rate was achieved for a potassium persulphate / sodium metabisulphite ratio of approximately 0.1-0.2

after which the rate steadily declined, also the polymerisation switched from case 2 to case 3 kinetics above a ratio of 1.

The kinetic study on porous nanoparticles found the dependence on the sodium dodecylsulphate and the potassium persulphate to be  $[\text{SDS}]^{0.78}$  and  $[\text{KPS}]^{0.26}$  compared to  $[\text{SDS}]^{0.6}$  and  $[\text{KPS}]^{0.4}$  found for styrene by Smith-Ewart.

Redox initiated porous nanoparticles suspended on a polybutylmethacrylate film were proposed as potential catalysts and were shown to increase substantially the rate of hydrolysis of ethyl formate.

Chitosan was successfully incorporated into polystyrene latex using a flexible diamine coupling agent, porous nanoparticles can also be functionalised with chitosan post polymerisation.

## **6.0 Further Work**

This study on the preparation of porous nanoparticles has concentrated on the most common monomer system used in the preparation of macroreticular resins, this being styrene co-divinylbenzene. These co-polymers led to rather brittle thin films. Other co-polymer for example acrylic and methacrylic monomers plus a cross-linker such as ethylene-glycol-dimethacrylate systems may prove more suitable for inclusion into such films. The increased hydrophilicity may be helpful for maintaining an even distribution of particles throughout the film and also aid in increasing the cohesiveness of the final film.

The use of active ingredient in the porogens used for the formation of porous nanoparticles may allow the prospect of developing materials suitable for sustained release applications. Sparingly soluble species or oil soluble species could be included in the polymerisation mixture at the beginning of the process or active species could be adsorbed into the porous network after the particles have been formed and their ability to be released over time examined. The possibility of forming selectively reactive particles using templating may also be investigated, while these do not not enhance gross adsorptive properties low level uptakes such as used in detector devices would be of interest.

A much more detailed investigation into the unusual rheological properties of such low solids dispersions of porous nanoparticles is required using other surfactant types and co-polymer systems.

## References

- <sup>1</sup> Sherrington, D. C., *Chemistry in Industry*, 1991, 7<sup>th</sup> Jan, 15
- <sup>2</sup> Hodges, I. C., *PhD Thesis*, Nottingham Trent University, February 2002
- <sup>3</sup> Seidl, J., Malinsky, J., Dusek, K. & Heitz, W., *Adv. Polym. Sci.*, 1967, 5, 11
- <sup>4</sup> Hassanein, M., Aly, El S., A., Abbas, Y. A., El-Signey, S. M., *Macromol Chem.*, 1993, 194, 1817
- <sup>5</sup> Ford, W. T., El-Hamshany, H., Stefanithis, I., Spivy, H. O., Hassanein, M., Selim, A., *New J. Chem.*, 1996, 20 (5), 549
- <sup>6</sup> Hassanein, M., Abdel-Hay, I., El-HafnawyEl-Esawy, T., *Eur. Polym. J.*, 1994, 30 (3), 335
- <sup>7</sup> Zhu, W., Ford, W. T., *J. Polm. Sci., A, Polym. Chem.*, 1992, 30, 1305
- <sup>8</sup> Fitch, R. M., in "Macromolecules", Benoit, H., Rempp, P. (Eds.), Pergamon Press, Oxford, 1992
- <sup>9</sup> Hopkins, A., Williams, A., *J. Chem. Soc., Perkin Trans.*, 1983, 2, 891
- <sup>10</sup> Kinato, H., Nakamura, K., Ise, N., *J. Appl. Biochem.*, 1982, 4, 34
- <sup>11</sup> Hassanein, M., Ford, W. T., *Macromol.*, 1988, 21, 525
- <sup>12</sup> Turk, H., Ford, W. T., *J. Org. Chem.*, 1988, 53, 460
- <sup>13</sup> Ford, W. T., Chandran, R., Turk, H., *Pure Appl. Chem.*, 1988, 60, 395
- <sup>14</sup> Chandran, R. S., Srinivasan, S., Ford, W. T., *Langmuir*, 1989, 5 (4), 1061
- <sup>15</sup> Bernard, M., Ford, W. T., Taylor, T. W., *Macromol.*, 1984, 17, 812
- <sup>16</sup> Thaigarajan, V. S., Huang, Z., Scriven, L. E., Schottel, J. L., Flickinger, M. C., *J. Colloid Interf. Sci.*, 1999, 215 (2), 244
- <sup>17</sup> Marchionna, F., *Latex and its Industrial Applications*, The Rubber Age Publishing Co., New York, 1933
- <sup>18</sup> Gilbert, R. G., *Emulsion Polymerization, A Mechanistic Approach*, Academic Press, London, 1995
- <sup>19</sup> Smith, W. V. & Ewart, R. H., *J. Chem. Phys.*, 1948, 16, 592
- <sup>20</sup> Matsumoto, T. & Ochi, A. *Kobunshi Kagaku*, 1965, 22, 481
- <sup>21</sup> Fitch, R. M., Prenosil, M. P., Sprick, K. J., *J. Polym Sci., Part C*, 1969, 27, 95
- <sup>22</sup> Arai, M., Arai, K., Saito, S., *J. Polym. Sci. Chem. Ed.*, 1979, 17, 3655
- <sup>23</sup> Goodall, A. R., Wilkinson, M. c., Hearn, J., *J. Polym. Sci. Polym. Chem. Ed.*, 1977, 15, 2193
- <sup>24</sup> Feeney, P. J., Napper, D. H., Gilbert, R. G., *Macromol.*, 1984, 17, 2520
- <sup>25</sup> Feeney, P. J., Napper, D. H., Gilbert, R. G., *Macromol.*, 1987, 20, 2922
- <sup>26</sup> Shaw, D. J., "Introduction to Colloid and Surface Chemistry" 4<sup>th</sup> Ed., Butterworth-Hienemann, 1992
- <sup>27</sup> Goodwin, J. W., Hearn, J., Ho, C. C., Ottewill, R. H., *Br. Polym. J.*, 1973, 5, 347
- <sup>28</sup> Ottewill, R. H., & Shaw, J. N., *Kolloid Z. u. Z. Polymere*, 1967, 218, 34
- <sup>29</sup> Smith, W. V., Ewart, R. H., *J. Phys. Chem*, 1948, 16, 592
- <sup>30</sup> Harkins, W. D., *J. Am. Chem. Soc.*, 1947, 69, 1428
- <sup>31</sup> Kolthoff, I. M. & Miller, I. K., *J. Am. Chem. Soc.*, 1941, 73, 5118
- <sup>32</sup> Bartlett, P. D. & Cotmann, J. D., *J. Am. Chem. Soc.*, 1949, 71, 1419
- <sup>33</sup> Fronaeus, S. & Ostman, C. O., *Acta Chem. Scand.*, 1955, 9, 902
- <sup>34</sup> Bacon, R. G. R., *Trans Faraday Soc.*, 1946, 42, 140
- <sup>35</sup> Baxendale, J. H., Evans, M. G. & Park, G. S., *Trans. Faraday Soc.*, 1946, 42, 155
- <sup>36</sup> Bury, K. L., Peterson, J. H., *J. Am. Chem. Soc.*, 1951, 73, 5195
- <sup>37</sup> Fordham, J. W. L., & Williams, H. L. *J. Am. Chem. Soc.*, 1951, 73, 4855
- <sup>38</sup> Starkweather et. al., *Ind. Eng. Chem.*, 1947, 39, 210
- <sup>39</sup> Bacon, R. G. R., *Q. Rev. Chem. Soc.*, 1955, 9, 287
- <sup>40</sup> Keight, D. V., Padget, J. C., & Towns, C. R., *PRI Polymer Latex III Conference*, London, June 1989
- <sup>41</sup> Blackley, D. C., "Emulsion Polymerisation", Applied Science Publishers, 1975
- <sup>42</sup> Orr & Williams, *J. Am. Chem. Soc.*, 1955, 77, 3715
- <sup>43</sup> Morgan, *Trans. Faraday Soc.*, 1946, 42, 169
- <sup>44</sup> Ivanhoff, S. S. & Yurzhenko, A., *Kolloid Zh.*, 19960, 22, 120
- <sup>45</sup> Morris, C. E. M. & Parts, A. G., *Makromol. Chem.*, 1968, 119, 212
- <sup>46</sup> Friend, J.p. & Alexander, A. E., *J. Polym. Sci. Pt. A-1*, 1968, 6, 1833
- <sup>47</sup> Allen, P. W., *Polym. Sci.*, 1958, 31, 206
- <sup>48</sup> Sturzenhoffecker, F., *Angew. Chem.*, 1959, 71, 198
- <sup>49</sup> Wilkinson, M. J., Hearn, J. & Steward, P. S., *Adv. Colloid Interface Sci.*, 1999, 81, 77
- <sup>50</sup> McCarvill, W. T., Fitch, R. M., *J. Colloid Interface Sci.*, 1978, 64 (3), 403
- <sup>51</sup> Goodall, A. R., Hearn, J., Wilkinson, M. C., *J. Polym. Sci. Chem. Ed.*, 1979, 17, 1019
- <sup>52</sup> Everett, D. H., Gultepe, M. E., Wilkinson, M. C., in "Polymer Colloids II", Fitch, T. M. (Ed.), Plenum Ptes, New York, 1980, 313

- <sup>53</sup> Ahmed, S. M., El-Asser, M. S., Powlic, G. H., Pohlein, G. W., Vanderhoff, J. W., *J. Colloid Interf. Sci.*, 1980, **73** (2), 388
- <sup>54</sup> Harding, I. H., Healy, T. W., *J. Colloid Interf. Sci.*, 1982, **89** (1), 185
- <sup>55</sup> Zahka, J., Min, L., *Chem. Eng. Prog.*, 1977, **December**, 53
- <sup>56</sup> Labib, L. E., Robertson, A. A., *J. Colloid Interface Sci.*, 1978, **67** (3), 543
- <sup>57</sup> Wilkinson, M. C., Hearn, J., Chainey, M., *Brit. Polym. J.*, 1981, **13**, 82
- <sup>58</sup> Wilkinson, M. C., Hearn, J., Steward, P. A., *Adv. Coll. Int. Sci.*, 1999, **77**, 165
- <sup>59</sup> Vanderhoff, J. W., Van den Hull, H. F., Tausk, R. J. M., Overbeek, J. T. H. G., in *"Clean Surfaces; Their Preparation and Characterisation for Interfacial Studies"*, Goldfinger, G.(Ed), Marcel Deckler, New York, 1970
- <sup>60</sup> Schenkel, J. H. & Kitchener, J. A., *Nature*, 1958, **182**, 131
- <sup>61</sup> Van den Hull, H. F., Vanderhoff, J. W., *J. Colloid Interf. Sci.*, 1969, **28** (2), 336
- <sup>62</sup> McCann, G. D., Bradford, E. B., Van den Hull, H. J., Vanderhoff, J. W., *J. Colloid Interf. Sci.*, 1971, **36** (1), 159
- <sup>63</sup> Vanderhoff, J. W., Van den Hull, H. J., *J. Macromol. Sci. Chem.*, 1973, **A7** (3), 677
- <sup>64</sup> Chen, S. F., PhD Thesis, Bristol University, 1974
- <sup>65</sup> Chonde, Y., & Krieger, I. M., *J. Colloid Interf. Sci.*, 1980, **77** (1), 138
- <sup>66</sup> Harding, I. H., & Healy, T. W., *J. Colloid Interf. Sci.*, 1982, **89** (1), 185
- <sup>67</sup> Staudinger, H. et al, *Chem. Ber.*, 1935, **68**, 1618
- <sup>68</sup> D'Alelio, G. F. *Production of synthetic polymeric compositions comprising sulphonated polymerizates of (poly)vinyl(aryl) compounds and treatment of liquid media therewith*, US Pat 2,366,007, 1945
- <sup>69</sup> Bundy, R. H., & Boyer, R. F., *"Styrene and it's Polymers, Copolymers and Derivatives"*, New York, Reinhold Publ. Corp., 1952
- <sup>70</sup> Bailey, D. C. & Lange, S. H., *Chem. Rev.*, 1981, **81**, 109
- <sup>71</sup> Kaneko, M. & Tsuchida, E., *J. Polym. Sci., Macromol. Rev.*, 1981, **26**, 397
- <sup>72</sup> Akelah, A. & Sherrington, D. C., *Chem. Rev.*, 1981, **81**, 557
- <sup>73</sup> Gribnau, T. C. J., Visser, J., Nivard, R. J. F., (Eds), *"Affinity Chromotography and Related Techniques"*, Elsevier, Amsterdam, 1982
- <sup>74</sup> Brooks, B. W., *Macromol. Chem. Macromol. Symp.*, 1990, **35/36**, 121
- <sup>75</sup> Kun, A. A. & Kunin, R., *J. Polym. Sci.*, 1967, **16**, 1457
- <sup>76</sup> Kun, A. A. & Kunin, R., *J. Polym. Sci.*, 1968, **6**, 2089
- <sup>77</sup> Millar, JH. R., Smith, D. G., Marr, W. E., Kressman, T. R. E., *J. Amer. Chem. Soc.*, **85**, 1963, 218
- <sup>78</sup> Kunin, R. & Meitzner, E., *J. Amer. Chem. Soc.*, 1962, **84**, 305
- <sup>79</sup> Seidel, J., Malinsky, J., Dusek, K., *Plasteicheskie Massej.*, 1963, **12**, 7
- <sup>80</sup> Bakhshae, M., Pethrick, R. A., Rashid, H., Sherrington, D. C., *Polym. Comm.*, 1985, **26**, 185
- <sup>81</sup> Milsson, H., Mosbach, R., Mosbach, K., *Biochem. Biophys. Acts*, 1972, **268**, 253
- <sup>82</sup> Seidel, W. K., & De Jong, G. J., *J. Appl. Poly. Sci.*, 1973, **17**, 2835
- <sup>83</sup> Bortel, E., *Prezmy. Chem.*, 1965, **44**, 255
- <sup>84</sup> Haupke, K. & Hoffman, H. Z., *Chem.*, 1968, **8**, 463
- <sup>85</sup> Mikes, J. A. *London Conference*, 1970
- <sup>86</sup> Tager, A. & Tailipotkina, M., *Bysokomol Sodein*, 1968, **10(A)**, 1065
- <sup>87</sup> Chung, D. Y., Bantholin, M., Guyot, A., *Agnew. Makromol, Chem.*, 1982, **103**, 109
- <sup>88</sup> Haupke, K. & Hoffman, H. Z., *Chem.*, 1968, **8**, 463
- <sup>89</sup> Guyot, A. & Bartholin, M., *Prog. Poym. Sci.*, 1982, **8**, 277
- <sup>90</sup> Braconnot, H. *Ann. Chim. (Paris)* 1811, **79**, 265
- <sup>91</sup> Odier, A. *Mem. Soc. Histoire Nat. (Paris)* 1823, **1**, 29
- <sup>92</sup> Lassaigne, J. L. *Comp. Rend.* 1843, **16**, 1087-1089
- <sup>93</sup> Ledderhose, G & Hoppe-Seyler, *Z. Physiol. Chem.* 1878, **2**, 213-227
- <sup>94</sup> Gilson, E. *Bull. Soc. Chim. (Paris)* 1894, **3**, 1099
- <sup>95</sup> Rouget, C. *Comp. Rend.* 1859, **48**, 799-795
- <sup>96</sup> Hoppe-Seyler, F. *Ber. Deut. Chem. Gesell.* 1894, **27**, 3329
- <sup>97</sup> Purchase, E.R. & Braun, C.E. *Org. Synth.* 1946, **26**, 36-37
- <sup>98</sup> Diehl, J.M. & Van Iterson, G. *Kolloid Z.* 1935, **73**, 253
- <sup>99</sup> Meyer, K.H. & Wehrli, M. *Helv. Chim. Acta.* 1937, **20**, 253
- <sup>100</sup> Van Iterson, G. Mwyer, K.H. & Lotmar, W. *Rec. Trav. Chem.* 1936, **55**, 61
- <sup>101</sup> Heyn, A.N.J. *Protoplasma*, 1936, **25**, 372
- <sup>102</sup> Heller, K. Claus, L. & Huber, J. Z. *Naturforsch.* 1959, **14-B**, 476
- <sup>103</sup> Zeichmeister, L. & Toth, G. *Physiol. Chem.* 1934, **223**, 53

- 104 Karrer, P. & Hoffmann, A. *Helv. Chim. Acta.* 1929, **12**, 616
- 105 Karrer, P. & Van Francois, G. *Helv. Chim. Acta.* 1929, **12**, 986
- 106 Wisselingh, V. *Jahrb. Wiss. Botan.* 1898, 31:619
- 107 Rudall, K.M. *J. Polym. Sci.* 1969, **C28**, 83
- 108 Rudall, K.M. *Adv. Insect. Physiol.* 1963, **1**, 257
- 109 Rudall, K. M. & Kenchington, W. *Biol. Review*, 1973, **48**, 597
- 110 Dweltz, N.E. *Bioch. Biophys. Acta.* 1961, **51**, 283-289
- 111 Blackwell, J. *Biopolymers*, 1969, **7**, 281-289
- 112 Rudall, K.M. *Symp. Soc. Exp. Biol.* 1955, **9**, 49-71
- 113 Roberts, G.A.F. "Chitin Chemistry", Macmillan, 1992, 55-82
- 114 Araki, Y. & Ito, E. *Eur. J. Biochem.* 1978, **55**, 77-78
- 115 Kregar, D.R. *Bioch. Biophys. Acta.* 1954, **13**, 1-9
- 116 Rutherford, F.A. & Austin, P.R. in "Proceedings of the First International Conference on Chitin & Chitosan", Muzzarelli, R.A.A. & Poyser, E.R. (Eds.) M.I.T.S.G, 1978, 182
- 117 Sannan, T. Kurita, K. & Gardner, J. *J. Appl. Polym. Sci.* 1988, **27**, 4251
- 118 Roberts, G.A.F. in "Chitin Handbook", Muzzarelli, R.A.A. & Peter, M.G. (Eds.) European Chitin Soc. 1997, 129-130
- 119 Maghami, G.G. & Roberts, G.A.F. *Macromol. Chem.* 1988, **189**, 2239
- 120 Gummow, B.D. & Roberts, G.A.F. *Macromol. Chem.* 1985, **186**, 1239
- 121 Domszy, J.G. & Roberts, G.A.F. *Macromol. Chem.* 1985, **186**, 1671
- 122 Filar, L.J. & Wirik, M.G. Ref. 118, p169-181
- 123 Broussignac, P. *Chem. Ind. Genie. Chim.* 1968, **99**, 1241
- 124 Hayes, E.R. & Daries, D.H. Ref. 29, p406-420
- 125 Castle, J.E. Deschamps, J.R. & Tice, K. in "Chitin, Chitosan and Related Enzymes", Zikakis, J.P. (Ed), Academic Press, London, 1984, p273
- 126 Muzzarelli, R.A.A. & Rochetti, R. in "Chitin in Nature and Technology", Muzzarelli, R.A.A. Jeuniaux, C. & Gooday, G.W. (Eds), Plenum Press, N.Y. 1986, p385
- 127 Darnen, S.E. & Rudall, K.M. *Disc. Faraday Soc.* 1950, **9**, 251
- 128 Moore, G.K. & Roberts, G.A.F. Ref. 118, p421-429
- 129 Sannan, T. Kurita, K. Ogura, K. & Iwakura, Y. *Polymer*, 1978, **19**, 458
- 130 Muzzarelli, R.A.A. Tanfani, F. Scarpini, G. & Latzera, G. *J. Biochem. Biophys. Methods*, 1980, **2**, 299-306
- 131 Miya, M. Iwamoto, R. Yoshikawa, S. & Mima, S. *Int. J. Biol. Macromol.* 1980, **2**, 323
- 132 Radhakrishnamurthy, B. Dalferes Jr. E.R. & Berenson, G. S. *Anal. Biochem.* 1978, **26**, 61
- 133 Holan, Z. & Votruba, J. *J. Chromatog.* 1980, **190**, 67
- 134 Hirano, S. & Yamaguchi, R. *Biopolymers*, 1976, **15**, 1685
- 135 Saito, H. Taketa, R & Hirano, S. in "Chitin and Chitosan" Hirano, S. & Takura, S. (Eds.) The Japanese Society of Chitin and Chitosan, Tottori, 1982, p71
- 136 Muzzarelli, R.A.A. in "Natural Chelating Polymers", Pergamon Press, Oxford, 1977
- 137 Hauer, H. Ref. 118, p263
- 138 Yaku, F. & Koshijima, T. Ref. 29, p386
- 139 Blair, H.S. & Ho, T.C. *J. Chem. Tech. Biotechnol.* 1980, **31**, 6
- 140 Muzzarelli, R.A.A. Tanfani, F. Emanuelli, M. & Gentile, S. *J. Appl. Biochem*, 1980, **2**, 380
- 141 Muzzarelli, R.A.A. "Chitin", Pergamon Press, 1977, 140
- 142 Yoshinara, T. & Subramanian, V. in "Environmental Biogeochemistry" Vol. 2, Nriagu, J.D. (Ed.) Ann Arbor Science Publ. Ann Arbor, 1976, 541
- 143 Mazengarb, S. A., *MPhil Thesis*, Nottingham Trent University, 2003
- 144 Fontana, F., *Memorie Mat. Fis. Soc. Ital. Sci.*, 1777, **1**, 679
- 145 Scheele, C. W., "Chemical Observations on Air and Fire", 1780, 182
- 146 de Saussure, N. T., *Gilbert's Ann. der Physik*, 1814, **47**, 113
- 147 Mitscherlich, E., *Pogg. Ann.*, 1843, **59**, 94
- 148 Kayser, H., *Wied. Ann.*, 1881, **14**, 451
- 149 Brunauer, S., Deming, L. S., Deming, W. S., and Teller, E., *J. Amer. Chem. Soc.* 1940, **62**, 1723
- 150 IUPAC (Sing K. S. W., et al), *Pure and Appl. Chem.*, 1985, **57** (4), 603
- 151 Brunauer, S., Emmett, P. H., & Teller, E., *J. Amer. Chem. Soc.*, 1938, **60**, 309
- 152 Langmuir, I., *J. Amer. Chem. Soc.*, 1916, **38**, 2221
- 153 Langmuir, I., *J. Amer. Chem. Soc.*, 1918, **40**, 1361
- 154 Dubinin, M. M., *Zhar. Phys. Chem.*, 1960, **34**, 959
- 155 Lowell, S. & Shields, J.E., "Powder Surface Area and Porosity, Chapman & Hall, London, 1984

- 
- <sup>156</sup> Craig, V. S. J., Ninham, B. W., Pashley, R. M., *J. Phys. Chem.*, 1993, **97**, 10192-10197
- <sup>157</sup> Karaman, M. E., Ninham, B. W., Pashley, R. M., *J. Phys. Chem.*, 1996, **100**, 15503-15507
- <sup>158</sup> Pashley, R. M., *J. Phys. Chem.*, 2003, **107**, 1714-1720
- <sup>159</sup> Gregg, S. J. & Langford, J. F., *Trans. Faraday Soc.*, 1969, **65**, 1394
- <sup>160</sup> Roberts, G. A. F., in "Chitin Chemistry", Macmillan, 1992
- <sup>161</sup> Osborn, A.G.; Douslin, D.R., Vapor-Pressure Relations for 15 Hydrocarbons, *J. Chem. Eng. Data*, 1974, **19**, 2, 114-117. [
- <sup>162</sup> Ambrose, D.; Sprake, C.H.S.; Townsend, R., Thermodynamic Properties of Organic Oxygen Compounds. XXXVII. Vapour Pressures of Methanol, Ethanol, Pentan-1-ol, and Octan-1-ol from the Normal Boiling Temperature to the Critical Temperature, *J. Chem. Thermodyn.*, 1975, **7**, 185-190
- <sup>163</sup> Besley and Bottomley, Vapour Pressure of Toluene from 273.15 to 298.15 K, *J. Chem. Thermodyn.*, 1974, **6**, 577-580.
- <sup>164</sup> Chainey, M., Hearn, J., & Wilkinson, M. C., *J. Colloid. Int. Sci.*, 1987, **117**, 477
- <sup>165</sup> Hodges, I. C., Hearn, J. & Wilkinson, M. J., *American Chemical Soc.I*, 2001
- <sup>166</sup> Bacon, R. G. R., *Q. Rev. Chem. Soc.*, 1955, **9**, 287
- <sup>167</sup> Flockhart, B. D., *J. Colloid Interf. Sci.*, 1961, **16**, 484
- <sup>168</sup> Gregg, S. J., Langford, J. F., *Trans. Faraday Soc.*, 1969, **65**, 1394
- <sup>169</sup> Ambrose, D.; Sprake, C.H.S.; Townsend, R., *J. Chem. Thermodyn.*, 1975, **7**, 185-190.
- <sup>170</sup> Osborn, A.G.; Douslin, D.R., *J. Chem. Eng. Data*, 1974, **19(2)**, 114-117.
- <sup>171</sup> Sanbe, H., Hosoya, K. & Haginaka, J., *Analytical Sciences*, 2003, **19**, 715
- <sup>172</sup> Bacon, R. G. R., *Q. Rev. Chem. Soc.*, 1955, **9**, 287
- <sup>173</sup> Craig, V. S. J., Ninham, B. W. & Pashley, R. M., *J. Phys Chem*, 1993, **97**, 10192-10197
- <sup>174</sup> Karaman, M. E., Ninham, B. W. & Pashley, R. M., *J. Phys Chem*, 1996, **100**, 15503-15507
- <sup>175</sup> Pashley, R. M., *J. Phys Chem*, 2003, **107**, 1714-1720
- <sup>176</sup> Steward, P., "Modification of the Permeability of Polymer Latex Films", PhD Thesis, The Nottingham Trent University, 1995
- <sup>177</sup> Marie, M., Lanndfester, K. & Antonietti, M. *Biomacromol.*, 2002, **3**, 475
- <sup>178</sup> Hsu, S. C., Don, T. M. & Chiu, W. Y., *Polymer Degradation and Stability*, 2002, **75(1)**, 73